INFORMATION TO USERS

This manuscript has been reproduced from the microfilm master. UMI films the text directly from the original or copy submitted. Thus, some thesis and dissertation copies are in typewriter face, while others may be from any type of computer printer.

The quality of this reproduction is dependent upon the quality of the copy submitted. Broken or indistinct print, colored or poor quality illustrations and photographs, print bleedthrough, substandard margins, and improper alignment can adversely affect reproduction.

In the unlikely event that the author did not send UMI a complete manuscript and there are missing pages, these will be noted. Also, if unauthorized copyright material had to be removed, a note will indicate the deletion.

Oversize materials (e.g., maps, drawings, charts) are reproduced by sectioning the original, beginning at the upper left-hand corner and continuing from left to right in equal sections with small overlaps. Each original is also photographed in one exposure and is included in reduced form at the back of the book.

Photographs included in the original manuscript have been reproduced xerographically in this copy. Higher quality 6" x 9" black and white photographic prints are available for any photographs or illustrations appearing in this copy for an additional charge. Contact UMI directly to order.

U·M·I

University Microfilms International
A Bell & Howell Information Company
300 North Zeeb Road Ann Arbor MI 48106-1346 USA
313 761-4700 800 521-0600

Order Number 9304750

Melting of mantle minerals at high pressures: Experimental study and thermodynamic evaluation

Zhang, Jianzhong, Ph.D.

City University of New York, 1992

U·M·I
300 N. Zeeb Rd.
Ann Arbor, MI 48106

Melting of Mantle Minerals at High Pressures: Experimental Study and Thermodynamic Evaluation

By

Jianzhong Zhang

A dissertation submitted to the Graduate Faculty in Earth and Environmental Sciences in partial fulfillment of the requirements for the degree of Doctor of Philosophy, The City University of New York

1992

This manuscript has been read and accepted for the Graduate Faculty in Earth and Environmental Sciences in satisfaction of the dissertation requirement for the degree of Doctor of Philosophy.

July 27, 1992
Date

Chair of Examining Committee

September 15, 1992
Date

Executive Officer

Supervisory Committee

The City University of New York

Abstract

Melting of Mantle Minerals at High Pressures: Experimental Study and Thermodynamic Evaluation

By

Jianzhong Zhang

Advisor: Professor Surrendra K. Saxena

Melting and subsolidus relations of mantle minerals have been experimentally determined for pyrope $Mg_3Al_2Si_3O_{12}$ between 10 and 16 GPa, SiO_2 polymorphs (coesite and stishovite) between 9 and 14 GPa, and brucite $Mg(OH)_2$ between 6 and 22 GPa using a split-sphere multianvil apparatus. Compared with the previous studies, the present determinations provide several new features which have not been reported earlier or predicted theoretically. These results are:

1) The melting curve of pyrope shows an increase in dT/dP slope at pressures above 10 GPa, which is considerably different from that of other mantle minerals;

2) The melting temperatures of coesite are independent of pressure between

11 and 13.5 GPa. The predicted melting curve of coesite that showed a temperature maximum around 8 GPa and a large negative slope at higher pressures has not been confirmed.

3) The coesite-stishovite-liquid triple point is bracketed between 13.5 and 13.8 GPa at 2800 °C which is 600 °C higher than the previous estimation.

4) Stishovite is melted for the first time through a static experiment. The melting temperature at 14 GPa is 2850 °C, and is 300 °C higher than those obtained from shock wave measurements at 16 to 30 GPa;

5) The dT/dP slope of the coesite-stishovite transition determined from 2000 to 2800 °C is two and half times smaller than indicated by the previous studies below 1400 °C;

6) The dehydration of brucite is terminated at a pressure between 8 and 10 GPa with a melting curve arising from it. The melting of brucite is reported for the first time and the melting temperatures are found independent of pressures between 12 and 22 GPa.

The experimental results have been thermodynamically evaluated. The procedure includes the selection of thermodynamic data on the related phases, extrapolation of heat capacity for solids beyond the melting temperatures, a modification of third order Birch-Murnghan equation at high temperature, and evaluation of data on liquid phases through analysis of the melting curves.

Acknowledgements

My thanks are due to my advisor Professor S. K. Saxena for his continuous advice and encouragement toward my Ph. D. degree. The thesis benefited highly from the suggestions and comments of my supervisory committee members, Professors G. Harlow, C. T. Herzberg and C. E. Nehru. Special thanks are due to Professor R. C. Liebermann for appointing me as a Predocroral Fellow at Mineral Physics Institute of State University of New York at Stony Brook and to Professor D. J. Weidner for his generous support which made it possible to work at KEK in the synchrotron X-ray study and to improve my understandings in the field of high pressure research by visiting laboratories in Japan. I am very grateful to Professors T. Gasparik and C. T. Herzberg for their continueous guidance throughout the entire experimental work. Discussions with Drs. G. Ganmanian, K. Leinenweber, and Y. Wang, and with many graduate students at Stony Brook on the experimental detail are greatly appreciated. I am also grateful to Dr. Y. Fei for his help in obtaining Raman spectra at the Geophysical Laboratory and many useful discussions. Finally, my thanks are due to my Brooklyn colleagues for their helpful daily discussions, especially to Dr. N. Chartterjee, E. Majewaski, and P. Shi.

The graduate school of the City University of New York made completion of my doctoral education possible, but the credits also go to those Institutes and Universities to which I closely related through personal contacts, especially to Mineral Physics Institute of State University of New York at Stony Brook, Department of Geological Sciences of Rutgers University, and Geophysical Laboratory of Carnegie Institute of Washington.

Table of Contents

List of Tables

List of Figures

Chapter 1

Introduction

Extensive melting remains a plausible mechanism for the differentiation of the early Earth into the core, mantle and crust. The homogeneous accretion models of planetary formation (e.g., Sasaki and Nakazawa, 1986) have suggested that the proto-Earth was covered by a molten layer that extended to a depth greater than 1000 km. Recent independent estimates suggested that melting extended to all depths in the upper mantle, transition zone, and possibly the lower mantle as well (e.g., Anderson, 1982; Walker, 1983; Herzberg and O'Hara, 1985; Ohtani et al., 1986; Scarfe and Takahashi, 1986; Ito and Takahashi, 1987; Herzberg, 1990).

To understand quantitatively the picture of melting in the early Earth, melting relations on appropriate compositions, such as peridotite, komatiite, and chondrite, are needed. In this respect, melting curves of minerals provide an important end-member reference frame that is essential for a comprehensive understanding of melting and crystallization behaviors in these chemically complex systems. Particularly, melting curves provide information on temperatures and compositions in multi-component systems. Furthermore, melting studies of simple compositions are also useful in evaluating thermochemical and thermophysical data of liquid phases along the melting curves. Such data are crucial for modeling of the early evolution of the Earth from magma ocean and for understanding magma generation and transportation in the upper mantle and transition zone.

The development of high pressure and high temperature techniques makes it possible to simulate the physical conditions of the Earth's interior. The uniaxial split-sphere multianvil apparatus (USSA-2000) at Stony Brook has capability to reach a maximum pressure of 26 GPa which corresponds to the depth of the uppermost lower mantle. Using a 10/5 sample assembly, a temperature of 2900 ^{o}C has been obtained in this study, which is the highest temperature ever reported using this technique and which makes it possible to melt mantle minerals at high pressures.

Through thermodynamic modeling all available physical and chemical information can be taken into account in assessing possible processes in the Earth's interior. In this regard, calorimetric measurements and independent determinations of physical properties of phases can be used to calculate phase equilibrium relations and compare them with high-pressure experimental studies. Ideally, the two sets of data should be consistent with one another. However, such comparisons are generally inconclusive because of uncertainties of calorimetric measurements, problems in pressure and temperature calibrations, and because of the lack of reversals in phase equilibrium studies. Therefore, a more practical approach is to evaluate the available thermochemical and thermophysical data using the constraints provided by the experimental phase equilibrium studies. The method will be particularly useful for silicate liquids because the relevant measurements are either fragmentary or have larger uncertainties.

In this research the melting relations of pyrope $Mg_3Al_2Si_3O_{12}$, SiO_2 polymorphs (coesite and stishovite), and brucite $Mg(OH)_2$ were experimentally determined

within the limit of high pressure apparatus at Stony Brook. The subsolidus phase transformation of SiO_2 polymorphs and dehydration of brucite are also examined. The specific motivations for the study include:

1. Aluminous garnet has been recently found on the liquidus of peridotitic and chondritic melts at pressures above 12 to 14 GPa (e.g., Takahashi and Scarfe,1985; Kato and Kumazawa,1986; Ohtani,1987; Ito and Takahashi, 1987; Herzberg et al., 1990). All these melting experiments indicate an increasing thermal stability of garnet and a change of liquidus phase from olivine to garnet at elevated pressure. On the other hand, the early studies on the melting of pyrope (Irifune and Ohtani, 1986) showed a dramatic decrease in dT/dP slope above 7 GPa and a considerably flat melting curve at higher pressures. We found that it is difficult to reconcile this melting curve with the studies in multicomponent systems. One major objective of this work is to experimentally examine if the reported flattening of pyrope melting curve at high pressures is real, or if it is a combined artifact of the experimental and the extrapolation methods used in previous investigation.

2. Jackson (1976) predicted that the melting curve of coesite had a temperature maximum around 8 GPa and a large negative slope at higher pressures. This melting relation has most recently received more attention because of the discovery of amorphization of quartz and coesite at room temperature and pressures of 25 to 30 GPa and 30 to 35 GPa, respectively (Hemley et al., 1988). By analogy with the amorphization of ice I at 77 K and 1 GPa (Mishima et al.,1984), the transformations of quartz-glass and coesite-glass have subsequently been interpreted in terms of the crossing of the

metastable negative extensions of their melting curves. In this regard, experimental constraint on the melting of coesite to the coesite-stishovite-liquid triple point becomes significant.

3. Melting temperature of stishovite has never been reported from a static experimental study. Using the shock wave data (e.g., Schmitt and Ahrens, 1989), it is possible to estimate a minimum constraint but with an uncertainty of 300-500 °C in temperature. Because of the expected very high melting point, the melting of stishovite has somehow become a technical target in laboratories.

4. The coesite-stishovite transformation boundary has been extensively used in laboratories for the pressure calibration at high temperatures. However, the boundary determined by previous studies up to 1400 °C and 9.6 GPa (Yagi and Akimoto,1976; Suito, 1977; Pacalo and Gasparik, 1990) may not be quite accurate in view of the inherent kinetic problems at low temperatures. As pointed out by Yagi and Akimoto (1976) from their in situ X-ray study, the transformation reaction at the phase boundary is very sluggish and coesite is metastably present within the stability field of stishovite. From consideration of kinetics, it is expected that determination of the phase boundary will be favored at higher temperatures.

5. The dehydration of brucite has become of interest recently because of the theoretical prediction that there exists a temperature maximum in the dehydration curve. At this point, it is believed that either an equation of state for water can be refined from data on brucite and periclase through thermodynamic

calculation (Johnson et al., 1991) or it can be actually obtained from the volumes of these two phases measured by in situ X-ray (Leinenweber et al., 1991). However, melting behavior of brucite has been completely ignored in all previous studies. One interesting thing observed on its analog, $Ca(OH)_2$, is that the dehydration of portlandite terminates at a pressure of about 100 bar with a melting curve rising from it (Wyllie and Tuttle,1960 and 1963; Irving et al., 1977). The major objectives of this work are to determine the melting curve of brucite at high pressures and to examine its relationship with the dehydration curve.

Details of the experimental techniques and procedures are described in Chapter 2. Equilibrium thermodynamics and relevant considerations used in the evaluation of the experimental data are discussed in Chapters 3. Experimental results, modellings and discussions of the data on pyrope, SiO_2 polymorphs, and brucite are, respectively, presented in Chapters 4, 5, and 6. Conclusions are given in the final Chapter along with discussions of the existing problems in this research and the suggested work for the future.

Chapter 2

Experimental Techniques and Procedures

2.1 High Pressure Apparatus

All experiments were carried out using a split-sphere multianvil apparatus (USSA-2000) located at Stony Brook. Detail of the technique has been given by Liebermann et al. (1985). The apparatus consists of a 2000-ton uniaxial press with a two-stage anvil system capable of achieving pressures as high as 26 GPa.The first-stage anvil system is a steel sphere split in six parts. The anvils are glued permanently into upper and lower guideblocks and enclose a cubic cavity, 60 mm on edge, which contains the second-stage anvil assembly. The second stage is assembled outside the press and consists of eight tungsten carbide cubes, 32 mm on edge, separated by pyrophyllite gaskets, teflon back-up gaskets and balsa wood spacers. The cubes are truncated at one corner and enclose an octahedral cavity that holds the sample assembly. The second stage is electrically insulated from the first stage by phenolic sheets. Electrical insulation between the adjacent cubes is provided by teflon tape.

2.2 High Pressure Sample Assembly

The sample assembly used in this study was described in detail by Gasparik (1989) and is shown in Figure 2.1. The diagram is a cross-section through a semisintered MgO octahedron with an edge length of 10 mm. Two types of the cube truncation edges, 4 and 5 mm, are used and are denoted, respectively, as

10/4 and 10/5 sample assemblies. Heating is provided by a lanthanum chromite sleeve with TZM (0.5% Ti + 0.1 %Zr +Mo) rings on both ends for better contact. The sample is placed in a rhenium capsule which is electrically insulated from the heater by an MgO sleeve. On average, the starting capsule volume is about 4 mm^3 (3 mm long x 1.3 mm diameter). The thermocouple was positioned axially and was in direct contact with the rhenium capsule. The wires are

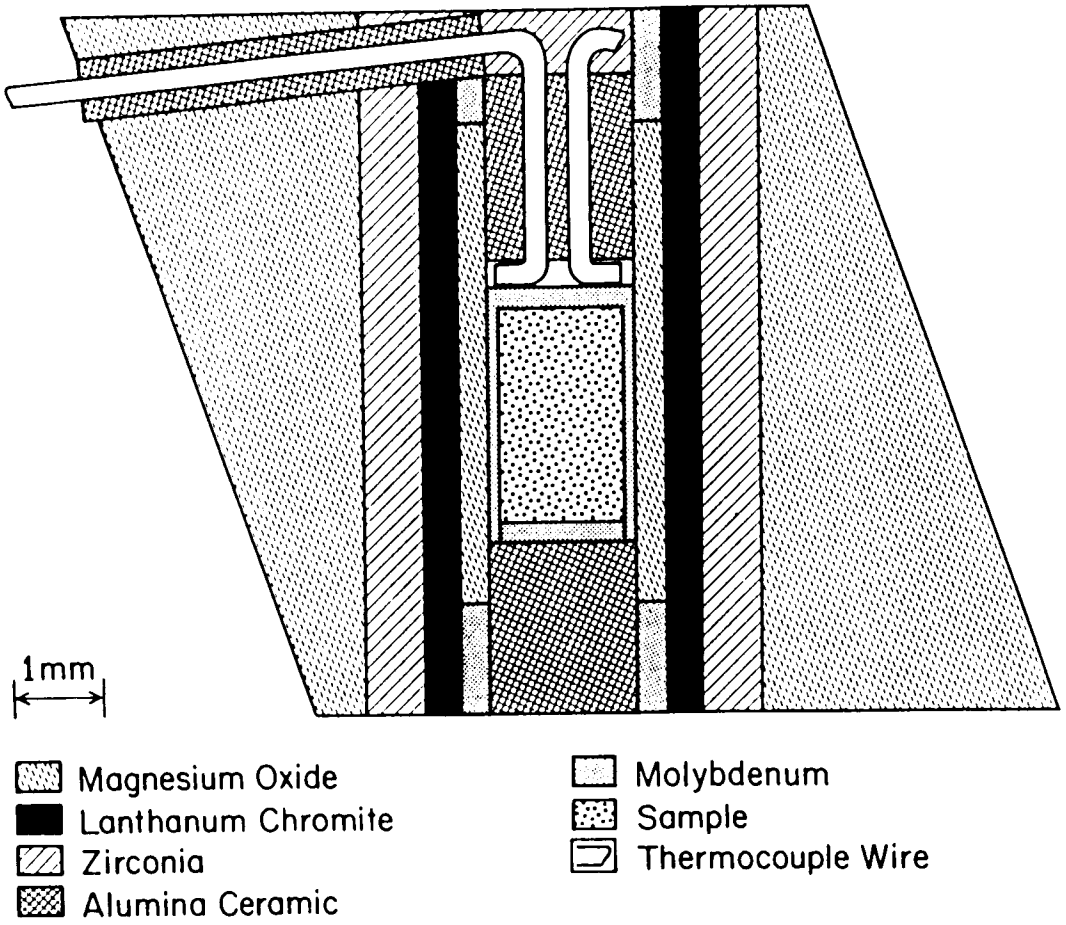

Figure 2.1 *The 10 mm sample assembly used in the experimental study.* After Gasparik (1989).

electrically insulated from the heater, TZM ring and tungsten carbide anvils with alumina ceramic tubes.

2.3 Pressure Calibration

The pressure calibrations for 10/5 and 10/4 sample assemblies at room and high temperature used in this study are the same as those carried out by Gasparik (1989, 1990), which are shown in Figure 2.2. These calibrations are based on the coesite-stishovite transition at 9.2 GPa and 9.6 GPa; the clinoenstatite to beta phase + stishovite transition at 16.5 GPa; forsterite to beta phase transition at 14.3 GPa and 15.2 GPa; beta phase + stishovite to ilmenite transition 17.5 GPa; majorite to ilmenite transition at 21.9 GPa, and majorite to perovskite trnasition 22.4 GPa. The 10/5 and 10/4 sample assemblies are able to reach the maximum pressures of 16.5 and 22.5 GPa, respectively. For these two configurations of the sample assemblies, a greater press load is generally required at high temperature to achieve a specific pressure than at room temperature. The sample pressures are reproducible to ±0.3 GPa.

2.4 Temperature Measurements

Temperature was monitored with a W3%Re/W25%Re thermocouple. In experiments performed at temperatures below 2400 °C, temperature was controlled to a few degrees within the set point by a Eurotherm controller. In experiments at higher temperatures, power was controlled manually, and the temperature was monitored by directly recording the thermocouple emf. The

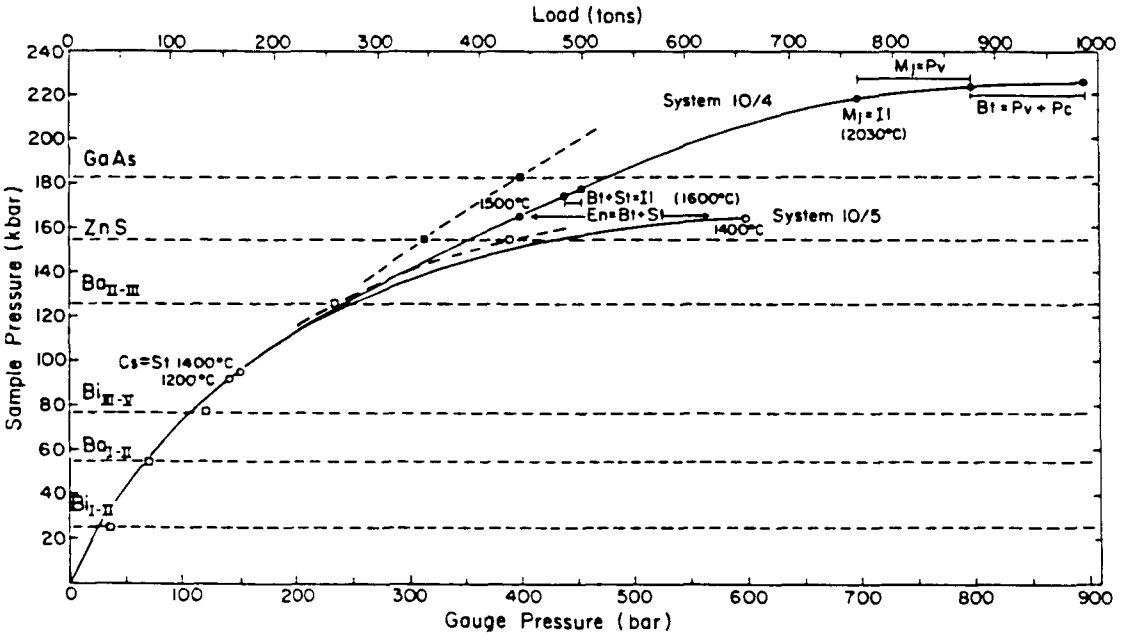

Figure 2.2 *Pressure calibrations of 10 mm sample assemblies at room temperature (dashed curve, calibrated only for 10/5 sample assembly) and high temperatures (solid curves). Open squares are the room-temperature calibration results obtained with the standard techniques by detecting the resistence change of calibrants shown on the left; Solid squares represent the results obtained using calibrants mixed with AgCl. Open and closed circles correspond, respectively, to the observations of the phase boundaries used for the high-temperature calibration for 10/5 and 10/4 sample assemblies. Cs = coesite; St = stishovite; En = enstatite; Bt = beta phase (modified spinel); il = ilmenite; Mj = majorite; Pv = perovskite; and Pc = periclase.*

present batch of thermocouple wires was calibrated by the manufacturer to 1800 °C; the emf-temperature relation was extrapolated to 2300 °C by the manufacturer and to 3000 °C by us using the calibration of Asamoto and Novak (1967) (Figure 2.3). No correction for the effect of pressure on thermocouple emf was applied.

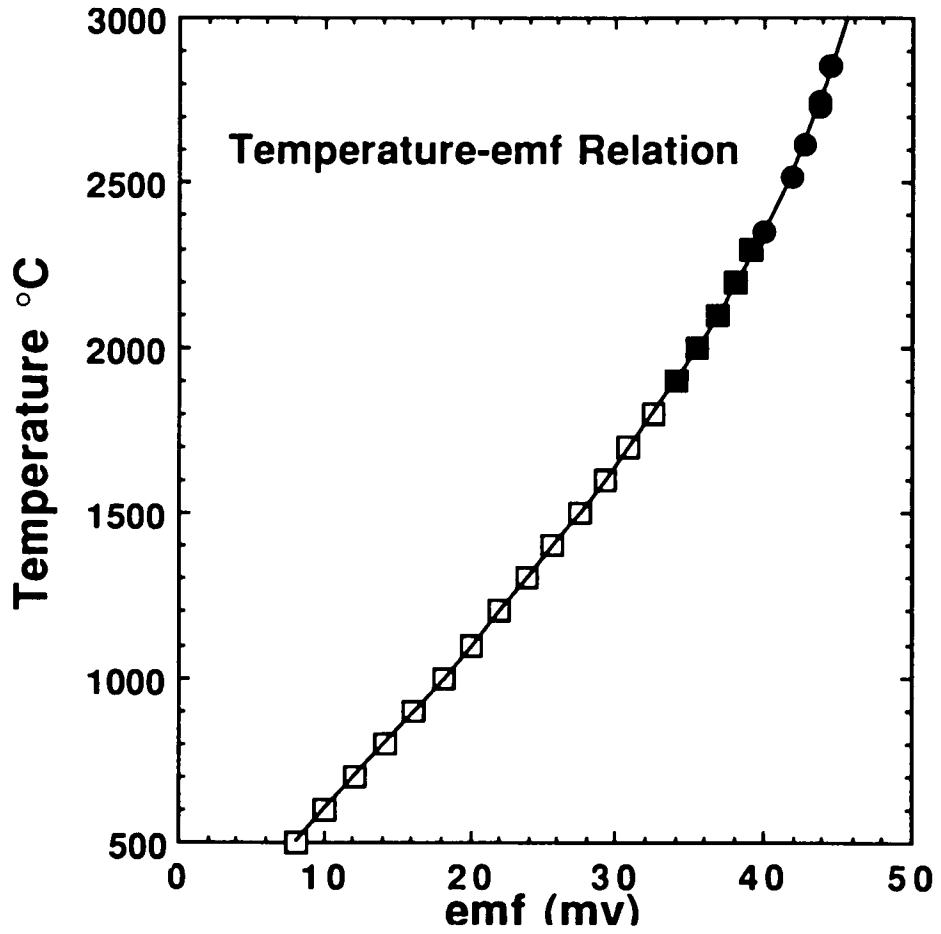

Figure 2.3 *Temperature - emf relationship for W3%ReM25%Re thermocouple calibrated and extrapolated by the manufacturer; and calibrated to 3000 °C by Asamoto and Novak (1967).*

An important temperature correction arises from the difference between the thermocouple junction (nominal temperature) and the hot spot (maximum temperature). The temperature distribution in the sample was estimated by Gasparik (1989) based on the solubility of enstatite in the diopsidic pyroxene coexisting with the enstatitic pyroxene and is illustrated in Figure 2.4a. The temperature increase from the center to the hotspot of the sample has generally been accepted and is approximately 50 °C. However, the temperature decrease from the center to the cold end of the sample (minimum temperature) has not been quite accurately determined, which is about 150 °C (Figure 2.4a) from Gasparik (1989) and 250 °C (Figure 2.4b) according to Presnall and Gasparik (1990). Since we did not study the detail of the temperature distributions in the high temperature range, the estimate from Gasparik (1989) has been adopted throughout the entire study. From the present experiments on the coesite-stishovite transition (see Chapter 5), it appears that the results are internally consistent with the 200 °C-temperature gradient of Figure 2.4a.

A minor difference can also be seen in Figures 2.4a and 2.4b in terms of the distribution of isotherms at the hot end. From the present melting experiments in a temperature range of 1000 to 2850 °C, it is found that the contour at the hot end at low temperatures may be different from that at high temperatures. The difference can be seen from Figures 5.2 and 6.2. in the following Chapters. Melting of brucite at 1200 °C always starts from the corner of the charge and forms two seperate loops, which are consistent with the configuration of Figure 2.4b; while the melting of coesite at 2800 °C indicates a flat temperature contour corresponding to Figure 2.4a.

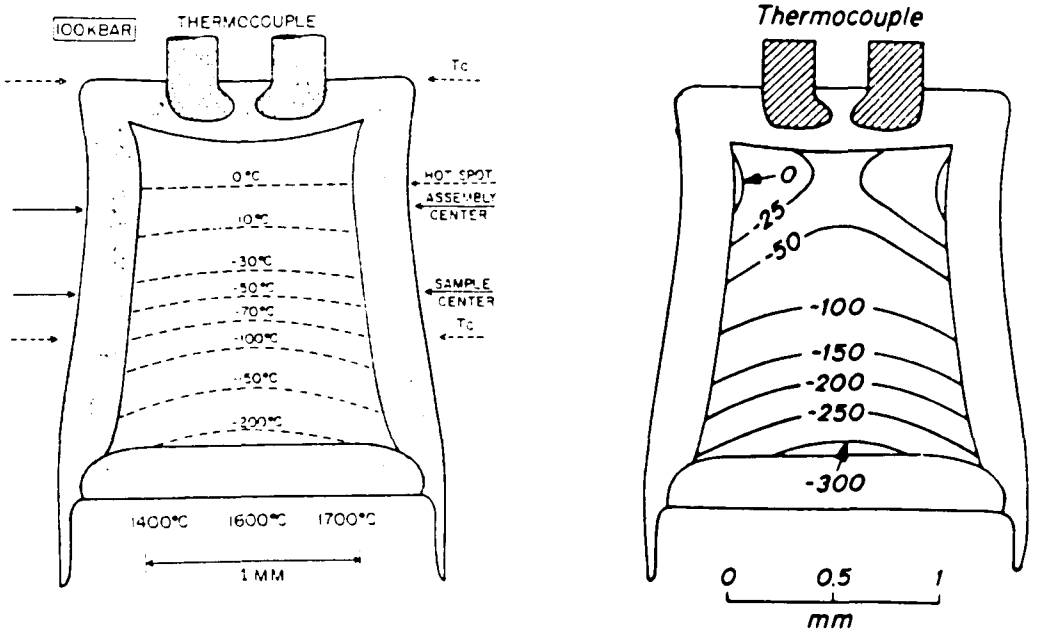

Figure 2.4 *Cross-section of an experimental charge in a 10 mm MgO sample assembly showing the temperature gradients. a) inferred from the enstatite-diopside data between 1400-1700 °C (Gasparik, 1989); and b) estimated from experiments on the melting of enstatite and forsterite-majorite eutectic between 2000 and 2150 °C (Presnail and Gasparik, 1990).*

The accurate measurement of temperature is attained by determining the location of the hot spot relative to the thermocouple junction, which has been discussed in detail by Herzberg et al. (1990). Error in temperature determination is estimated at ±30 °C if a phase boundary is located above the sample center. If a phase boundary is located below the sample center, the estimated temperature may present larger uncertainty, but may be well within ±75 °C

(Herzberg and Gasparik, 1991). Fortunately, it is worthwhile mentioning that, in all the experiments of this study, whether it is melting, phase transformation, or dehydration, only two experimental results (both on the coesite-stishovite transition) show the phase boundaries below the sample center, while all the others have the interfaces above the center and toward the hot spot.

2.5 Starting Materials

Starting material for the melting experiments of pyrope was synthesized from mixed powder of MgO, Al_2O_3, and SiO_2 according to pyrope stoichiometry at 5 GPa and 1400 °C for five hours using a girdle-anvil type high pressure apparatus. Optical observation indicated that the recovered sample consisted of more than 95% of pure pyrope and a small proportion of unreacted oxides (mostly of corundum). Microprobe analyses showed that in the middle of the sample were all clean pyrope (see Table 4.3), while the unreacted oxides were only observed at the very cold end of the sample because of the 200 °C-temperature gradient. Amorphous silica and reagent $Mg(OH)_2$ were used, respectively, for the melting and subsolidus experiments of SiO_2 polymorphs (coesite and stishovite) and brucite.

2.6 Anhydrous Experiments

Water is contained in the sample assembly as absorbed water along grain boundaries and as $Mg(OH)_2$, and is difficult to expel. In an attempt to ensure that all the data are anhydrous, the sample assembly is fired at 1100 °C for one and half hours. Firing is performed in an Argon atmosphere to prevent any

potential oxidation of parts in the assembly such as TZM rings and thermocouple wires. For the experiments on pyrope and silica, the sample capsule is enclosed in the assembly for firing immediately prior to running the experiments. For the experiments on brucite, the capsule is enclosed after the assembly is fired, and the entire assembly is stored in an oven of temperature of 110 °C for overnight prior to the experiment.

The following quenching method was utilized in all experiments. For each run, pressure was applied first, and temperature was then raised to the target value in a time period of 8 to 15 minutes by applying power to lanthanum chromite heater. In the experiments on the coesite-stishovite transition below 1400 °C, time to reach the target values is 3 to 4 minutes (for reasons, see Chapter 5). Although a run duration of 2 hours at 2400 °C is possible when a rhenium capsule is used (Presnall and Gasparik, 1990), the run time in this study is usually limited to ≤ 3 minutes for melting experiments on pyrope and to ≤ 20 minutes for the experiments on brucite to prevent potential power fluctuations and thermocouple contamination. Since all the melting experiments on coesite and stishovite are performed at extremely high temperatures, only several seconds of duration are allowed before the power shows fluctuations. Under this circumstance, quench has to be made to avoid ambiguity in temperature determination. However, for most compositions that have been studied above 2000 °C, the time required for a melt phase to form from crystalline material is about one second (Ohtani and Kumazawa, 1981; Herzberg et al., 1990). The experiment is terminated by shutting the power off, and the sample is able to cool to room temperature within one or two seconds.

2.7 Phase Identifications

The recovered capsule is cut along the cylindrical heater and half of it is prepared as a thin section for optical observation. Since all the experimental studies are on the simple composition, phase identification and determination of the presence or absence of melting can be basically carried out with the petrographic microscope. When melting happens, there usually exists a sharp boundary between the coexisting solid and liquid phases and the quench phase appears dark in color relative to the subsolidus one. Crystalline phases can be easily identified by their symmetry, birefringence, and sometimes by their refractory index and hardness reflected on the polished surface. The distinct features are summarized below.

Coesite has a low birefringence (i.e., 0.01), low interference colors, and grows as large prismatic crystals that exhibit inclined extinction because of their monoclinic symmetry. Stishovite is noticeably harder, has a high birefringence (i.e., 0.027), high interference colors, and grows as small equidimensional crystals. Brucite forms transparent plates with perfect basal cleavage. In contrast, periclase is characterized by its isotropic nature and high refractory index (n=1.73). Additionally, high hardness of periclase (H=5.5) is reflected in the polished surface of thin sections by rising high over brucite.

To confirm the optical observations on phase identifications and nature of melting, SEM, microprobe analysis, and Raman specstroscopy were used as necessary. SEM is very useful in determination of the nature of melting by examining the interface of the coexisted phases which is usually very sharp

in congruent melting; while the change from subsolidus phase(s) to a mixed liquid + crystal is gradual in incongruent melting. In microprobe analyses, pyrope always has a normal stoichiometry in the middle of the samples but sometimes slightly deficient in alumina content (about 0.65 wt.%) when they are very close to the melting interface (see Table 4.3). Brucite shows a MgO content of around 70 wt.% and periclase ranging from 95 to 100 wt.% (see Table 6.2). From Raman spectra (Figure 2.5), coesite shows strong Raman peak around 520 cm^{-1}, while stishovite around 750 cm^{-1}. Both spectra are considerably different from those obtained by Hemley et al. (1986) on silica

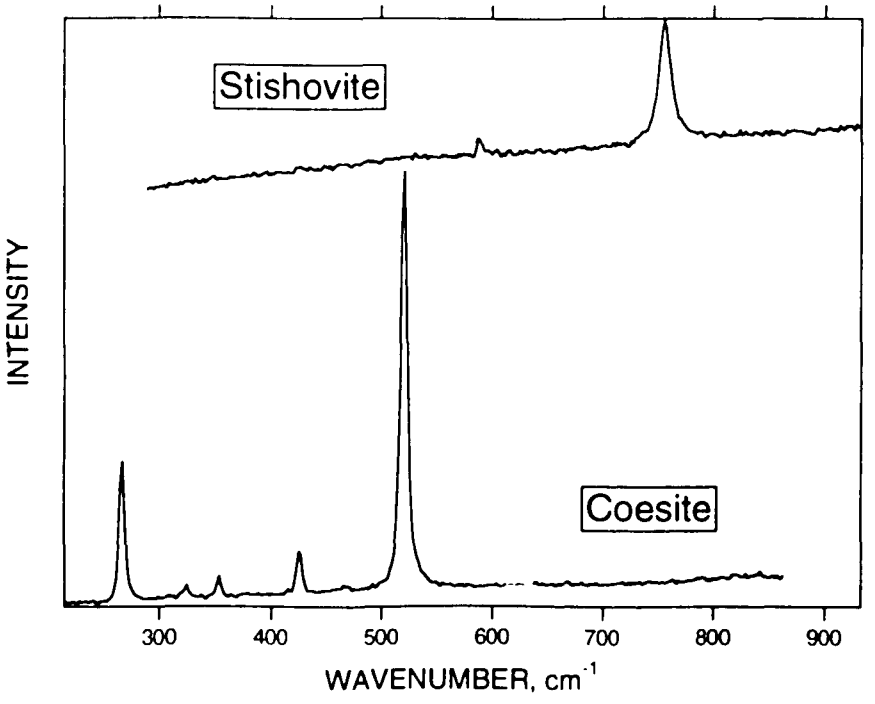

Figure 2.5 *Representative Raman spectra of coesite and stishovite obtained from experiments at 13.5 to 14 GPa and 2750 °C to 2850 °C.*

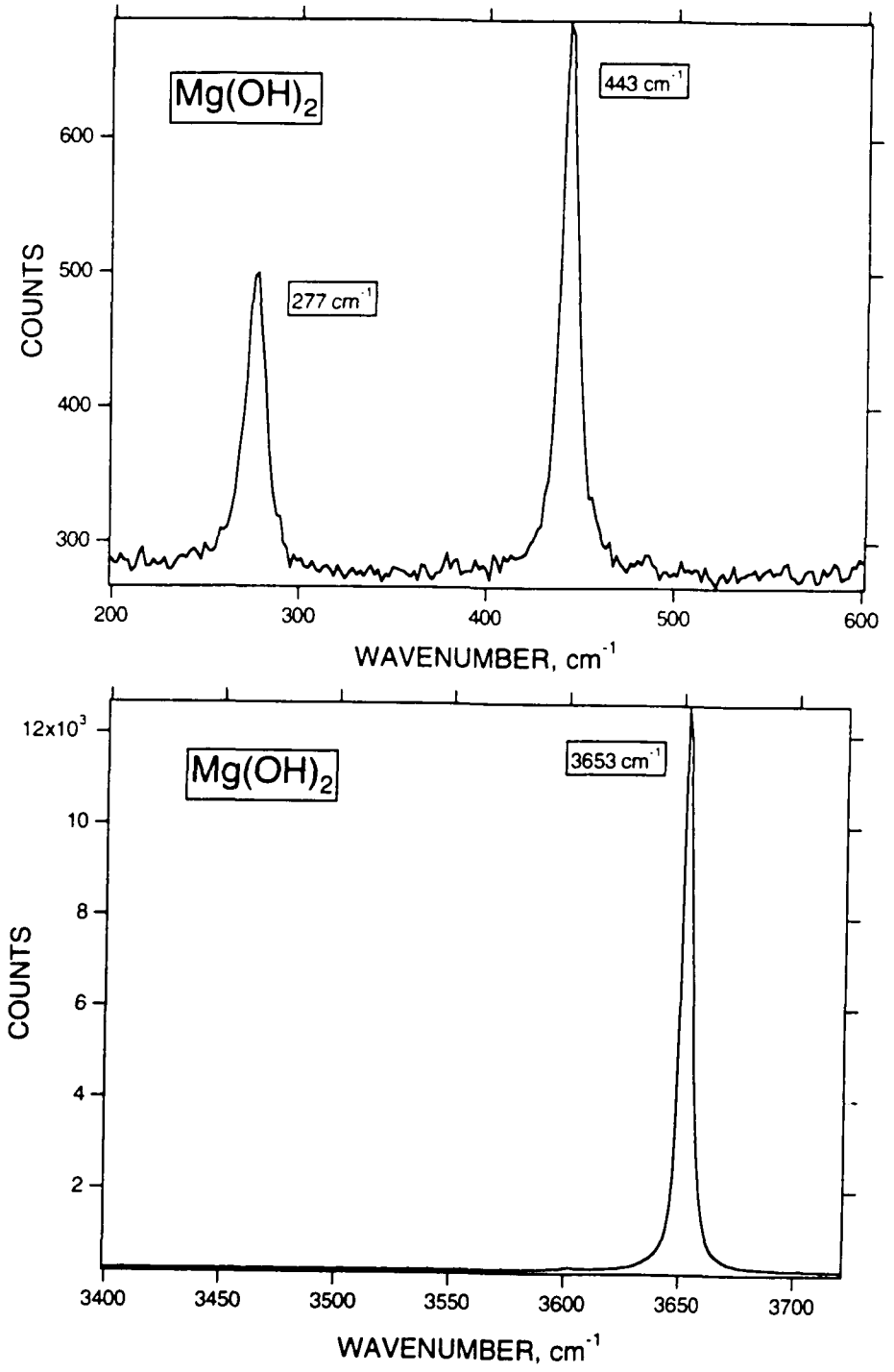

Figure 2.6 *Representative Raman spectra of brucite obtained from experiment at 10 GPa and 1200 °C.*

glass using the same technique. Brucite shows a sharp Raman absorption at 3653 cm^{-1} (Figure 2.6) that is generally assigned to the crystallographically bonded OH stretching for hydrous minerals (McMillan, 1989). It also has sharp Raman absorptions at 277 and 443 cm^{-1} (Figure 2.6), but these two peaks have not been properly interpreted in terms of their structural assignment (Mysen, personal communication). On the other hand, no Raman peaks was detected on periclase. Free water behaves differently from crystallographically bonded OH by showing a wide band of Raman shift between 3300 and 3700 cm^{-1} (McMillan, 1989).

Chapter 3

Thermodynamical Considerations

3.1 Gibbs Free Energy

The free energy of a reaction at high pressure and temperature is given by

$$\Delta G(P,T) = \Delta H^{o}_{T} - T\Delta S^{o}_{T} + \int_{1}^{P} \Delta V(P,T)dP$$

where ΔH^{o}_{T} and ΔS^{o}_{T} are the standard enthalpy and entropy of a reaction, respectively, at temperature T and 1 atm. They are given by

$$\Delta H^{o}_{T} = \Delta H^{o}_{298} + \int_{298}^{T} \Delta C_P dT$$

and

$$\Delta S^{o}_{T} = \Delta S^{o}_{298} + \int_{298}^{T} \frac{\Delta C_P}{T} dT$$

where ΔH^{o}_{298} and ΔS^{o}_{298} are the standard enthalpy and entropy of reaction at 298.15 K, ΔC_p is the heat capacity difference between products and reactants, and $\Delta V(P,T)$ is the volume change for the reaction.

The extrapolation of temperature and pressure dependence of the Gibbs free

energy of a solid or a liquid phase to high temperature and pressure is complicated by the nature of the heat capacity, C_p, and the behavior of molar volume, V(P,T). In order to obtain a suitable form of the Gibbs free energy at high pressure and high temperature, it is necessary to discuss the heat capacity at high temperature and the equation of state in detail.

3.2. Heat Capacity at High Temperature

The form of the heat capacity for high temperature extrapolation has been discussed by Haas and Fisher (1976), Lane and Ganguly (1980), Holland (1981), Berman and Brown (1985), Fei and Saxena (1987), and Richet and Fiquet (1991). Many different polynomials have been used in literature for fitting the measured heat capacity data. Application of these extrapolation at high temperature must be careful, because some of them are suitable only to a certain temperature range (e.g., Berman and Brown, 1985).

Recently, Saxena (1988) and Saxena and Zhang (1989) adopted another approach to extrapolate the measured heat capacity data by considering the following thermodynamic identity:

$$C_p = C_V + \alpha^2 V K_T T$$

where C_p and C_v are, respectively, heat capacities at constant pressure and constant volume; V is the molar volume at a temperature T, and α isobaric thermal expansion and K_T the isothermal bulk modulus.

Although the above equation is given in many books, no specific attention has been paid to the use of this relationship in data systematics. It was shown that the internal consistency of these data can be obtained through non-linear programming (Saxena, 1988; Saxena and Zhang, 1989), if C_p is available in certain temperature range and if the molar volume, thermal expansion and bulk modulus are known at 298 K. For most of the geologically interested materials, these data are generally available (e.g., Robie et al., 1978; Carmichael, 1982).

The following equations have been found useful to extrapolate the relevant parameters to high temperatures:

$$C_v = C_o + C_1 T^{-2} + C_2 T^{-4} + C_3 T^{-6} + \ldots$$

$$\alpha = \alpha_o + \alpha_1 T + \alpha_2 T^{-1} + \alpha_3 T^{-2}$$

$$K_T = 1/(\beta_o + \beta_1 T + \beta_2 T^2 + \beta_3 T^3)$$

where $C_o = 3Rn$, R is the gas constant, n the number of atoms in the chemical formula of one mole of the solid; C_i, α_i and β_i are the coefficients to be determined in the optimization procedure.

The choice of a suitable polynomial expression for C_v is the most difficult. The form given above follows the Debye heat capacity equation with the integral evaluated for moderate and high temperatures. However, it is not generally applicable at low temperatures. For example, the C_v equation will fail completely below a temperature of about 0.1θ (where θ is the Debye

temperature) for many solids.

For a Debye solid, the low-temperature limit for C_V is the "Debye T^3" law, that is, the temperature dependence is expressed in the form $C_V=A(T/\theta)^3$, where A is a constant. At high temperature as θ/T approaches unity, C_v approaches a constant value of 3Rn. For a non-Debye solid the departure of C_V from this model is commonly expressed by calculating θ_{cal} a number which varies with temperature and replaces θ in the original Debye C_v equation. By plotting θ_{cal} against temperature for a number of oxides and silicates, Kieffer (1979) showed that, for most oxides and silicates, the variation of θcal with temperature is linear at temperatures above 60 K, indicating that C_v must vary smoothly with temperature. It is assumed that our C_v equation is suitable in this consideration.

By considering the C_v - C_p relation, the variations of thermal expansion and bulk modulus will be constrained by the difference of these two heat capacities. For extrapolations beyond the melting temperature, it is important that our optimized C_p of the solid are such that above the melting temperature the C_p of the fictive solid should not exceed the C_p of the liquid. This constraint would ensure that in the phase equilibrium calculation the solid does not become stable at 1 bar above the temperature of melting. Although heat capacities for most of silicate liquids are not available, they can be reasonably estimated from the partial molar heat capacities of their oxide components, which will be discussed in detail later.

A non-linear program called MINUIT was used for the optimization. Detail

Table 3.1 Thermodynamic Data on MgO

T	C_p(E)	C_p(C)	C_v(C)	α(E)	α (C)	K_T(E)	K_T(C)	αK_T(C)
K	J mol^{-1}K^{-1}			10^6		(GPa)		
300	37.78	37.67	37.14	31.20	31.24	160.7	160.7	50.21
400	42.45	43-60	42.68	35.80	35.82	157.9	157.9	56.59
500	45.42	46.26	44.97	38.40	38.36	155.1	155.2	59.54
600	47.36	47.73	46.06	40.21	40.11	152.2	152.3	61.10
700	48.74	48.70	46.65	41.59	41.48	149.4	149.4	61.97
800	49.78	49.45	47.00	42.71	42.64	146.5	146.5	62.45
900	50.59	50.07	47.23	43.69	43.69	143.6	143.5	62.68
1000	51.23	50.64	47.39	44.61	44.66	140.7	140.5	62.73
1200	52.19	51.66	47.59	46.37	46.48	134.8	134.4	62.48
1400	52.85	52.63	47.71	48.10	48.21	128.8	128.4	61.91
1600	53.32	53.59	47.78	49.90	49.88	122.7	122.5	61.12
1800	53.66	54.55	47.83	51.69	51.53	116.6	116.8	60.21
2000		55.52	47.87		53.16		111.4	59.23
2500		58.10	47.92		57.18		99.7	56.98
3000		61.14	47.95		61.17		91.4	55.88

E = Experimental Data; C = Calculated Data;

The experimental data on α and K_T are from Anderson and Zou (1989), and C_p from Robie et al., (1978).

of the method has been discussed by James and Roos (1975) and by Saxena (1988). A favorable situation in such an approach is that the input data on

C_p, thermal expansion and bulk modulus are known in certain temperature ranges. As has been well known, it is possible to have various temperature polynomials fitting the experimental data with similar precision but with very different extrapolated data. Since in the range of extrapolation the main concern is the reference state for high pressure phase equilibrium calculation, it is proposed to use the Anderson-constraint that the product αK_T shows only a small variation with T at high temperature (Anderson and Zou, 1989), which is basically true for MgO as shown in Table 3.1. Practically, this can be achieved by a method of trial and error when few data are available on α and K_T. If this constraint is accepted, it will be very useful in the data extrapolation beyond the melting temperatures of solids.

Taking MgO as an example, the fitted equations to the experimental data on α and K_T are given by:

$$\alpha = 0.3754E\text{-}4 + 0.7907E\text{-}8T - 0.7836E\text{-}2T^{-1} + 0.9148T^{-2}$$

$$K_T = 1/(0.5951\ E\text{-}6 + 0.8233E\text{-}10T + 0.3264E\text{-}13T^2 + 0.1018E\text{-}17T^3)$$

The same extrapolation procedure has been applied to pyrope and brucite for thermodynamic considerations in the following Chapters. Since stishovite is involved in several other reactions in the system MgO - SiO_2, the extrapolated data on coesite and stishovite by Fei et al. (1990) are adopted for sake of the internal consistency. For convenience of phase equilibrium computation, C_p data calculated from the optimized C_v, α and K_T are refitted with a temperature polynomial of the form:

$$Cp = a + bT + cT^{-2} + eT^{-3} + gT^{-1}$$

making sure there is no loss of accuracy in the refitting procedure.

3.3. Equation of State at High Temperature

The contribution of $\int VdP$ to Gibbs free energy becomes significant at high pressure. Therefore, the use of a suitable equation of state at high pressure and temperature is necessary for phase equilibrium calculation. Experimental data on molar volumes are available either at high pressure and room temperature or at high temperature and 1 atm. The molar volume at high temperatures can be calculated from thermal expansion data obtained from C_p-C_v optimization using the equation:

$$V(1,T) = V_{298}[\exp(\int_{298}^{T} \alpha dT)]$$

The Murnaghan equation of state, which is based on the assumption that the bulk modulus changes linearly with pressure, is given by

$$P_M = \frac{K_{T,0}}{K'_{T,0}}\left[\left(\frac{V^o}{V}\right)^{K'_{T,0}} - 1\right]$$

The Birch-Murnaghan equation of state, which is based on the finite-strain theory, is expressed as

$$P_{B\text{-}M} = \frac{3}{2}K'_{T,0}\left[\left(\frac{V^o}{V}\right)^{\frac{7}{3}} - \left(\frac{V^o}{V}\right)^{\frac{5}{3}}\right]\left\{1 - \frac{3}{4}(4 - K_{T,0})\left[\left(\frac{V^o}{V}\right)^{\frac{2}{3}} - 1\right] + \ldots\right\}$$

where $K_{T,0}$ and $K_{T,0}' = ([\partial K_T/\partial P]_T)$ are the isothermal bulk modulus and its pressure derivative at 298 K, respectively. Very often, this equation is truncated after $[(V^o/V)^{2/3} - 1]$ term, which yields the so-called third order Birch-Murnaghan equation. As discussed by Jeanioz and Knittle (1986), the Birch-Murnaghan equation of state is considered a better expression than the Murnaghan equation of state for the pressure-volume relation at very high pressures.

The method of extrapolation of the existing data to high P-T space is still controversial. Anderson and Zou (1989) and Heinz and Jeanloz (1984) have expounded on the relationships among the various thermochemical and thermophysical variables. In Anderson and Zou's (1989) model, the simultaneous effect of pressure and temperature on volume is taken care of by the thermal pressure (P_{th}), i.e.

$$P = P_{B\text{-}M} + P_{th}$$

where P_{th} is calculated by

$$P_{th} = \int_{298}^{T} \alpha K_T dT$$

The calculation of thermal pressure has been simplified by assuming the product of αK_T is constant.

In this study, the third order Birch-Murnaghan equation of state is adopted to calculate $\int VdP$ but was modified in several aspects to consider the effect of

temperature on the molar volume (Saxena and Zhang, 1990):

i) the temperature dependence of the isothermal bulk modulus is included;

ii) V(1,298)/V(P,T) is replaced by V(1,T)/V(P,T); and

iii) K_T' is considered as a function of temperature as well in some cases when the calculated P - V relations at different temperatures are found crossover, and is expressed by $K_T' = K_{298}' + K_1' \ln(T/298)$, where K_1' is an empirical constant and can be estimated from phase equilibria or from shock wave pressure-volume relation (see Saxena and Zhang, 1990).

For computational convenience $\int PdV$ is calculated from the third order Birch-Murnaghan equation, instead of from $\int VdP$. The relation between $\int PdV$ and $\int VdP$ is given by

$$\int_1^P VdP = \int_{V(P,T)}^{V(1,T)} PdV + V(P - 1)$$

where

$$\int_{V(P,T)}^{V(1,T)} PdV = \frac{3}{2}K_T V(1,T)\{\frac{3}{4}(1+2X)[Y^{4/3} - 1] - \frac{3}{2}(1+X)[Y^{2/3} - 1] - \frac{1}{2}X[Y^2 - 1]\}$$

where

$$X = \frac{3}{4}[4 - (\frac{\partial K_T}{\partial P})_T]$$

and

$Y = V(1,T)/V(P,T)$

The temperature dependence of the bulk modulus accounts for part of the simultaneous effect of pressure and temperature on volume. The calculated results for MgO are close to that calculated by Anderson and Zou's thermal pressure model (Figure 3.1). However, the traditional method, in which the temperature dependence of the isothermal bulk modulus is not included, results in a significant overestimation of volume at high pressure and high temperature (Figure 3.1). This modification dose not significantly affect the phase equilibrium calculation where the phases in the reaction have similar thermal expansion and compressibility because only the volume change is concerned in the calculation, but it may play an important role in the reaction where the phases involved have very different thermophysical behavior. For example, in a melting reaction liquid generally has a much larger compressibility and a much smaller thermal expansion than solid.

3.4 Thermodynamic properties of silicate liquids

The direct measurements of thermodynamic properties on silicate liquids of compositions such as forsterite, enstatite, pyrope and silica are generally missing because of their high melting temperatures. However, the relevant data such as heat capacity, molar volume, compressibility, and thermal expansion can be approximately calculated from the partial molar properties of their respective oxide components. From a large quantity of measurements on enthalpies (e.g., Richet and Bottinga, 1984,1985; Stebbins et al., 1984), densities (e.g, Bottinga and Weill, 1970; Nelson and Carmichael, 1979; Lange

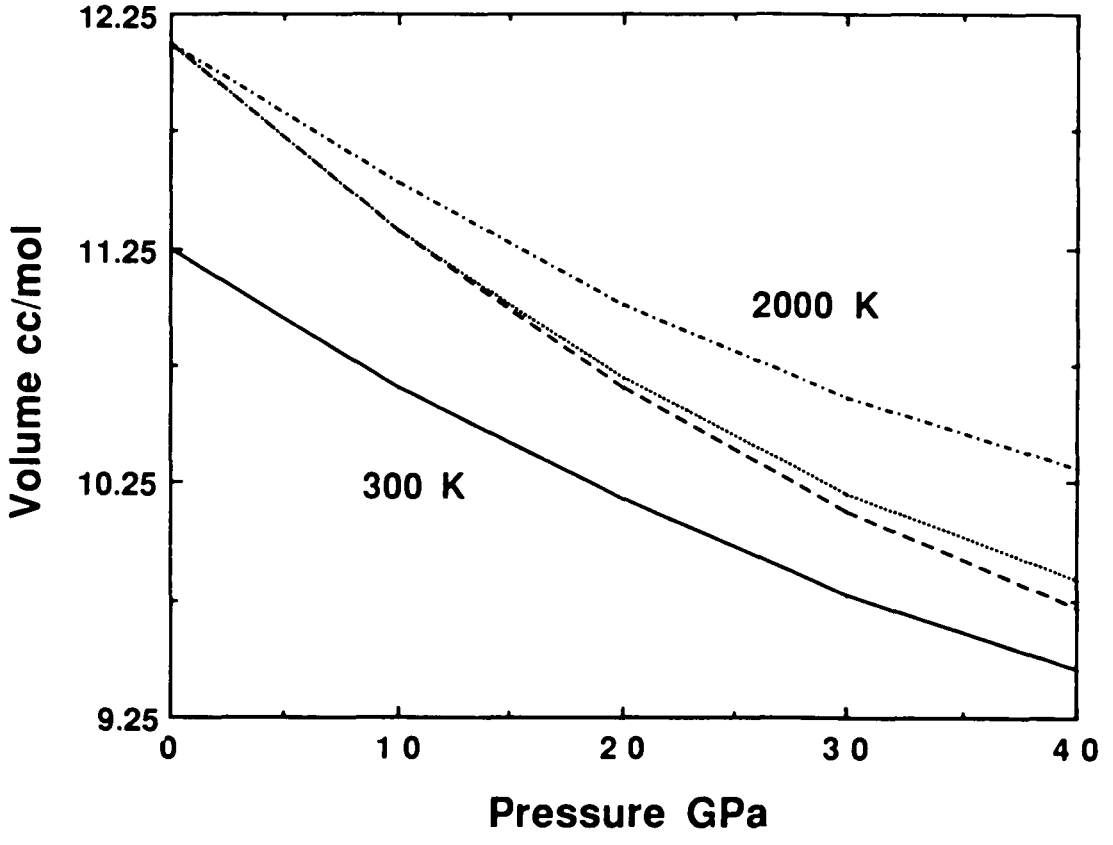

Figure 3. 1 *P- V- T relations of MgO calculated using different models at room and high temperatures. Solid curve: at 300 K. Dashed curve: this study; Dotted curve: Anderson and Zou's (1989) model; Dotted dash curve: using constant* K_T.

and Carmichael, 1987), and ultrasonic velocities (e.g., Rivers and Carmichael, 1987) for silicate liquids in the multicomponent system such as K_2O-Na_2O-CaO-MgO-FeO-Fe_2O_3-Al_2O_3-TiO_2-SiO_2, the partial molar properties of the oxide

components have been derived by aforementioned authors. In this regard, a simple ideal mixing model of the form:

$$M = \Sigma X_i M_i$$

is usually adopted, where M could be heat capacity, molar volume, thermal expansion or compressibility; M_i are the partial molar properties of the respective oxide components; X_i are the mole fractions in the calculations of heat capacity, molar volume and thermal expansion, and are the volume fractions in the calculations of compressibility.

3.5 Fugacity of H_2O

Many attempts have been made to model the equation of state for water (Helgeson and Kirkham, 1974; Holloway, 1977; Delany and Helgeson, 1978; Kerrick and Jacobs; Halbach and Chartterjee, 1982; Saxena and Fei, 1987). Data obtained by Halbach and Chatterjee (1982) using modified Redlich-Kwong equation and by Saxena and Fei (1987) using corresponding state equation in the virial format were generally adopted in calculations of reactions involving H_2O and in the modeling of multicomponent mixing of fluids (e.g., Kerrick and Jacobs, 1981; Saxena and Fei, 1988).

The fugacity of H_2O used in this study is from Saxena and Fei (1987a,b). In their computation, the compressibility "Z", a factor describing the deviation of a real gas from ideal behavior, was expressed as a polynomial of virial format in reduced pressure and temperature:

$$Z(P,T) = PV/RT = A + BP + CP^2 + DP^3 + ...$$

where A, B, C and D are coefficients that are dependent on temperature only.

Although it is contended that the virial equations of state are not useful at high pressures, especially at pressures near or above the critical pressure, Saxena and Fei (1987a, b) noted that the above polynomial could be used for generating an equation empirically, applicable particularly at high pressure - temperature ranges.

The constants in the above polynomial, obtained through regression analysis of the P-V-T data, are useful in computation of fugacity of pure gases from the following relation:

$$RTlnf(P,T) = RTlnf(1\ Kbar,T) + RT(Z_1/PdP + Z_2/PdP)$$

An expression for water fugacity at 1 Kbar that reproduces the data of Burnham et al. (1969), Halbach and Chartterjee (1982) and Haar et al. (1984) is given by:

$$RTlnf(1\ Kbar,T)=1000(-222.943+2.9865E\text{-}2T+35.9794lnT)$$

For pressures between 1 and 5 Kbar:

$$Z_1 = A + BP + CP^2$$

where

$A = -7.025E\text{-}1 + 1.1\ 60E\text{-}3T + 9.968E\text{+}I\ T^{-1}$

$B = 2.143E\text{-}1\ T^{-1} - 3.142E\text{-}1\ 4T^{3}$

$C = -2.249E\text{-}6T^{-1} - 1.459E\text{-}1\ T^{-3} + 2.169E\text{-}1\ 5T^{2}$

Above 5 Kbar,

$Z_2 = A + BP + CP^2 + DP^3$

where

$A = 1.4937 - 1.8626T^{-2} + 0.8000T^{-3} - 0.3941\ T$

$B = 4.2410E\text{-}2T^{-1} + 2.4097E\text{-}2T^{-2} - 8.9634E\text{-}3T^{-3}$

$C = -9.016E\text{-}7T^{-1} - 6.1345E\text{-}5T^{-2} + 2.2380E\text{-}5T^{-3} + 5.2335E\text{-}7\ln T$

$D = -7.6707E\text{-}9T^{-1} + 4.1108E\text{-}8T^{-2} - 1.4798E\text{-}8T^{-3} - 6.3033E\text{-}21T^{3}$

Chapter 4

Melting of Pyrope $Mg_3Al_2Si_3O_{12}$

4.1 Experimental Results

Experimental data were obtained at 10 to 16 GPa and 2050 to 2500 °C. The results are listed in Table 4.1 and illustrated in Figure 4.1 together with the earlier studies up to 10 GPa. Consistent with the previous studies between 3.5 and 7 GPa (Boyd and England, 1962; Irifune and Ohtani, 1986), pyrope melted congruently and liquid was quenched to the fine-grained crystalline pyrope. In contrast, pyrope melted incongruently to liquid plus spinel or aluminous enstatite below 3.5 GPa (Boyd and England, 1962).

Microprobe analyses of the present experiment at 13 GPa and 2300 °C are shown in Table 4.2. From these analyses it is clear that the half way to the cold end of the sample are all clean pyrope although the unreacted oxide spots (mostly of corundum) are observed optically and by SEM at the very cold end of the sample. For some unknown reasons pyropes that are just below the melting boundary are slightly defficient in the average content of Al_2O_3 but no corundum was observed. No rhenium is detected in the sample.

At 10 GPa the melting temperature of pyrope from this study was in excellent agreement with those determined by Irifune and Ohtani (1986). However, at higher pressures, the melting temperatures we found were 200 to 300 °C

higher than those extrapolated by Irifune and Ohtani (1986), who fitted their experimental data between 7 and 10 GPa to the Kraut-Kennedy.

Table 4.1 Experimental Results on the Melting of Pyrope

Run No.	P (Kbar)	emf (mV)	T (°C)	Time (Min.)	Phases
1057	100	36.76	2100	3.0	Py, Q-Py
1081	100	35.90	2050	3.0	Py
1094	130	36.60	2100	0.5	Py
1132	130	38.20	2200	1.0	Py
1137	160	37.73	2200	3.0	Py
1142	130	37.60	2190	3.0	Py
1145	160	38.90	2300	3.0	Py
1159	130	38.95	2300	3.0	Py, Q-Py
1169	160	40.10	2380	1.0	Py
1248	115	37.20	2150	3.0	Py
1251	145	38.65	2280	1.0	Py
1280*	145	38.90	2300	5 hr	Py
1328	160	41.50	2500	3.0	Py, Q-Py

Py = Stable pyrope; Q-Py = Pyrope quench ed from liquid

** Synthesis of pyrope for 5 hours.*

Within 3.5 and 16 GPa range, melting of pyrope has an initial melting slope of 82 °C/GPa (Boyd and England, 1962; Irifune and Ohtani, 1986). The slope

decreases with increasing pressure to about 20 °C/GPa at 9.0 to 10 GPa (Irifune and Ohtani, 1986). Between 10 and 16 GPa, our melting data indicate a slope that is 67 °C/GPA. Such anomalous melting behavior by showing a dramatic increase in the slope is substantially different from the Irifune and

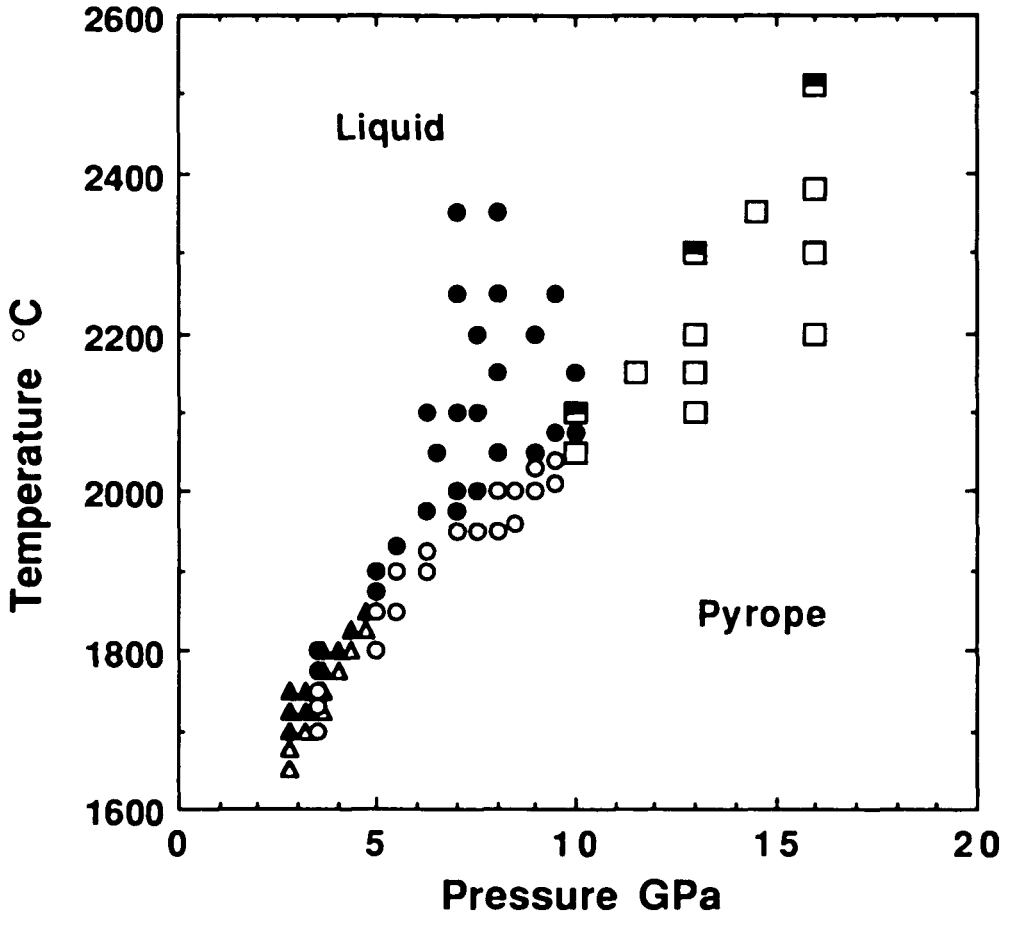

Figure 4.1 *Experimental results on the melting of pyrope. Triangles are from Boyd and England (1962); circles are from Irifune and Ohtani (1986); and squares are from this study; Open symbols are for solid and closed symbols for liquid.*

Ohtani's (1986) extrapolation and has not been observed in other mantle minerals such as forsterite (Ohtani and Kumazawa, 1981) and enstatite (Presnall and Gasparik, 1990) in the comparable pressure range (Figure 4.2). An increased melting slope has been reported on $(Mg_{0.9}Fe_{0.1})SiO_3$ perovskite but was observed above 60 GPa (Heinz and Jeanloz, 1987; Knittle and Jeanloz, 1989).

Table 4.2 Chemical compositions of pyrope from the experiment at 13 GPa and 2300 °C

Analysis #	SiO_2	Al_2O_3	MgO	CaO	FeO	Total
1	44.83	24.19	30.83	0.03	0.04	99.11
2	45.22	24.05	30.12	0.07	0.00	99.45
3	44.71	24.66	29.61	0.08	0.00	99.06
4	44.85	24.85	30.41	0.07	0.00	100.17
5	44.86	24.31	30.25	0.08	0.00	99.50
6	44.24	25.15	29.98	0.04	0.01	99.43
7	44.90	24.17	29.67	0.06	0.00	98.80
8	45.01	24.71	29.89	0.08	0.01	99.70
9	45.37	24.60	29.54	0.06	0.00	99.57
10	45.31	24.33	29.93	0.06	0.05	99.67
11	44.62	24.90	29.64	0.02	0.01	99.19
12	44.62	24.83	30.15	0.08	0.01	99.70
13	44.17	24.20	30.39	0.05	0.00	98.80
14	44.83	24.45	30.13	0.03	0.05	99.49
15	44.51	24.11	30.27	0.06	0.00	98.96
16	44.54	25.17	29.75	0.05	0.05	99.56
17	45.34	24.82	29.47	0.01	0.01	99.65
18	44.22	24.78	29.98	0.06	0.02	99.06
19	44.24	24.53	29.55	0.07	0.05	98.44
20	44.94	25.36	29.83	0.04	0.01	100.18
21	45.35	23.94	30.20	0.06	0.03	99.59

22	44.11	24.72	29.85	0.04	0.02	98.74
Average	44.76	24.58	29.97	0.055	0.017	99.36
23	45.62	24.21	29.96	0.05	0.00	99.85
24	44.97	25.31	30.05	0.03	0.08	100.44
25	45.42	24.99	30.10	0.06	0.04	100.61
26	44.90	25.72	29.73	0.04	0.03	100.42
27	45.31	25.36	29.82	0.04	0.00	100.52
28	45.29	24.93	30.11	0.05	0.03	100.42
29	45.23	25.45	29.57	0.03	0.02	100.30
30	46.66	24.85	29.58	0.06	0.00	101.14
31	45.28	25.40	30.11	0.00	0.01	100.80
32	45.13	25.55	29.51	0.05	0.04	100.29
33	45.84	25.43	29.62	0.04	0.02	100.94
Average	45.43	25.20	29.83	0.04	0.025	100.52

Notes: Analyses 1 to 22 are 50 to 100 micrometers below the liquid-pyrope interface; Analyses 23 to 33 are half way (about 1 mm) to the cold end of the sample.

From experimental studies in other systems, Gasparik (1990) and Herzberg et al. (1990) pointed out that a thermocouple entering through the side of an assembly, which was adopted by Irifune and Ohtani (1986), will generally read the melting temperatures at least 100 °C lower than that positioned axially. However, if such a difference does exist, it can only change the absolute values of temperature systematically while the melting slope will not be disturbed. In fact, at 10 GPa our melting temperature is only slightly higher than those of Irifune and Ohtani (1986). At 15 GPa the melting temperature obtained in Ito's laboratory at Misasa is 2350 °C (personal communication).

Underestimation of pressure is not possible. Using the same sample assembly and calibration scale at Stony Brook, melting curves of enstatite and coesite were observed to have slopes that decreased gradually with pressure (Presnall and Gasparik, 1990; Zhang et al., 1992; see Chapter 5). These results

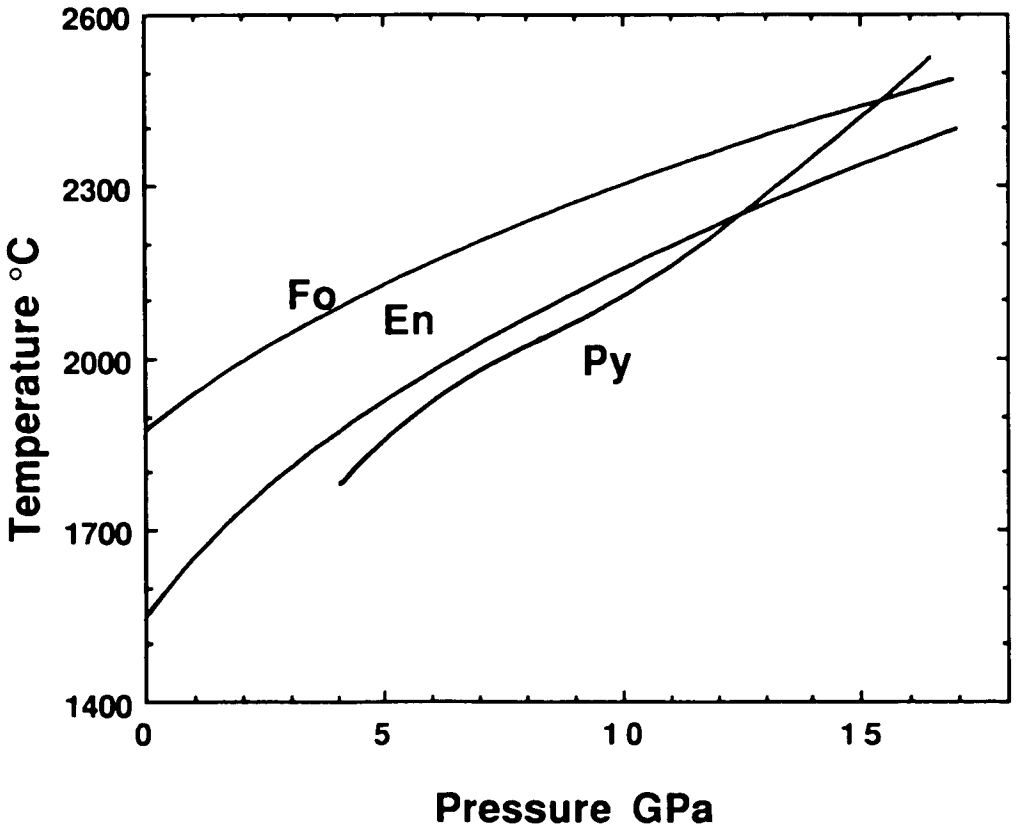

Figure 4.2 *Melting curves of the mantle silicates. Fo= orsterite (Davis and England, 1964; Ohtani and Kumazawa,1981); En=enstatite (Boyd et al, 1964; Presnaill and Gasparik, 1989); Py=pyrope (Boyd and England, 1962; Irifune and Ohtani, 1986; and this study).*

were also consistent with the previous studies (e.g., Boyd et al., 1964; Kanzaki, 1990). When all the information above is taken into account, it is unlikely that the anomalous melting behavior of pyrope above 10 GPa is an artifact of different experimental techniques. Instead, it may provide significant information on the physical changes of either crystalline pyrope or the coexisting liquid.

Table 4.3 Comparisons of d-spacing and intensity obtained from synthesis at 14.5 GPa and 2200 °C with those from JCDPS

d-spacing				relative intensity			
sample	JCDPs(py)	sample	JCDPs (cor)	sample	JCDPs (py)	sample	JCDPs (cor)
3.062	3.063	3.480	3.479	14	8	27	75
2.869	2.865	2.384	2.379	48	60	18	40
2.566	2.562	2.086	2.085	76	100	53	100
2.442	2.443	1.741	1.740	100	40	100	45
2.252	2.247	1.601	1.601	31	25	38	80
2.086	2.092	1.512	1.510	69	14	7	8
1.859	1.8588	1.404	1.404	24	16	19	30
1.811	1.8120	1.374	1.374	10	8	10	50
1.588	1.5890			49	30		
1.533	1.5312			71	50		
1.454	1.4551			11	2		
1.433	1.4320			34	10		
1.404	1.4102			25	4		
1.374	1.3696			13	4		

py = pyrope; cor = corundum

It has been well documented that a phase transformation in subsolidus phase will cause an increase in the slope of melting. To test the applicability of this theory to the present case, pyrope was synthesized at 14.5 GPa and 2200 °C for 5 hours, and the recovered sample was examined by X-ray diffraction. It is clear from the X-ray data (Table 4.3) that the recovered sample consists mostly of pyrope. Small amount of corundum is present and is probably due to an incomplete reaction among oxide mixture at the cold end of the sample. No other phase was identified. Since the experimental condition of synthesis is close to the melting point of pyrope, the possibility that there exists a phase transformation in crystalline pyrope is eliminated. On the other hand, we do not know if it is possible that a phase transformation does occur at high temperature and pressure but is not able to be recovered to the ambient condition.

In the following sections, thermodynamic approaches are applied to model the melting data of pyrope in the entire P-T space. Interpretations of this anomalous melting curve are offered.

4.2 Thermodynamic Evaluation along Melting Curve of Pyrope

4.2.1 Thermodynamic Calculation

Using the data listed in Table 4.4, a number of thermodynamic simulations were made by adjusting the physical properties of pyrope liquid. The following data on pyrope liquid are found to give an excellent description of the melting data below 10 GPa (Figure 4.3): V_{298} = 136.5 cm^3/mol (147.1 cm^3/mol at 1400°C,

using a thermal expansion coefficient α=5.65 x 10^{-5} /°C), K_T=18.5 GPa. However, under all circumstances, the thermodynamic simulations cannot yield a melting curve that shows an increase in the slope. For example, when a larger K_T' is used for liquid pyrope becomes more stable at high pressures, but this would result in the melting temperatures which are substantially higher than those of the experimental observations at low pressures (Figure 4.3). This will be also true if larger values of K_T and V_{298} are adopted. Comparisons of the recommended physical data on liquid with those calculated from the partial molar properties are given in Table 4.5.

Inability to model the melting data at high pressures through conventional thermodynamic approach indicates a possibility that certain physical change may occur in either subsolidus or liquid phases at high pressures. In the following sections, cation disordering in crystalline pyrope and stiffening of the pyrope liquid are considered to be alternate ways to yield a change in the melting slope around 10 GPa.

4.2.2 Cation Disordering

The slope of a univariant solid-solid equilibrium involving phases of fixed compositions can change significantly owing to the intracrystalline cation disordering. Examples of geological interest are found in the reactions: albite= jadeite + quartz, where albite undergoes an Al/Si order-disorder transition at about 600 °C corderite = Al orthopyroxene + spinel, where disordering of Al occurs in both orthopyroxene and spinel (Herzberg, 1983). Since the entropy of melting is always positive, arising from the liquid being always more

Table 4.4 Thermodynamic Properties of Pyrope and Liquid

	Pyrope	Liquid	Units
ΔH^o_{298}	-6291540	-5456710	J mol^{-1}
ΔS^o_{298}	226.70	11 59.6	J mol^{-1} K^{-1}
Heat Capacity			
a	519.70	630.00	
b	0.01388	0.035	
c	-0.5161	____	10^7
e	-0.5074	____	10^5
9	-0.4194	____	10^5
V_{298}	113.37	136.50	
Thermal Expansion			
α_o	0.2420	0.565	10^{-4}
α_1	0.2578	____	10^{-8}
α_2	____	____	
α_3	0.4421	____	
Compressibility			
β_o	0.5501	5.4054	10^{-6}
β_1	0.8643	____	10^{-10}
β_2	0.4798	____	10^{-13}
β_3	-0.1398	____	10^{-17}
K_T'	4.93	6.0	

*Pyrope: ΔH^o_{298} Charlu et al. (1975); ΔS^o_{298} Haselton and Westrum (1980); Heat capacity Tequi et aL (1991); V_{298} Robie et al. (1978); Thermal expansion, Skinner (1966); Compressibility and K_T' Webb (1989). Liquid: ΔH^o_{1570} and ΔS^o_{1570} Tequi et al. (1991); Heat capacity (Richet and Bottinga,1984); Thermal expansion; V_{298}, compressibility and K_T' This study. * At 1300 ^oC.*

disordered than the solid, cation disordering in the crystallographic site(s) of solid would decrease the entropy change of melting and thus increase the P-T slope of melting according to the Clayperon-Clausius relation.

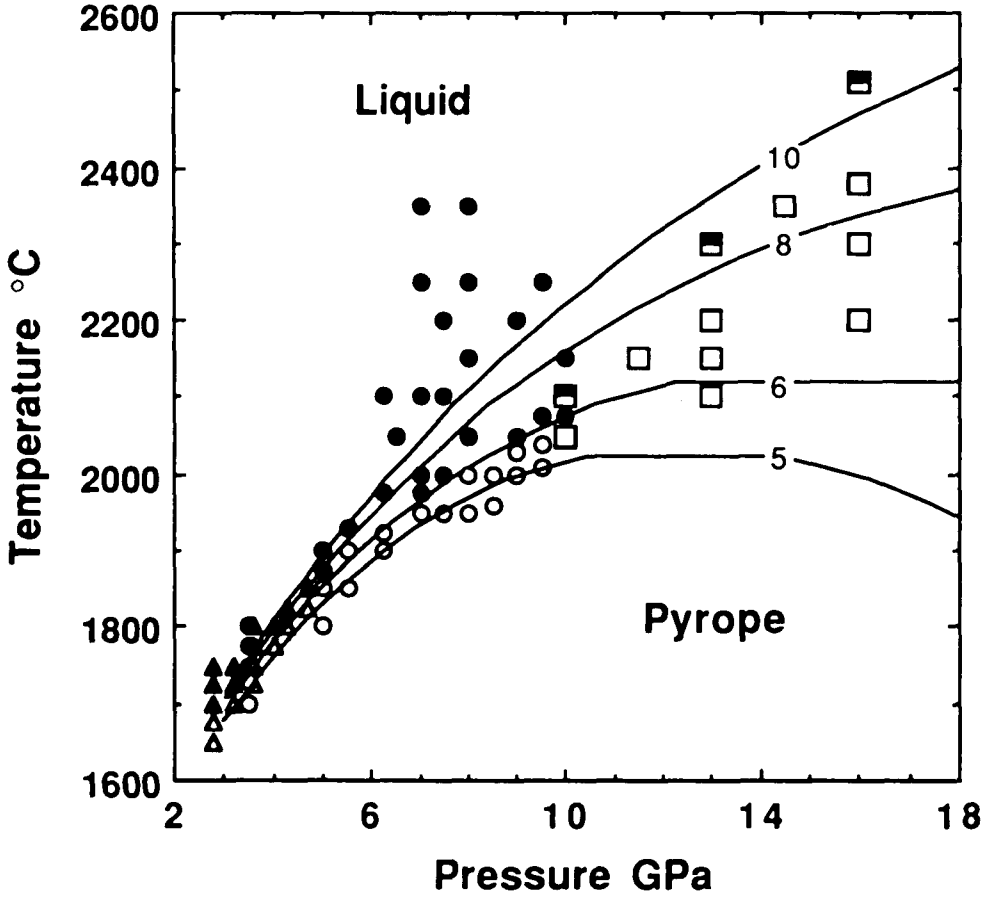

Figure 4.3 *The simulated melting curves of pyrope using the following data on pyrope liquid: V_{298} = 136.5 cm^3/mol; α = 5.65 x 10^{-5}/°C; and K_T = 18.5 GPa. Numbers along the melting curves are values of K_T'. Symbols have the same meanings as in Figure 4. 1.*

Table 4.5 Comparison of physical properties on pyrope liquid

Parameters		Studies	Units
V_{1673}	147.10	1	cm^3/mol
	153.07	2	
	154.10	3	
	153.68	4	
	152.16	5	
K_T	18.50	1	GPa
	18.78	5	
	11.30	6	
	11.90	7	
K_T'	6.00	1	
	22.33	7	

1. This study; 2. Bottinga and Weill (1970); 3. Nelson and Carmichael (1979); 4. Herzberg (1987); 5. Lange and Carmichael (1987); 6. Bottinga (1991); 7. Bottinga (1985, 1991).

Pyrope, with a structural formula $^{VIII}Mg_3{}^{VI}Al_2{}^{IV}Si_3O_{12}$, has Si on tetrahedral sites, Al on octahedral sites, and Mg on dodecahedral sites, in its completely order state. In the following model two types of cation disorderings are assumed to occur among different crystallographic sites: i) Mg-Al mixing on dodecahedral and octahedral sites; and ii) Al-Si mixing on octahedral and tetrahedral sites.

It should be mentioned that the recent spectroscopic studies on the pyrope endmember (McMillan et al.,1989) have not suggested the above assumptions

of cation disordering. However, the pyrope sample they used was synthesized at 900-1000 °C and may not be suitable for discussions in the present temperature range. Mg-Al-Si disordering was indeed observed by McMillian et al. (1989) but confined to the octahedral sites in pyrope-majorite garnet series which was synthesized at the similar temperature.

Since no data are available on the site occupancies of cations and interaction parameters, it is impossible to quantitatively characterize the contribution of disordering to the free energy of an ordered pyrope. However, the present case is simple in the sense that we are only interested in the entropy of disordering and its effect on the melting slope of pyrope. From statistical thermodynamics the geometric configurational entropy can be obtained by

$$S_C = - R[\Sigma\Sigma X_{ij} \ln X_i]$$

where R is the gas constant and X_{ij} the cation site occupancy of fth atom (j = Mg, Al, Si) on ith crystallographic site (i = d, dodecahedral site preferred by Mg, o, octahedral site preferred by Al, t, tetrahedral site preferred by Si). For the mixing of Mg and Al between dodecahedral and octahedral sites, the configurational entropy is given by

$$Sc(Mg/Al) = -R[X_{Mg}^{d} \ln X_{Mgd} + X_{Mg}^{o} \ln X_{Mg}^{o} + X_{Al}^{d} \ln X_{Al}^{d} + X_{Al}^{o} \ln X_{Al}^{o}]$$

A similar equation can be written on the Al/Si mixing between octahedral and tetrahedral sites. In view of the foregoing discussion, a practical way to estimate the effect of cation disordering on the P-T slope of pyrope melting is to find the

maximum entropy of disordering which can be attained by assuming pyrope to be completely disordered. For a completely disordered pyrope, calculation of the configurational entropy should consider two factors: 1) Al is expected to be equally distributed into dodecahedral and tetrahedral sites; and 2) each site should have the same Al/Mg or Al/Si ratio as in the crystal itself. As a result, the completely disordered pyrope can be expressed with a structural formula of the form

$$[^{VIII}(Mg_{0.75}Al_{0.25})^{VI}(Mg_{0.75},Al_{0.25})][^{Vi}(Al_{0.25},Si_{0.75})^{IV}(Al_{0.25},Si_{0.75})]O_6$$

and the configurational entropy is therefore calculated to be 18.7 J/mol K.

From the data in Table 4.4 the entropy changes of melting (ΔS_f) are calculated to increase from 226 to 255 J mol^{-1} K^{-1} between 2100 and 2500 ^oC. It means that the completely disordering of cations in pyrope will decrease the value of ΔS_f by only less than 10 percent. Assuming the disordering has no significant effect on the volume of pyrope, which is approximately true for albite (Holm and Kleppa, 1968), the resultant increase in the slope of melting $\Delta(dT/dP)$ is about 3 $^oC/GPa$. This small number is far insufficient to satisfy the melting temperatures observed in this study. It infers that the cation disordering in pyrope at high temperatures is unlikely a way to yield the anomalous increase in the melting slope around 10 GPa.

Although the value of 18.7 J mol^{-1} K^{-1} is obtained in a somewhat arbitrary way, it comes out with a very useful interpretation. However, the above implication may not be true for the melting of other minerals if an order - disorder

transformation occurs in subsolidus solid. It largely depends on the difference between the melting and configurational entropies. Compared with the melting entropies of other minerals such as quartz (ΔS_f=7.58 J mol^{-1} K^{-1} at 1633 K, see Chapter 5) and fayalite (ΔS_f=89.3 J mol^{-1} K^{-1}at 1620 K, Stebbins and Carmichael, 1984), pyrope has an enormously high values of ΔS_f.

4.2.3 Stiffening of the liquid

From previous melting experiments on pyrope and spectroscopic studies on aluminosilicate liquid, there are two observations which strongly indicate a dramatic structural change in pyrope liquid. One is that phases quenched from liquid of pyrope composition change from aluminous enstatite to pyrope above 7 GPa (irifune and Ohtani, 1986). Another is the appearance of six-coordinated Al^{3+} in albite liquid above 6 GPa (Ohtani et al., 1985). Since both of the observations are pressure-induced, it will be reasonable to consider that certain physical properties in pyrope liquid may be significantly modified at pressures above 6-7 GPa.

In the calculations of phase equilibrium between pyrope and its liquid, thermodynamic data in Table 4.2 are all fixed except for K_T' which is manually changed by a method of trial and error to fit the melting data between 10 and 16 GPa. The resultant values which give the best fit are: K_T'= 6.3 at 10 GPa; K_T'= 8.3 at 13 GPa, and K_T'= 10.3 at 16 GPa. K_T' is smoothly changed from 6.0 to 6.3 in the pressure range of 7 to 10 GPa, while it maintains constant at 6.0 below 7 GPa. The calculated melting curve of pyrope by this procedure in the entire experimental P-T space is shown in Figure 4.4.

It is not surprising from Figure 4.4 that this procedure will always lead to an excellent agreement between the calculations and the experimental data. However, the following observations and reasoning provide physical backgrounds for the adjustment of data in different pressure ranges:

1) Below 6 GPa the quench albite liquids showed the same ^{27}Al NMR spectra

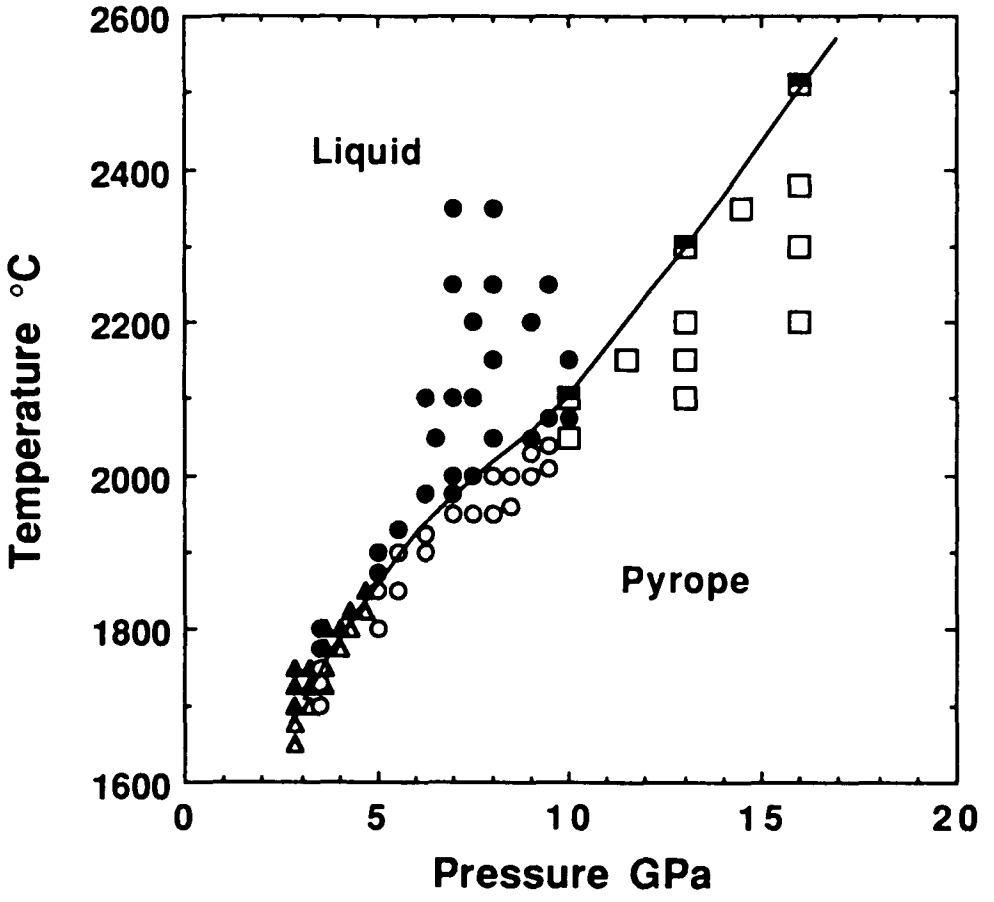

Figure 4.4 *Calculated melting curve of pyrope in the experimental P-T space by changing values of K_T' above 7 GPa.*

(Ohtani et al., 1985). In this pressure range it is generally accepted that compression of liquid is accomplished by decreases in the Al-O-Si and Si-O-Si bond angles without any involvement of significant structural change (Ohtani et al., 1985; Williams and Jeanloz, 1988).

2) A new ^{27}Al NMR peak emerged in albite liquid at 6 GPa and became larger at 8 GPa (Ohtani et al., 1985). Structural assignment of the new peak suggest that Al^{3+} in the liquid was in octahedral coordination. Further analysis implied that the concentration of the six-coordinated Al^{3+} increased with pressure. According to Stolper and Ahrens' (1987) proposal, such close octahedral packing of oxygen atoms will make the liquid more difficult to compress.

3) At 10 GPa Williams and Jeanloz (1988) inferred that aluminum in fivefold and sixfold coordinations contributed to the observed Infrared spectral changes in anorthite glass. From molecular dynamics computer simulation (e.g., Angel et al., 1982 and 1987), a similar conclusion has been derived. Both studies further suggest that a large proportion of Al^{3+} are probably in six coordination above 10 GPa in aluminaosilicate liquid. Following Stolper and Ahrens (1987), a consequence of changing coordination from IV to VI is likely to be a change from corner-sharing tetrahedra to edge- or face-sharing polyhedra, which will significantly stiffen the liquid.

The values of K_T' obtained by the above procedure and by fitting the melting curve of Irifune and Ohtani (1986) are both used to calculate the isothermal P-V relations. The results at 2000 K are shown in Figure 4.5. Although pyrope liquid with a constant value of $K_T' = 6$ has small absolute volumes above 10 GPa, it

does not stiffen very much at higher pressures. In contrast, the pyrope liquid with the increased K_T' values stiffens considerably at pressures above10 GPa, which is in accord with the analysis of coordination change of Al^{3+} in silicate liquid with increasing pressures.

From the shock wave studies on the pressure-volume relations, Rigden et al. (1988, 1989) found that diopside liquid was considerably stiffened at pressures above 25 GPa. As a result, it is difficult to describe its P-V relation using a single set of data on bulk modulus and its pressure derivative according to

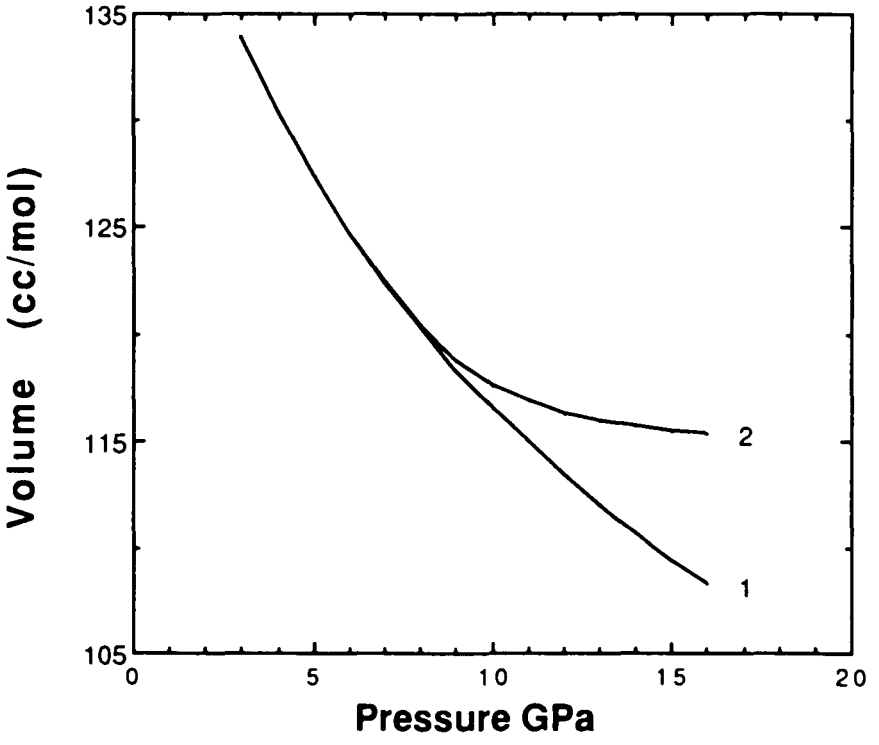

Figure 4.5 *Isothermal P-V relation of pyrope liquid at 2000 K.1: K_T' = 6.0 obtained by fitting the melting curves of Irifune and Ohtani (1986); 2: K_T' values are obtained by fitting thep resent melting data.*

the third order Birch-Murnghan equation. It means that above 25 GPa the stiffened diopside liquid must have a different and larger K_T' value. These observations are highly consistent with the prediction from molecular dynamics simulation that Si^{4+} becomes six- coordinated in silicate liquid at pressures above 20 GPa (eg., Angell et al, 1982 and 1987).

4.3 Discussions

Aluminous garnet, as an important component in garnet lherzolite models of the upper mantle, has been recently found on the liquidus of peridotitic and chondritic melts at pressures above 12 to 14 GPa (e.g., Takahashi and Scarfe, 1985; Kato and Kumazawa, 1986; Ohtani, 1987; Ito and Takahashi, 1987; Herzberg et al., 1990). All these experimental results indicated an increasing thermal stability of garnet and a change of liquidus phases from olivine to garnet at elevated pressure. Such change has recently been emphasized because fractionation of garnet is considered to play a significant role in the generation of komatiitic magmas and gross mantle differentiation (e.g., Ohtani and Sawamoto, 1987; Herzberg and Gasparik, 1991).

Melting curves of mantle minerals will provide an end-member reference frame that is essential for a comprehensive understanding of high pressure melting behavior in more complex multicomponent systems. The liquidus curve of a phase in multicomponent systems will be quantitatively related to its melting curve in a one component system. This concept was developed by Herzberg (1983) and was applied to explain why magmas on the anhydrous solidus become increasingly magnesian with increased pressure by

considering Fo - En binary system. It is also useful to apply this concept to relate the melting data of pyrope with those of peridotitic and chondritic compositions, despite garnets in these systems are alumina deficient relative to pyrope. As shown in Figure 4.2, the melting slope of pyrope above 10 GPa is larger than that of forsterite. As a result, the melting curve of pyrope will gradually converge with that of forsterite at increased pressure. At a certain point when forsterite has lower melting temperature than pyrope it will no longer be the liquidus phase and will be replaced by pyrope.

From the above consideration, the melting curve of pyrope between 10 and 16 GPa is qualitatively in excellent agreement with the observations in the multicomponent systems. On the other hand, if the melting curve of pyrope is flat above 10 GPa, as suggested by Irifune and Ohtani (1986), it will not be consistent with the observations that garnet is present as liquidus phase of ultramafic magmas at high pressures.

Chapter 5

Melting and Subsolidus Relations of SiO_2 Polymorphs

5.1 Experimental Results

The experimental results are listed in Table 5.1 and shown in Figure 5.1. In most of the experiments two or more silica phases were synthesized in the same run because of the 200 °C temperature gradient across the sample (Figure 2.4a). In subsolidus experiments, coesite was distributed in the hot end and stishovite in the cold end, an the contact between them was usually very sharp. In melting experiments, the interface was observed to be very sharp between the liquid and coesite, but somewhat diffuse between stishovite and liquid. Liquid SiO_2 does not quench to a glass at pressures of 12 to 14 GPa, but instead quenches to coesite crystals that were typically as large as primary coesite. Kanzaki (1990) reported liquid as glass at pressures between 4.5 and 6 GPa, but he could not preserve it at 8 GPa. He interpreted this highest pressure result to be due to a temperature fluctuation-induced crystallization, but it is more likely that he formed quenched coesite as well.

Inspection of Figure 5.1 demonstrates that the slope of the melting curve of coesite is almost flat but slightly positive. Three experiments performed in the pressure range of 13.5 to 14 GPa yield a very tight constraint on the location of the coesite - stishovite - liquid triple point. As shown in Figures 5.2a and b, the experiment at 13.5 GPa and 2750 °C (Run #1317) contained liquid in the hot spot, coesite in the middle and stishovite in the cold end of the sample.

Table 5.1 The Experimental Results

Run No.	P(GPa)	emf(V)	T(°C)	Time	Phases
1256	12.0	39.99	2350	3 min	Cs, Cs
1292	14.0	42.80	2625	3 min	St, St
1297	13.0	43.80	2750	3 sec	Q-Cs,Cs
1317	13.5	43.80	2750	3 sec	Q-Cs,Cs,St
1327	13.8	43.80	2750	3 sec	Q-Cs, St
1329	11.0	43.00	2650	3 sec	Cs,Cs
1347	13.8	43.80	2750	3 sec	Q-Cs,St
1348	11.0	35.50	2000	10 min	Cs,St
1354	12.5	39.99	2350	10 min	Cs,St
1362	14.0	44.40	2855	3 sec	Q-Cs,St
1363	12.0	43.70	2740	3 sec	Q-Cs,Cs
1364	13.0	41.80	2520	5 min	Cs, St
1381	11.3	35.45	2000	25 min	Cs,St
1382	12.3	39.99	2350	30 min	Cs, St
1452	9.6	25.69	1400	4 hr	Cs,Cs
1464	10.2	25.69	1400	4 hr	Cs,St
1467	9.0	18.11	1000	4 hr	Cs,Cs
1468	9.6	18.11	1000	4 hr	Cs,St,Cs

Cs=Coesite; St=Stishovite; Q-Cs=Coesite quenched from liquid.

** For each run, phases are arranged in order as they appear from the cold end to the hot spot; e.g., Cs, St meanig Coesite at hot end, and stishovite at cold end.*

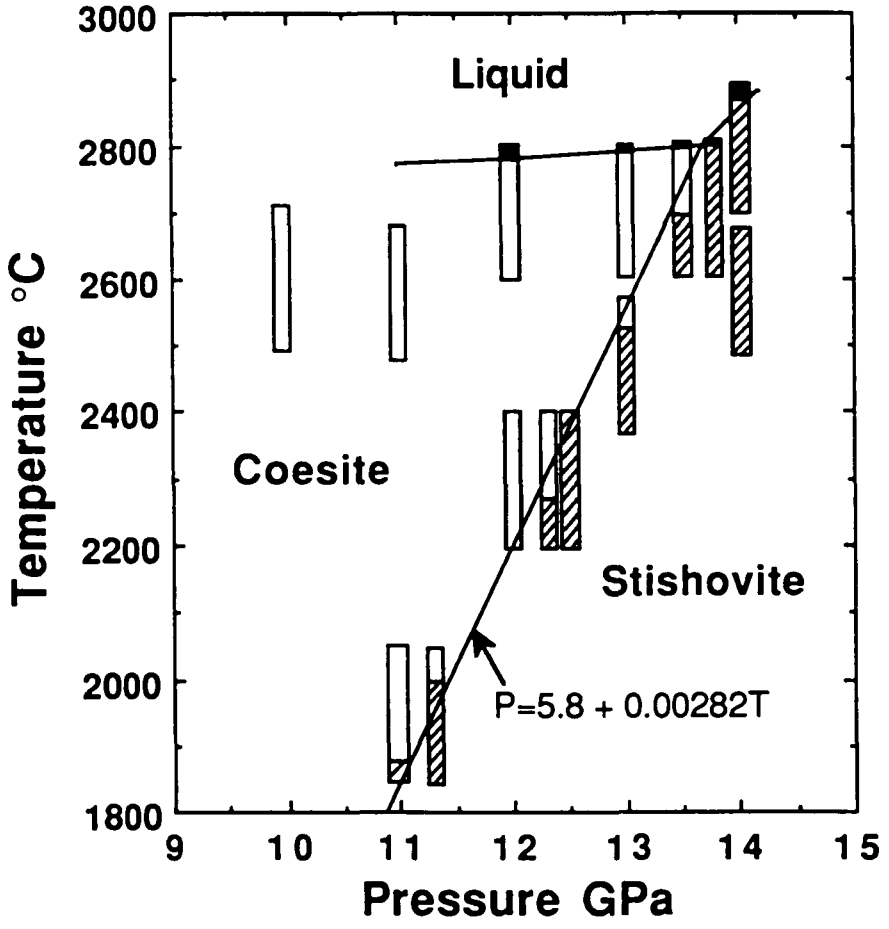

Figure 5.1 *Experimental results on the melting of coesite and stishovite, and the coesite-stishovite transformation. Closed symbols, quenched liquid, Open symbols, coesite; and slash symbols: stishovite. Each bar represents a single experiment, and the length of the bars corresponds to the 200 °C temperature gradient shown n Figure 2.4a.*

0.5 mm

a)

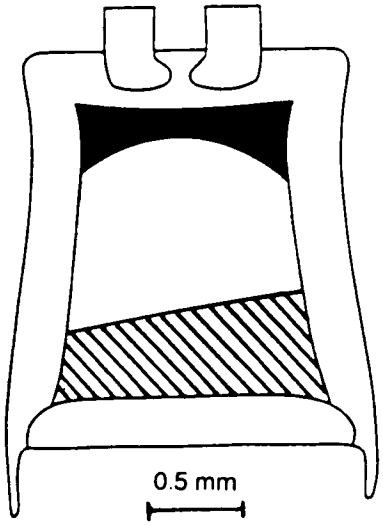

Liquid

Coesite

Stishovite

b)

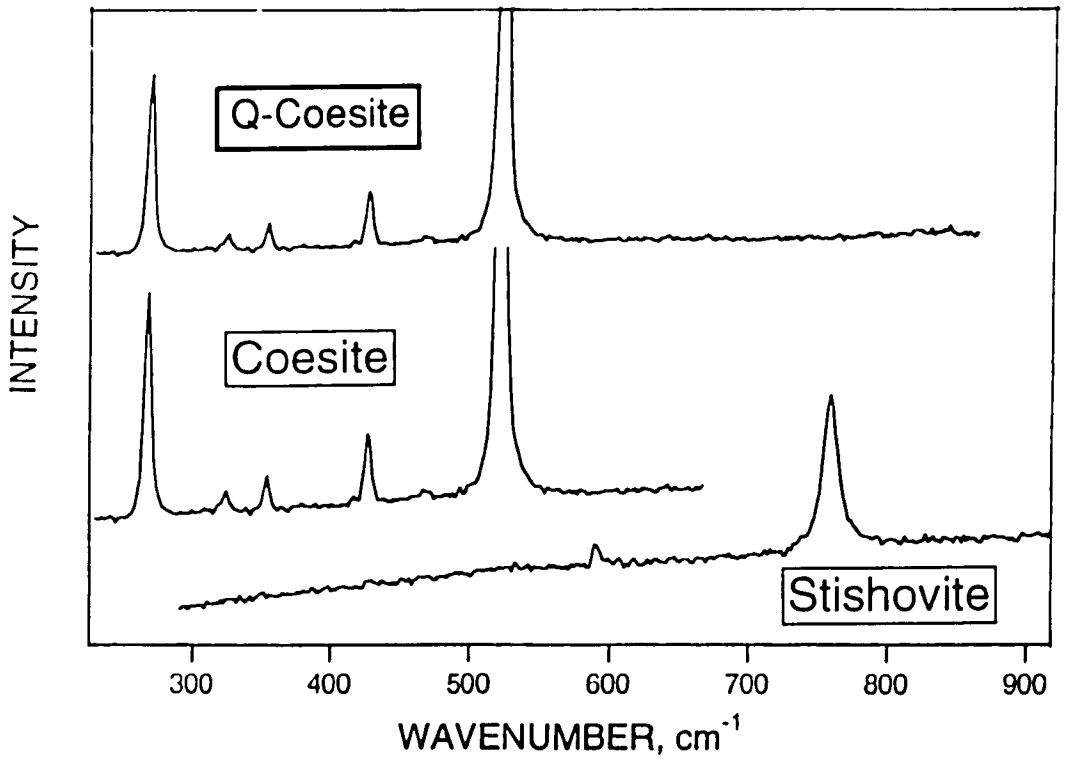

c)

Figure 5.2 *a) A photograph of the experimental results at 13.5 GPa and 2750 °C (Run # 1317). b) A sketch of a); c) Representative Raman spectra obtained from three different phases of Run # 1317 .*

The respective Raman spectra are shown in Figure 5.2b. This experiment is especially noteworthy because it was conducted at conditions that are very close to the triple point.

At 13.8 GPa and 2750 °C (Run # 1327), the charge contains mostly stishovite with crystals that range from large in the cold end to very fine in the hot end.

Coesite was detected in the hot spot by its Raman spectrum but it could not be observed optically. Since the interface between coesite and stishovite was diffuse, the observed coesite is interpreted as quenched liquid. The triple point is therefore bracketted between 13.5 and 13.8 GPa at 2800 °C. At 14 GPa and 2850 °C, both stishovite and quench coesite were abundant, each occupying about half of the sample.

The coesite-stishovite transformation between 2000 and 2800 °C is linear and can be best described by the following equation:

$$P = 5.8 + 0.00282\ T$$

where T is in °C and P in GPa. The dT/dP slope in this temperature range is about 355 °C/GPa. However, for several experiments that were performed at temperatures of 1000 and 1400 °C, the results are rather ambiguous for determination of the phase boundary and are described below in detail.

At 1000 °C and 9 GPa and 1400 °C and 9.6 GPa, pure coesites were synthesized without stishovite. At 1400 °C and 10.2 GPa the experimental charge (Run # 1464) contained a mixed phase of coesite+stishovite toward the cold end and pure coesite in the rest of the sample. The interface between them is not as sharp as observed above 2000 °C. In another experiment at 9.6 GPa and 1000 °C (Run # 1468), the observation was even more ambiguous. The experimental charge contained pure coesite in the very cold end, a mixed phase of coesite and stishovite in the middle, and pure coesite in the hot end of

the sample. In both cases, half of the charges consisted of very fine-grained crystals which were difficult to identify optically. Identification of phases was determined by Raman spectroscopy.

5.2 Comparisons and discussions of the experimental results

Comparisons of the present experimental results with previous studies are shown in Figures 5.3 and 5.4. The melting temperatures of coesite reported by Kanzaki (1990) were corrected downward to the temperature-emf relation calibrated by Asamoto and Novak (1967). It can be seen that there is a very good agreement on the melting of coesite in these two independent studies. However, as shown in Figure 5.4, the flat coesite melting curve determined in this study substantially disagrees with the Jackson's (1976) prediction in that the melting curve of coesite had a temperature maximum of ~2750 ^{o}C at about 8 GPa and a large negative melting slope at higher pressures. The coesite-stishovite-liquid triple point constrained by this study is about 600 ^{o}C higher than that estimated by Davis (1972) from the shock wave data. Since Jackson's (1976) prediction was made to reconcile his work on the melting of quartz with this estimated triple point, he was clear to point out that his melting relation on coesite was conjectural and that Davis' (1972) triple point may be 300-500 ^{o}C too low.

Although the melting curve of stishovite was not able to be determined because of the technical limitation, the present melting experiments on stishoviteat 14GPa provides a reference point. Inspection of Figure 5.4 shows that the melting temperature we obtained at 14 GPa could be 300 ^{o}C higher

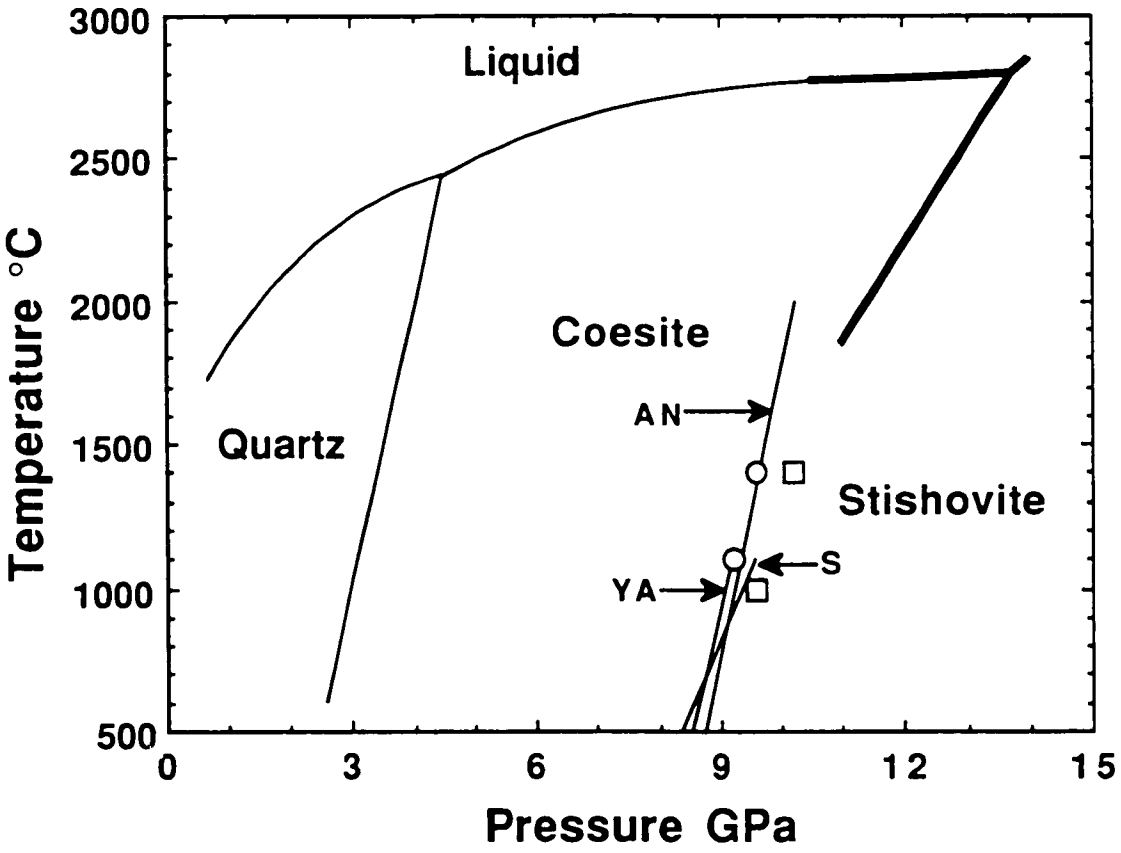

Figure 5.3 *Review of the static experimental data on the melting and subsolidus relations of SiO_2. The melting data are from Jackson (1976) between 0.7 and 2.5 GPa, and from Kanzaki (1990) between 3.0 and 8.0. The bold lines are from this study. YA=Yagi and Akimoto (1976), S=Suito (1977), and AN=Akaogi and Navrotski (1984). Both circles (Pacalo and Gasparik, 1990) and squares (this study) represent the observed phase transformation boundaries.*

than those inferred by Schmitt and Ahrens (1989) from the shock wave experiments at pressures between 16 and 30 GPa. Since the shock wave data place a minimum constraint on the melting temperatures of stishovite, Schmitt and Ahrens (personal communication) considered that their reported

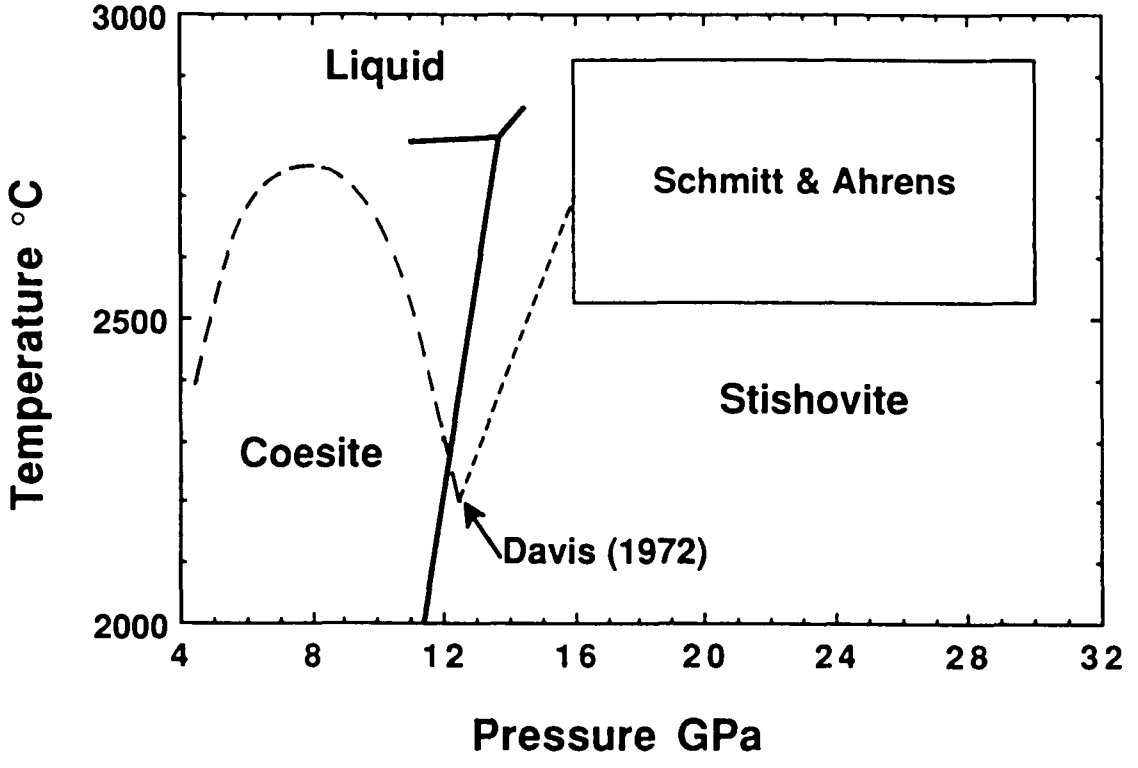

Figure 5.4 *Comparisons of the present experimental results (bold lines) with thermodynamic calculations on the melting of coesite and stishovite (Jackson, 1976; dash cueve and line, respectively) and the coesite-stishovite-liquid triple point (Davis, 1972), and with the shock-wave melting on stishovite (Schmitt and Ahrens, 1989).*

values are in reasonable agreement with ours. However, from the difference in temperature values of two sets of data, it is likely that their proposed melting curve of stishovite in the lower mantle may underestimate the melting temperatures by at least 300 °C.

As shown in Figure 5.3, the dT/dP slope of the coesite-stishovite boundary above 2000 °C is two and half times smaller than indicated by the in the situ X-ray study of Yagi and Akimoto (1976) below 1100 °C and by the quench experiments of Pacalo and Gasparik (1990) between 1050 and 1400 °C. In these two independent studies amorphous silica and a mixed phase of coesite + stishovite were, respectively, used as the starting materials. A linear extrapolation of these results to high temperatures yields a boundary which is located at pressures that are much lower than the present observations. For example, at 2800°C the extrapolated phase boundary of Yagi and Akimoto's (1976) result is about 2.5 GPa lower than constrained by the coesite-stishovite-liquid triple point of this study. Since melting of coesite and stishovite occurred instantaneously and had no kinetic difficultty, the coesite-stishovite-liquid triple point is considered to be an excellent constraint on the coesite-stishovite phase boundary.

It is emphasized that our higher pressure values for the coesite-stishovite transformation cannot be an artifact of the pressure calibration scale. Although the temperatures in this study (e.g., 2800 °C) are considerably higher than those at which the pressure calibration was made (up to 1600 °C, Figure 2.2), there are a number of observations indicating that this scale is valid over a

wide temperature range. As shown in Figure 5.5, using this calibration scale the forsterite to beta phase transition of the composition Mg_2SiO_4 was observed at 2240 °C (Presnall and Gasparik, 1990), and was consistent with the linear extrapolation of the forsterite-beta phase boundary determined at lower temperatures (Katsura and Ito, 1989). Any downward correction in pressure that is larger than 0.5 GPa would result in the formation of modified spinel in the stability field of forsterite and a phase boundary that is thermodynamically inconsistent with the calorimetric measurements (Akaogi et al., 1989). Similarly, it will affect the linearity of the orthoenstatite-clinoenstatite transformation boundary that was determined up to 2100 °C (Pacalo and Gasparik, 1990).

Another important observation in this regard is the melting behavior of pyrope determined up to 2500 °C in this study. As can be seen in Figure 4.1, any downward correction in pressure will lead to a more unusual melting curve that is theoretically difficult to model. For example, it requires very large K_T' values for pyrope liquid above 10 GPa such that the liquid phase is almost incompressible.

As mentioned before, a linear extrapolation of the low temperature data on the coesite-stishovite transformation to 2800 °C will yield a phase boundary that is about 2.5 GPa lower than obtained by this study. If this difference is due to the pressure calibration scale used at Stony Brook, the resultant phase relations of the forsterite-beta phase transition and the melting of pyrope will become completely unreasonable. For example, at 2240 °C the phase transformation will take place at a pressure of 14 GPa; while at 1200 °C the pressure for

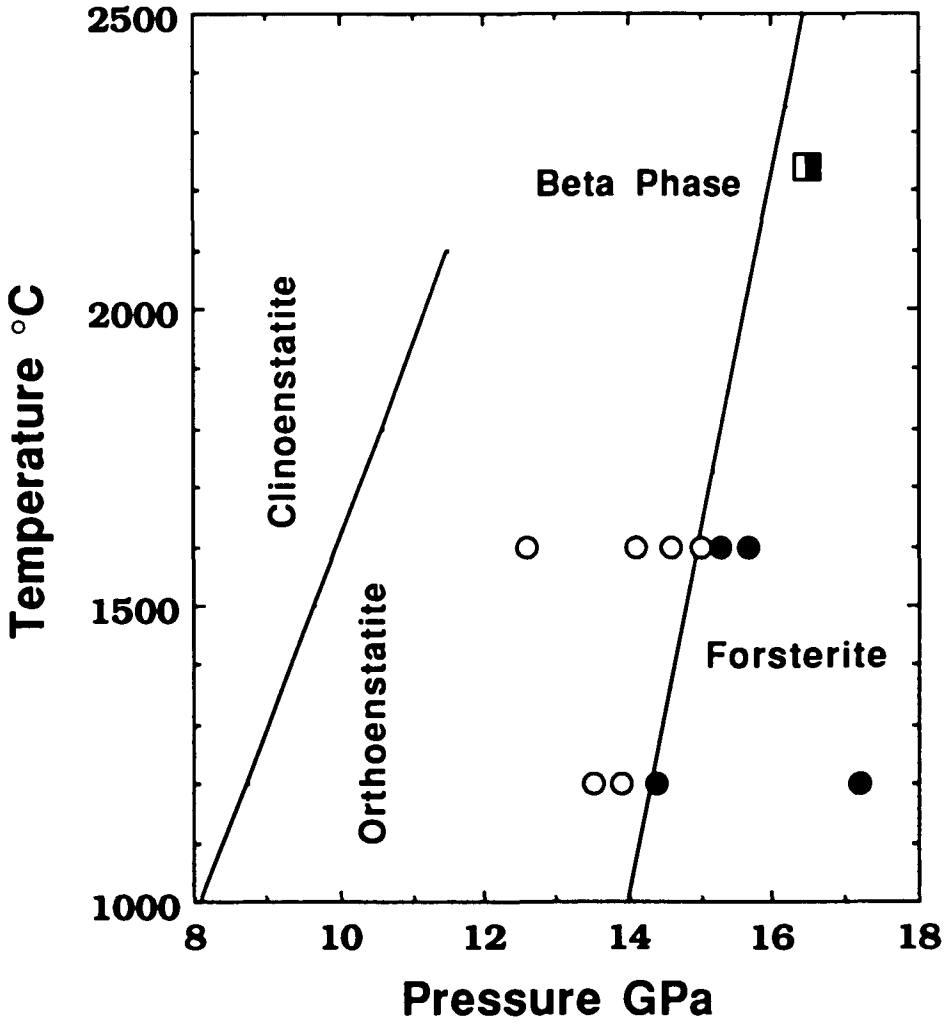

Figure 5.5 *Other phase equilibria obtained in Stony Brook using the same sample assembly provide supporting evidence for the validity of the pressure calibration scale (Figure 2.2) at very high temperature. Forsterite-beta transition: circles = Katsura and Ito (1989); Squares = Presnail and Gasparik (1990); Open symbols: forsterite; Closed symbols: beta-phase. Forsterite-beta phase boundary is from Akaogi et al. (1989). Orthoenstatite-clinoenstatite transition boundary was obtained Pacalo and Gasparik (1990).*

this transformation is around 14.5 GPa.

With regard to the significant change in the slope of the coesite-stishovite transformation, the following possibilities are considered. First, it is likely that all the experiments including those in this study performed at temperatures below 1400 °C did not position the phase boundary correctly because of the inherent kinetic problems. From the in situ X-ray study of Yagi and Akimoto (1976), there were two competing observations that made their results ambiguous. One observation was that once stishovite was well crystallized above 700 °C it was almost impossible to transform it into coesite near the phase boundary even at 1000 °C. This points to the desirability of using amorphous silica as a starting material and of reaching the target temperature as quickly as possible to avoid growth of stishovite crystals. On the other hand, as also pointed out by Yagi and Akimoto (1976), amorphous silica always first crystallized into coesite rapidly at approximately 200 °C in the stability field of stishovite. This so-called metastable coesite did not breakdown to stishovite at least up to 500 to 600 °C. From our experimental results at 10.2 GPa and 1400 °C (Run # 1464) and at 9.6 GPa and 1000 °C (Run # 1468), it is likely that such metastable coesite could be stable even to about 1400 °C. This arises from stishovite being more difficult to be nucleated than coesite, a consequence of requiring sufficient thermal energy to change the coordination number of Si^{4+} from 4 to 6. In this regard, it raises a problem, that is, whether the previously determined phase boundaries below 1400 °C were metastable or in equilibrium.

In view of the observed problems at low temperatures, all the experiments on the coesite-stishovite transformation in our preliminary report (Zhang et al., 1991) were performed at temperatures above 2000 °C. We had no definite evidence to indicate that the above kinetic problems would persist at such high temperatures. However, the experimental results in this P-T space are clearly more internally consistent than those of Yagi and Akimoto (1976), which actually indicated a slightly negative slope if a line is drawn to best fit all the experiments with coexisting coesite and stishovite. In addition, metastable coesite has not been observed in any experiments above 2000 °C. Stishovite always exists under the phase boundary while coesite above it. When all this information is taken into account, we could conclude that the precise determination of the coesite-stishovite transformation would be favored at high temperatures.

An alternate way to reconcile the low temperature data with the high temperature ones is to consider the phase boundary to be strongly curved. Mathematically, there would be no difficulty, and the following equation gives a good description of the data in the entire P-T space:

$$P = 7.95 + 0.910 \times 10^{-3}T + 0.415 \times 10^{-6}T^2$$

where T is in °C and P in GPa. Thermodynamic analysis of this consideration will be given in the next section.

The third possibility is that coesite has a second order and nonquenchable phase transformation. If this is true, the predicted kink in the transformation

boundary will be located somewhere at a pressure between 10 and 11 GPa and a temperature between 1500 and 1800 °C. To test this possibility, further work such as TEM to characterize samples recovered from low and high temperatures and in situ X-ray study are needed.

5.3 Thermodynamic evaluation and discussion

Thermodynamic data used in the evaluation of the experimental results are listed in Table 5.2. Four SiO_2 phases: β-quartz, coesite, stishovite, and liquid are considered. Thermodynamic evaluation of the subsolidus phase relations between the three polymorphs have been made recently by several authors such as Akaogi and Navrotsky (1984) and Kuskov and Fabrichnaya (1987). Fei and Saxena (1986) and Fei et al. (1990) started with the thermochemical data on quartz from Robie et al. (1978), and evaluated the thermochemical data on ΔH°_{298} and ΔS°_{298} for coesite and stishovite by synthesizing the data from the phase equilibrium studies for the quartz-coesite transformation (Bohlen and Boettcher, 1982), for the coesite-stishovite transformation (Yagi and Akimoto, 1976) and from the calorimetric measurements from Akaogi and Navrotsky (1984). Their data systematization on stishovite also consider several phase transformation boundaries in the system $MgO\text{-}SiO_2$ involving stishovite (Fei and Saxena, 1986).

5.3.1 Coesite-stishovite transformation

From the available elastic data on coesite and stishovite listed in Tables 5.2 and 5.3, entropy changes ranging between -11 and -13.5 J $K^{-1}mol^{-1}$ are required to

Table 5.2 Thermodynamic Data

Parameters	Quartz	Coesite	Stishovite	Liquid
ΔH^{o}_{298} (J mol^{-1})	-910700	-908000	-859000	-897910
ΔS^{o298} (J K^{-1} mol^{-1})	41.46	38.73	34.38	49.04
V_{298} (cm^3/Mol)	23.80	20.64	14.01	26.71
K_{298} (GPa)	68.42	96.00	314.0	14.43
K_{298}'	6.40	8.40	6.40	4.50
$(dK/dT)_p$ (GPa/K)	___	-0.02	-0.047	___
α_o (10^{-4})	-0.065	0.0543	0.1023	0.100
α_1 (10^{-8})	___	0.832	1.3500	___
α_3	___	-0.061	___	___
a	78.812	78.746	58.129	81.37
b(10^{-3})	1.205	0.6974	7.002	___
c(10^{7})	0.1731	-0.2963	-1.2689	___
e(10^{9})	0.1202	0.5858	1.7928	___
g(10^{4})	-1.2130	-0.6689	1.7040	___

Quartz: ΔH^{o}_{298} and ΔS^{o}_{298} (Robie et al., 1978); V_{298}, and α, Skinner (1966); K_{298} and K_{298}', Carmichael (1982); Coesite: ΔH^{o}_{298} and ΔS^{o}_{298} Fei and Saxena (1986); V_{298}., Robie et al. (1978); K_{298} and K_{298}', Levien and Prewitt (1981); (dK/dT)P, Watanabe (1982); α, Skinner (1966), modeled by Fei and Saxena (1986); Stishovite: ΔH^{o}_{298} and ΔS^{o}_{298} Fei and Saxena (1986); C_P, Robie et al., (1 978); K_{298} and K_{298}', Weidner et al. (1982); (dK/dT), Watanebe (1982); Liquid: ΔH^{o}_{298}, ΔS^{o}_{298} and K_{298}', estimated in this study; V_{298}, α and K_{298}, Lange and Carmichael (1987); C_p (Richet and Bottinga, 1984).

Table 5.3 Elastic data on coesite and stishovite

References	K_{298} (Kbar)	K_{298}'
coesite		
Basset and Barnett (1970)	1260	4.0
Akimoto (1975)	972	___
Weidner and Carleton (1 977)	1137	___
Levien and Prewitt (1981)	960	8.4
Stishovite		
Akimoto (1975)	3430	___
Liebermann (1976)	2500	6.0
Sato (1 977)	2810	5.0
Chung(1979)	2930	4.1
Weidner et al. (1982)	3160	___

fit the observed boundary of the coesite-stishovite transition between 2000 and 2800 °C. The entropy change at temperatures less than 1000 °C is - 4.2±1.7 J $K^{-1}mol^{-1}$ (Akaogi and Navrotsky, 1984; Fei and Saxena, 1986) and is thermodynamically consistent with the Yagi and Akimoto's (1976) results. It is found that the required three-fold increase in the entropy change of the transition at temperatures above 2000 °C cannot be predicted with any existing heat capacity data base. For example, from thermochemical data listed in Table 5.2, the calculated entropy changes range from -2.23 to -3.13 J $K^{-1}mol^{-1}$ between 2000 and 2800 °C.

These calculations suggest that it is unrealistic to fit all the experimental data as a curve, a possibility proposed before to reconcile the phase boundary at low temperatures with that at high temperatures. However, the calorimetric measurements on stishovite are only applicable to about 400 °C. The extrapolated heat capacity data on both coesite and stishovite may not be suitable in this high temperature range. If ΔH^{o}_{298} and ΔS^{o}_{298} in Table 5.2 are accepted, the heat capacity of coesite above 2000 °C should be larger than or that of stishovite be smaller than the existing extrapolations.

5.3.2 Modeling of melting data on quartz and coesite

The high-pressure melting relations of SiO_2 predicted by Jackson (1976) have received attention because of several recent important observations. The most interesting one is the transformation of ice I to an amorphous phase by pressurizing it at 77 K to its extrapolated melting point of 1 GPa (Mishima et al., 1984). Sinc it has been well known that the melting temperature of ice I decreases with increasing pressure, such pressure-induced amorphization has subsequently been interpreted in terms of the crossing of the metastable extension of its melting curve (Mishima et al.,1984). They further predicted that similar transformation will probably occur in all other solids that have negative melting volumes when a transformation to a crystalline solid is too slow.

Discovery of amorphizations of crystalline quartz and coesite at 25 to 35 GPa and 300 K (Hemley et al., 1988) provides an insight into the Mishima et al.'s (1984) prediction. By integrating the P-V data on quartz, coesite and silica glass, Hemley et al. (1988) demonstrated that the volume changes at high

pressures for the quartz-glass and coesite-glass transformations were consistent with the negative metastable extension of the coesite melting curve predicted by Jackson's (1976). On the other hand, as indicated by Yagi and Akimoto (1976) and by us in this study, transformation of coesite to stishovite has proven to be difficult even up to about 1400 ^{o}C within the stability field of stishovite. When this information is taken into account, it seems to demonstrate that the Mishima et al.'s (1984) prediction can be applied to quartz and coesite, and perhaps to other crystalline materials such as carbon and boron nitride as indicated by Tan and Ahrens (1990) from results of the shock wave studies.

In view of the substantial difference in the melting relations of coesite between the Jackson's (1976 prediction and this study, an attempt has been made to test the amorphization of quartz and coesite by combining the experimental studies on the melting of these two SiO_2 polymorphs (Jackson, 1976; Kanzaki, 1990) with thermodynamic considerations.

With the thermodynamic data in Table 5.2, the melting curve of quartz has been successfully modeled with K_T'=4.3. The extrapolated metastable point at 1 bar is 1417 ^{o}C at which ΔH^{o}_{1690} and ΔS^{o}_{1690} for SiO_2 liquid are, respectively, -802150 J mol^{-1} and 164.91 J mol^{-1} K^{-1}. The resultant enthalpy and entropy of melting are thus, respectively, 12780 J mol^{-1} and 7.58 J mol^{-1} K^{-1}. If these differences remain at 298K, we obtain for SiO_2 liquid ΔH^{o}_{298}=-897910 J mol^{-1} and ΔS^{o}_{298}=49.04 J mol^{-1}K^{-1}. For comparison, the entropy of melting obtained by Richet et al. (1982) from calorimetric measurement on silica glass is 5.5 J mol^{-1}K^{-1}. But this value will result in the melting temperatures that are much higher than those of Jackson (1976) and Kanzaki (1990).

When the same data on SiO_2 liquid are used to the melting curve of coesite the resultant melting temperatures are lower than Kanzaki's (1990) and higher than ours. To fit the melting data between 4.5 and 13.7 GPa, a reasonable simplification has been adopted, that is, to extrapolate the coesite data on thermal expansion and bulk modulus to 2500 K and to keep them constant at higher temperatures. The reason for this treatment is that the temperature effects on these parameters are not included for SiO_2 liquid. By doing so, it is found that a value of ΔS^{o}_{298}=45.2 J mol^{-1} K^{-1} for coesite can give an excellent fit to the melting data of coesite in the entire P-T space (Figure 5.6). Obviously, this value is not real because it is not consistent with the quartz-coesite transition. However, this fictive value could simply mean that the thermochemical data in Table 5.2 may underestimate the entropy of coesite by about 6.5 J mol^{-1} K^{-1} at high temperatures if ΔS^{o}_{298}=38.73 J mol^{-1} K^{-1} is correct. Specifically, for example, at 2360 °C ΔS^{o}2633=189.39 J mol^{-1} K^{-1} for coesite is needed to be in equilibrium with SiO_2 liquid; while the calculated value from Table 5.2 is 182.92 J $mol^{-1}K^{-1}$. To increase the entropy of coesite a larger heat capacity at this temperature is required, which is consistent with the previous discussion on the coesite-stishovite transition.

Although the above analysis indicates an inconsistency between the experimental results and thermochemical data, optimization of data on coesite and stishovite is not attained for the following reasons : 1) As discussed before, the coesite-stishovite phase transition below 1000 °C may not be correct. At this stage, we are not sure whether these results should be included in the data systemization; 2) Phase boundary between 1000 and 2000 °C has not been well constrained. In situ X-ray study in this

temperature will be conducted in the near future; and 3) if there exists a nonquenchable phase transformation of coesite, we should not use a single set of data to describe these two phases. It is expected to provide a test also from the in situ X-ray study.

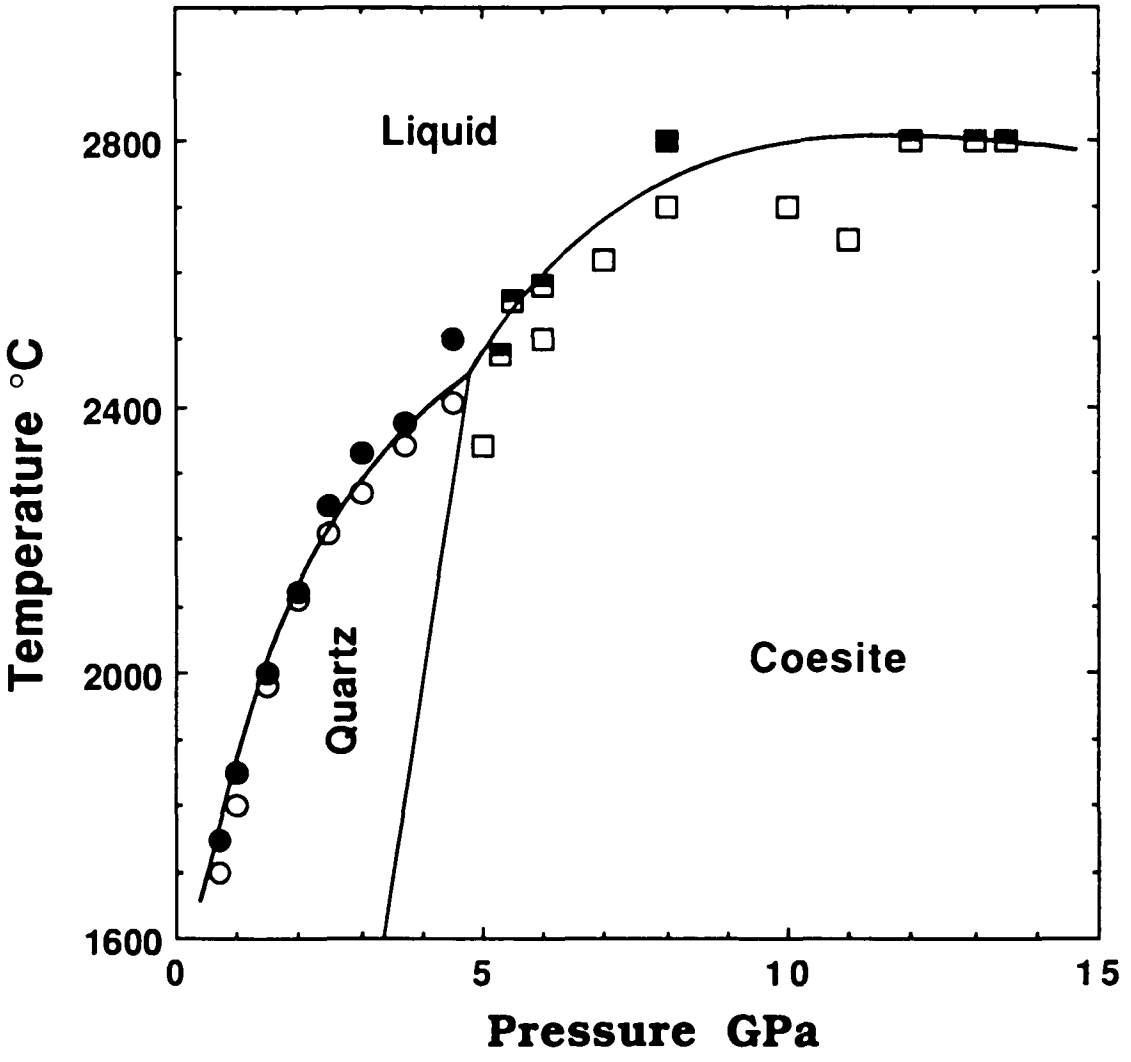

Figure 5.6 *Comparisons of the calculated melting curves of quartz and coesite with the experimental results. Circles = quartz (Jackson, 1976; Kanzaki, 1990); Squares = coesite (Kanzaki, 1990 and this study); Closed symbols: liquid, Open symbols: coesite.*

If the data on SiO_2 liquid in Table 5.2 are accepted, it becomes rather easy to test the aforementioned proposal for the room temperature amorphizations of quartz and coesite by minimizing the Gibbs free energy at 298 K. At this condition both heat capacity and thermal expansion actually have no effect on the equilibrium calculation. The only data we need are those at 298 K. This will place the metastable melting points at about 13 GPa for quartz, and 28 to 32 GPa for coesite when ΔH^{o}_{298} and ΔS^{o}_{298} are considered, respectively, in the ranges of -905000 to -910000 J mol^{-1} and 35 to 40 J mol^{-1} K^{-1}. It implies that the amorphization of coesite observed at 30 to 35 GPa by Hemley et al. (1988) could be interpreted in terms of the crossing of the negative metastable extension of its melting curve, while the quartz-glass transformation should have occurred at much lower pressure than that demonstrated by Hemley et al. (1988).

Chapter 6

Melting and Dehydration of Brucite $Mg(OH)_2$

6.1 Experimental Results

Experimental results are summarized in Table 6.1 and illustrated in Figure 6.1. The most important observation in this study was that brucite melted incongruently to liquid plus periclase at pressures above 10 GPa, represented by the following univariant reaction:

$$\text{Brucite} = \text{Liquid} + \text{Periclase}$$

where liquid was quenched to a crystalline phase with the MgO content ranging from 45 to 66 wt.% (Table 6.2). In comparison, the unreacted brucite generally has the MgO content greater than 67 wt.% and close to 70 wt.%. Periclase has the MgO content between 95 and 100 wt.%. Two possibilities are considered for some of them to have low MgO content: 1) periclase may be overlaped with brucite; and 2) surface of the thin sections may not be well polished.

A typical sketch of melting relation of brucite is shown in Figure 6.2 based on the microscopic observations for the experiment at 10 GPa and 1200 °C (Run # 1409). Because of the 200 °C temperature gradient, we observed the following variations in the sample. Above the melting boundary it contained two loops of liquid between which it was a mixed phase of liquid and periclase. Right below the melting boundary it consisted of coarse plates of brucite with

scattered, very fine grains of periclase. Stable brucites occupied the rest of the sample, but the crystals became smaller toward the cold end. The estimated melting temperature was slightly lower than 1250 °C.

Table 6.1 Results on the Melting and Dehydration of Brucite

Run No.	P (GPa)	T (°C)	Time (Min.)	Phases
1394	10	1150	20	Br
1397	10	1050	20	Br
1398	10	950	20	Br
1401	8	1150	20	Br
1402	12	1140	20	Br
1403	14	1150	20	Br
1405	16	1150	20	Br
1406	18	1150	20	Br
1409	10	1200	20	Q-liq,Per,Br
1410	16	1200	20	Q-liq,Per,Br
1411	20	1250	20	Q-liq,Per,Br
1415	12	1200	20	Q-liq,Per,Br
1416	20	1200	20	Q-liq,Per,Br
1420	8	1200	20	Q-liq,Per,Br
1421	22	1200	20	Q-liq,Per,Br
1425	6	1150	20	Per,Br
1426	6	1200	14	Q-liq,Per,Br

Br =Brucite; Per=Periclase; Q-liq=Quench Liquid.

Phases are listed according to the order observed from the hot spot to the cold end. Details are in the text.

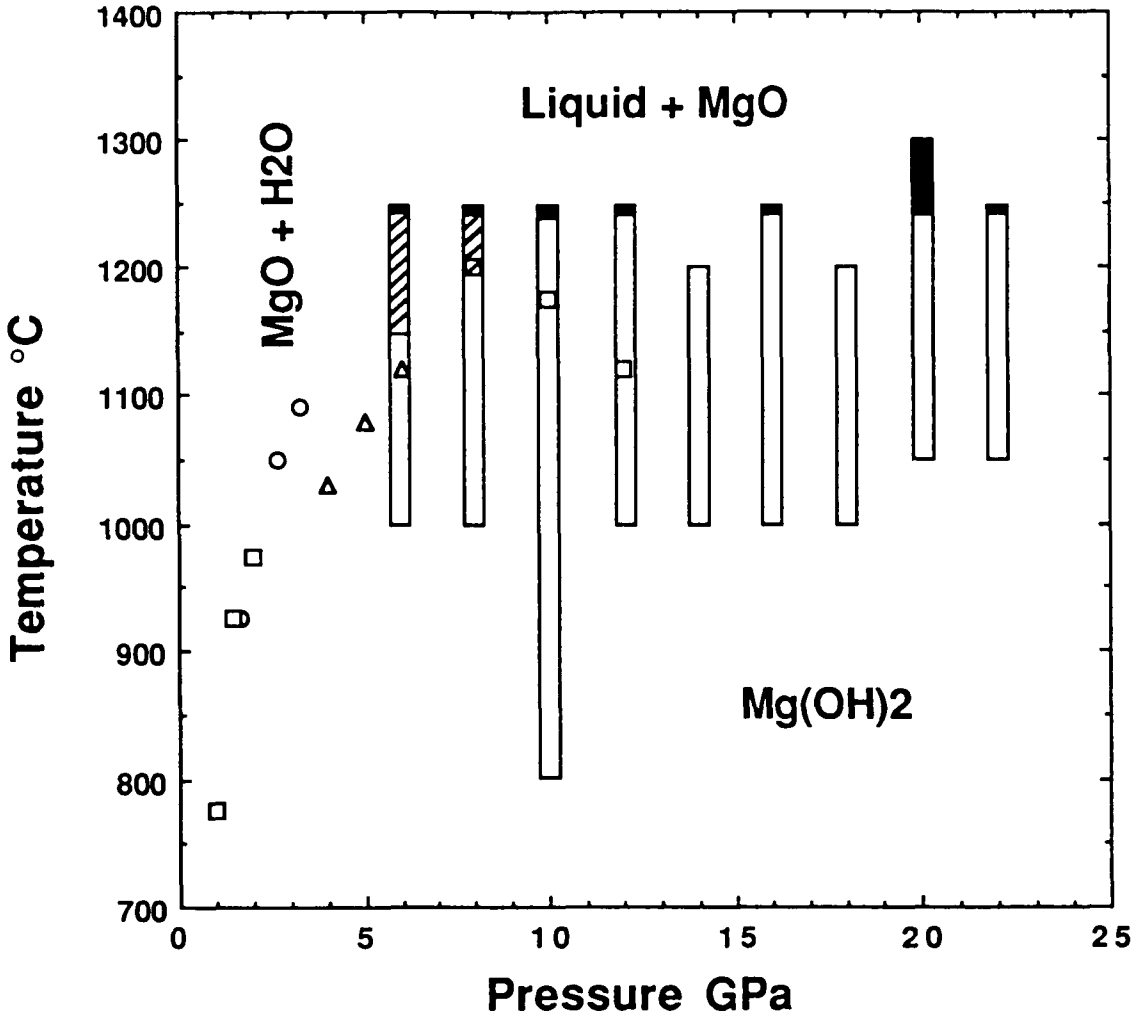

Figure 6.1 *Experimental results on the melting and dehydration of brucite. The long bars are from this study. Closed symbols : quench liquid; Open symbols: stable brucite; and Slash symbols: periclase. The length of each bar represents the temperature range covered by one or more experiments, and includes the 200 °C temperature gradient. For the previous experimental studies, Circles: Irving et al. (1977); Triangles: Kanzaki (1991); and Squares: Johnson et al. (1991). All these symbols represent the temperatures and pressures at which dehydration of brucite occurs.*

Table 6.2 Microprobe Analyses of the samples at 8 and 10 GPa

Analysis #	MgO	CaO	Al_2O_3	SiO_2	Total
P = 10 GPa; T = 1050 °C (Run # 1397)					
1	0.70909	0.00055	0.00172	0.00102	0.71238
2	0.69898	0.00017	0.00100	0.00140	0.70155
3	0.71727	0.00001	0.00141	0.00139	0.72008
4	0.67136	0.00022	0.00242	0.00253	0.67653
5	0.69114	0.00016	0.00035	0.00131	0.69296
6	0.67690	0.00036	0.00077	0.00119	0.67922
P = 10 GPa; T = 1150 °C (Run # 1394)					
7	0.68744	0.00004	0.00016	0.00155	0.68919
8	0.70513	0.00019	0.00207	0.00157	0.70896
9	1.02744	0.00029	0.00843	0.00015	1.03631
10	1.00719	0.00012	0.00105	0.00016	1.00852
11	0.97503	0.00063	0.00713	0.00032	0.98311
P = 10 GPa; T = 1200 °C (Run # 1409)					
12*	0.98425	0.00000	0.00032	0.00042	0.98499
13	0.69280	0.00000	0.00046	0.00165	0.69491
14*	0.95871	0.00000	0.00043	0.00041	0.95955
15*	0.98905	0.00005	0.00290	0.00050	0.99250
16*	0.59381	0.00000	0.00642	0.00154	0.60177
17*	0.45750	0.00336	0.00936	0.00226	0.47248
18*	0.98995	0.00002	0.00127	0.00020	0.99144
19*	0.64284	0.00001	0.00980	0.00168	0.65433
20*	0.94798	0.00004	0.00178	0.00044	0.95024
21*	0.96124	0.00002	0.00896	0.00030	0.97052
22*	0.95933	0.00029	0.00072	0.00039	0.96073
23*	0.98049	0.00000	0.00031	0.00044	0.98124

P = 8 GPa; T = 1200 °C (Run # 1420)

24*	1.00313	0.00000	0.00141	0.00000	1.00454
25	0.72991	0.00014	0.00022	0.00166	0.73193
26*	0.99930	0.00001	0.00113	0.00001	1.00045
27*	0.66636	0.00081	0.01965	0.00385	0.69067
28*	0.64169	0.00000	0.01489	0.00328	0.65986
29*	0.66512	0.00092	0.01216	0.00354	0.68174
30	0.69783	0.00000	0.00015	0.00116	0.69914

* *Analyses were made above the melting or dehydration interface*

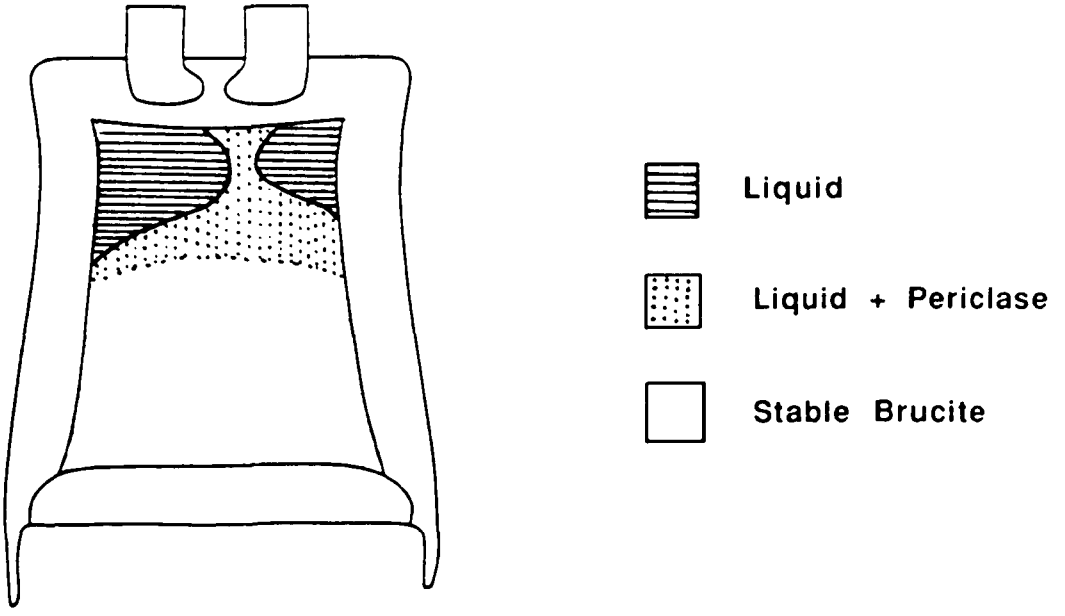

Figure 6.2 *A sketch of the experimental charge on brucite at 10 GPa and 1200 °C (Run # 1409).*

The quench liquid and stable brucite were not only different in compositions, they were also quite different texturally in the polished section under microscope. Stable brucites formed transparent plates with a white sugary texture and recrystallized into giant crystals before it melted. They also showed perfect basal cleavage, which is due to weak bonding between the adjacent octahedral layers. In contrast, the quench liquid appeared yellowish in color, shiny but less transparent on the surface, and grew in an elongated and sub-radial fashion. {0001} cleavage observed in stable brucite was invisible. The presence of periclase above the melting boundary was further confirmed by its high refraction relative to brucite, and by its hardness, which makes the polished surface of sample appeared not very flat.

Most of the experiments in this study were designed in a way that a series of experiments was conducted either at the fixed pressure by changing temperatures or at the fixed temperature by changing pressures (Table 6.1 and Figure 6.1). In this procedure, it would give us a clear base line to determine the slopes of melting and dehydration curves. This has been done by examining variations in the amount of the quench liquid and periclase in the recovered samples. It will also record any chemical and textural changes in the experimental pressure and temperature ranges.

At 10 GPa and a temperature range of 950 to 1150 ^{o}C, three experiments showed the following textural variations. At 950 ^{o}C (Run #1398) the sample contained fine grains of brucites. At 1050 ^{o}C (Run #1397) brucites were fine grained at the cold end , but grew to medium-grained crystals at the hot end. At further 100 ^{o}C higher (Run #1394), giant crystals of brucite were found, together

with scattered, fine grained periclase at the hot spot. This was consistent with the observation at 1200 °C (Run #1409) right below the melting boundary.

In a wide pressure range of 12 to 22 GPa, all the recovered samples at 1150 °C showed similar characteristics, and were basically the same as that at 10 GPa and 1150 °C. To emphasize, melting was not observed, and only trace amount of very fine-grained periclase appeared within giant crystals of brucite at the hot spot. However, when temperature was increased by 50 °C, brucite melted incongruently at 12, 16, 20 and 22 GPa. The melting temperatures were all 1250 °C, and thus independent of pressure. Dehydration of brucite was also observed in this study but at low pressures. At 6 GPa and 1150 °C (Run # 1425), the sample contained abundant medium-grained crystals of periclase, together with small amount of fine-grained brucite formed presumably from rehydration during the quench. Immediately below them were giant crystals of brucite that have been observed right below the melting boundaries above 10 GPa. The interface between periclase and brucite was not as sharp as the melting boundary, but somewhat diffused. Melting was also observed at this pressure (Run #1426) at about 1250 °C, and was attributed to that of periclase + H_2O. At 8 GPa, we observed the dehydration at 1200 °C and melting at 1250 °C. The quench liquid was similar both texturally and compositionally to that observed above10 GPa.

6.2 Comparisons of the experimental data

Comparisons of this study with the previous experimental results are also

shown in Figure 6.1. Using the quench method, our dehydration temperatures are consistent with the extrapolation of the data of Irving et al. (1977). Observations below and above the dehydration boundaries in this study agree with theirs as well. In both studies, however, it is found difficult to have a definitive explanation for the occurrence of small periclase grains below the defined dehydration and melting boundaries. Certainly, it cannot be explained in terms of reactions for a bulk composition $Mg(OH)_2$ in the binary system. For example, at constant pressure brucite and periclase can coexist at only one temperature for this composition. A small proportion of air sealed into the capsule could be a plausible reason. As pointed out by Wyllie (1962), a fraction of 1 wt.% of an inert gas under these conditions would cause incipient dehydration more than100 ^{o}C below the real reaction temperature.

Compared with the results from the in situ DTA measurements, our results on the dehydration are in excellent agreement with those of Johnson et al. (1991) at 8 GPa. But temperatures in both studies are slightly higher than those of Kanzaki (1991) when his data are extrapolated to high pressure. At 10 GPa agreement is also found between Johnson et al. (1991) and this study in terms of temperature, but our observation and interpretation are completely different. Within 2 to 12 GPa pressure range, they reported a temperature maximum in the dehydration curve around 8 GPa, which has not been confirmed by this study in the pressure range of 6 to 22 GPa. The DTA study has its advantage to detect the reaction in situ by recording endothermic and exothermic signals as a function of temperature, but such a study can not tell the relevant chemical and physical processes that happen in the sample.

In their preliminary report from the in situ X-ray studies, Leinenweber et al. (1991) suggested a turnover of the dehydration curve at even lower pressure and temperature (~6 GPa and 1050 °C). Since all these experiments were conducted without using capsules, contamination of the sample (reagent $Mg(OH)_2$) with the surrounding materials such as boron nitride sleeve and loss of water in an open system are possible reasons for their observations. They have most recently conducted several new experiments in which I was got involved by using the same technique but the sample was enclosed in the capsule made of the plantum foil, 25 micrometers in thickness. These new data indicated that brucite did not breakdown even at 3 GPa because no periclase peaks were observed. Instead it melted at 1150 to 1250 °C in a pressure range of 3 to 12 GPa, judged from the X-ray patterns in which the brucite peaks disappeared and the background increased significantly when temperature was higher than 1150 °C. It is clear that these results are qualitatively in excellent agreement with our quench experimental studies. Since all these discussions are purely based on the analyses of the X-ray data, the final conclusion will not be derived until further information is obtained from the recovered samples (for instance, periclase may exist below 8 GPa but too small to be detected by X-ray with a beam size of 100 x 200 micrometers).

Through theoretical considerations Saxena (1989) and Duffyand Ahrens (1991) have also predicted a temperature maximum in the dehydration curve of brucite around 8 GPa. This arises from water being more compressible than the coexisted solids. However, as will be discussed in the following section, other parameters such as compressibility data on brucite will significantly affect the extrapolated dehydration curve at high pressures.

Previous studies (e.g., Wyllie and Tuttle, 1963) have noticed that periclase tended to react with H_2O during quench, rendering it difficult to locate the boundary. However, there was no report indicating that complete rehydration was possible. For the following reasons we consider that the dehydration did not take place between 10 and 22 GPa. 1) The decomposition of brucite was observed at 6 and 8 GPa; 2) Brucite that presumably formed by reaction of periclase with vapor during the quench was texturally different from the untransformed stable material. Crystals of secondary brucite usually exist as interstitial, feathery fine grains within periclase crystals; and 3) The quench rates in this study were 10 to 20 times faster than those in Irving et al.'s (1977) experiments such that the former were able to preserve abundant large crystals of periclases.

Although this study was the first one among the literatures to demonstrate the relationship between dehydration and melting of brucite, similar phase relation has been reported on $Ca(OH)_2$. According to Wyllie and Tuttle (1960,1963), the dehydration of portlandite terminated at about 100 bars and 780 ^{o}C with a melting curve rising from it. The melting temperatures were observed almost independent of pressure up to 30 Kbars (Wyllie ant Tuttle, 1960; Irving et al., 1977). The similarity of the phase relations in these two analogous systems is shown in Figure 6.3.

By considering the temperature - composition phase equilibrium in a binary system MgO - H_2O, the present experimental results on the dehydration and melting of brucite at pressures of 6, 8 and 10 GPa are schematically illustrated in Figures 6.4a, 6.4b and 6.4c, respectively. Solubility of MgO in water at these

conditions is unknown and is not considered in the phase diagrams. The melting relations between 12 and 22 GPa are basically the same as shown in Figure 6.4c. Following the Robertson and Wyllie's (1971) analyses, the line a-b-c-d in Figure 6.4c is a saturation boundary of vapor along which the subsolidus assemblage can be fully hydrated, or the liquid formed by complete melting can be saturated. In this study, the subsolidus phase with a bulk composition of $Mg(OH)_2$ is water- saturated prior to melting (the line a-b). Once reaching the point m, brucite melts incongruently into periclase plus liquid which is water - undersaturated. In other words, liquid would not be in equilibrium with a vapor phase. That is why free water or water bubble was not observed in this study. In contrast, by using reagent $Ca(OH)_2$ mixed with excess water as a starting material, Wyllie and Tuttle (1960, 1963) observed either a menicus in the quench sample which indicated the former coexistence of liquid and vapor phase or small bubbles occurred within the quench liquid. These two features were not observed in our recovered samples.

6.3 Thermodynamic evaluation of the experimental data

Thermodynamic data used in the evaluation are listed in Table 6.3. Because of the dehydration of brucite at 1 bar and about 500 ^{o}C, heat capacity was only available to 700 K (King et al., 1975). From the experimental studies on the dehydration reaction up to 3.3 GPa (Barnes and Ernst, 1963; Irving et al., 1977; al.,1977; Schramke et al., 1982), Saxena (1989) extrapolated the heat capacitydata on brucite up to 1400 K and optimized data on thermal expansion, bulk modulus and its pressure derivative. His data on heat capacity and thermal expansion are adopted in this study. Elastic data on K_T

and K_T' for brucite have been most recently determined from the shock wave measurements between 12 and 60 GPa (Duffy and Ahrens, 1991) and from studies using the diamond anvil cell up to 80 GPa (Fei, unpublished). These data are listed in Table 6.3. Fugacity of water is calculated from equations given in Chapter 3.

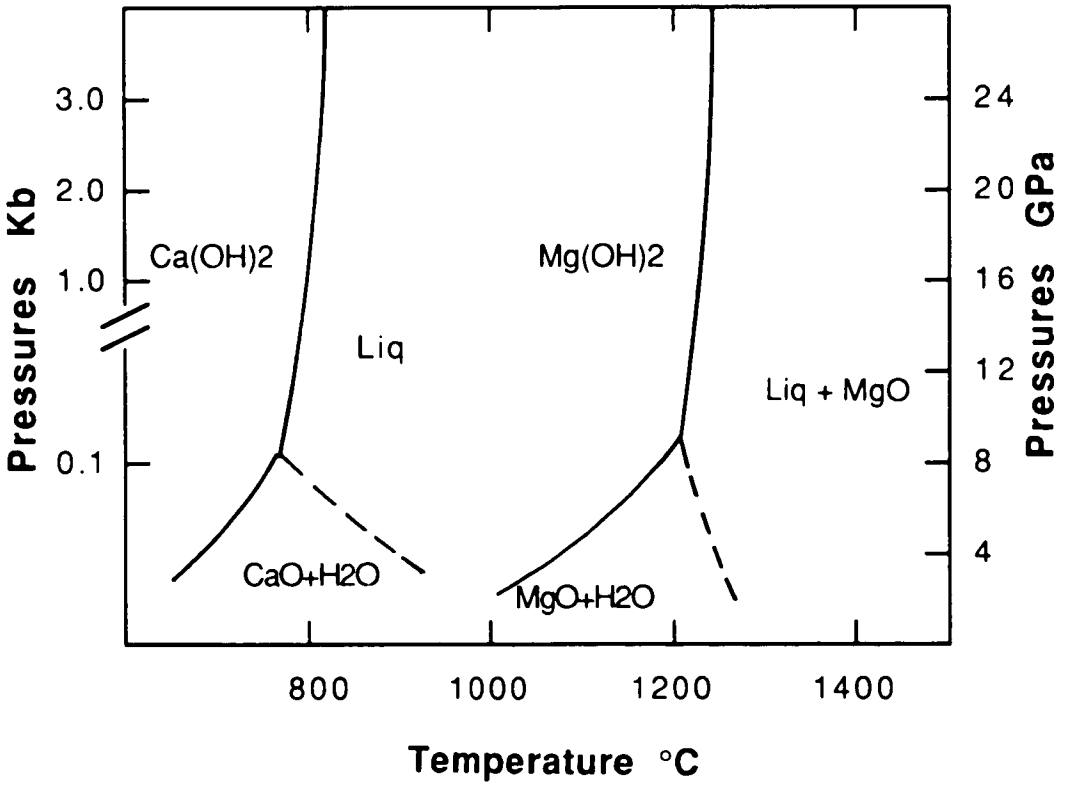

Figure 6.3 *P- T projection of univariant equilibria in the systems CaO - H_2O (left) and MgO - H_2O (right). The invariant point for MgO - H_2O system has not been well constrained, but it will be located at a temperature around 1200 °C and a pressure between 8 and 1 0 GPa.*

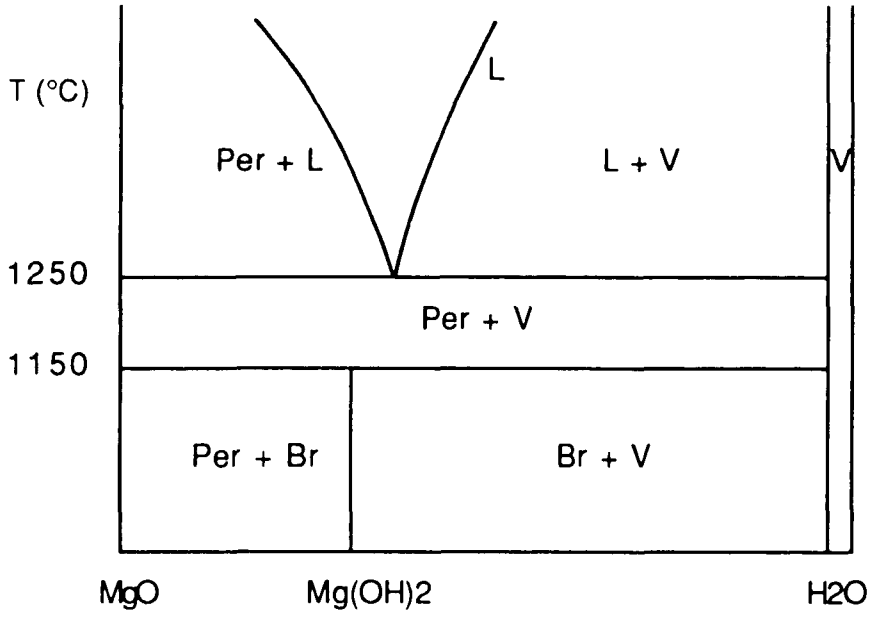

A) P = 6 GPa

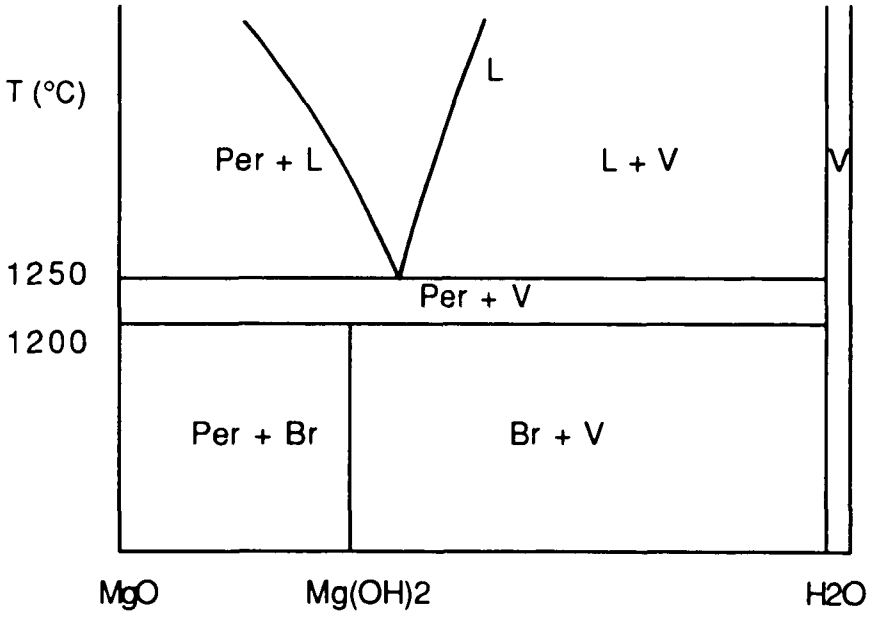

B) P = 8 GPa

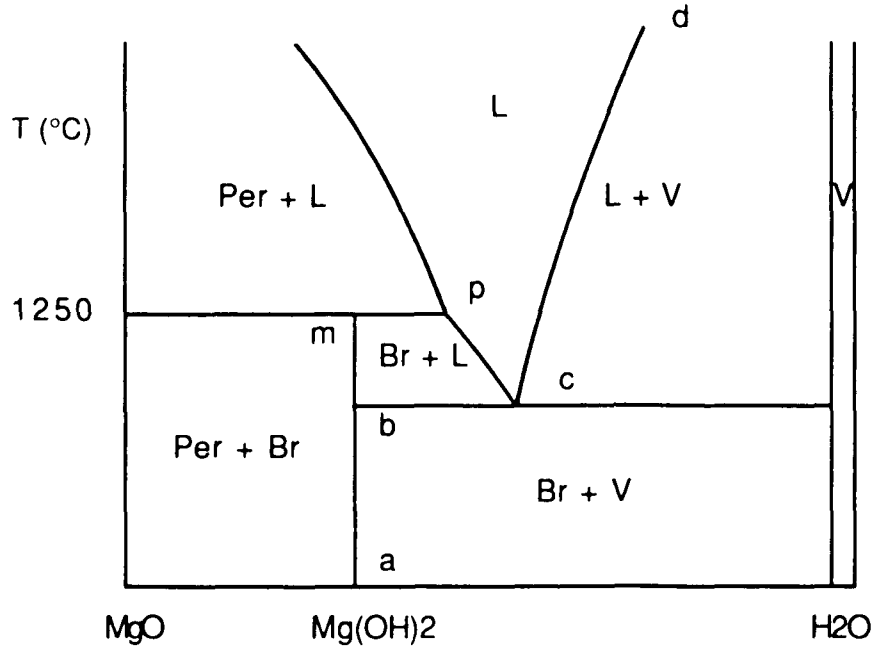

C) P ≥ 10 GPa

Figure 6.4 *Schematic isobaric temperature-composition sections for the system MgO-H_2O showing phase relations of dehydration and melting reactions of brucite at the increased pressures. Br = Brucite; Per = Periclase; V = Vapor, and L= Liquid.*

With thermodynamic data in Table 6.2, a number of simulations have been made using different elastic data on brucite given in Table 6.3. Typical results of calculations are shown in Figure 6.5. As can be seen, the calculated dehydration curves are all in good agreement with the experimental results at low pressures. However, both Saxena's (1989) and Duffy and Ahrens' (1991) data on K_T and K_T' predict a temperature maximum at 8 to 10 GPa in the dehydration curves and a large negative dT/dP slope at higher pressures. For

Table 6.3 Thermodynamic data on brucite and periclase

Parameters	Brucite	Periclase	Units
ΔH^o_{298}	-924500	-601490	J mol^{-1}
AS^o_{298}	63.60	26.94	J mol^{-1} K^{-1}
Heat capacity			
a	103.01	43.57	
b	1.6533	0.5480	10^{-2}
c	-0.2746	-0.1678	10^{7}
e	-0.1365	-631000	10^{3}
9	-0.1141	3.3390	10^{3}
V_{298}	24.63	11.25	cm^3/mol
Thermal expansion			
α_o	0.8754	0.3754	10^{-4}
α_1	1.8090	0.7910	10^{-8}
$\alpha 2$	-2.2180	___	10^{-2}
α_3	0.5943	-0.7836	
Compressibility			
β_o		0.5951	10^{-6}
β_1		0.8233	10^{-10}
β_2		0.3264	10^{-13}
β_3		0.1018	10^{-17}
K_{298}'		4.17	

Brucite: ΔH^o_{298}, ΔS^o_{298}, and V_{298}, Robie et al. (1978); Heat capacity and thermal expansion, Saxena (1989); Compressibility, see Table 6.3; Periclase: ΔH^o_{298}, ΔS^o_{298} , V_{298}, and heat capacity, Robie et al. (1978); Thermal expansion and compressibility, Saxena and Zhang (1988); Ki, Anderson and Zou (1989).

Table 6.4 Elastic data on brucite

References	K_{300} (GPa)	K_{600} (GPa)	K_{298}'
Saxena (1989)	57.12		4.71
Duffy and Ahrens(1991)	51±4		5.0±0.4
Fei (unpublished)*	54.90	48.10	4.70

* $K_T' = 1/(1.5640E\text{-}6 + 8.5837E\text{-}10T)$

comparison, Fei's unpublished data are consistent with the experimental observations in the entire P-T space.

It is clear from Figure 6.5 that K_T and K_T' values have a significant effect on the extrapolation of dehydration curves at high pressures. At room temperature Fei's data are comparable with those of Saxena's (1989) and Duffy and Ahrens' (1991). However, by considering a linear extrapolation of Fei's data obtained between 300 and 600 K, the stability field of brucite has been markedly extended at pressures above 10 GPa. This is because brucite is significantly more compressible than periclase. As a result, the dehydration curve of brucite will not turn over at least up to 30 GPa, and will be metastably over the melting curve as shown in Figure 6.5.

A number of calculations were also made to test the effect of the standard entropy of brucite (ΔS^o_{298}) on the dehydration curves. The results are shown in Figure 6.6. The best value to fit all the experimental data is 63.6 J mol^{-1} K^{-1},

which compares with a value of 63.18 J mol^{-1} K^{-1} from Robie et al. (1978) and of 64.4 J mol^{-1} K^{-1} from Holland and Powell (1991).

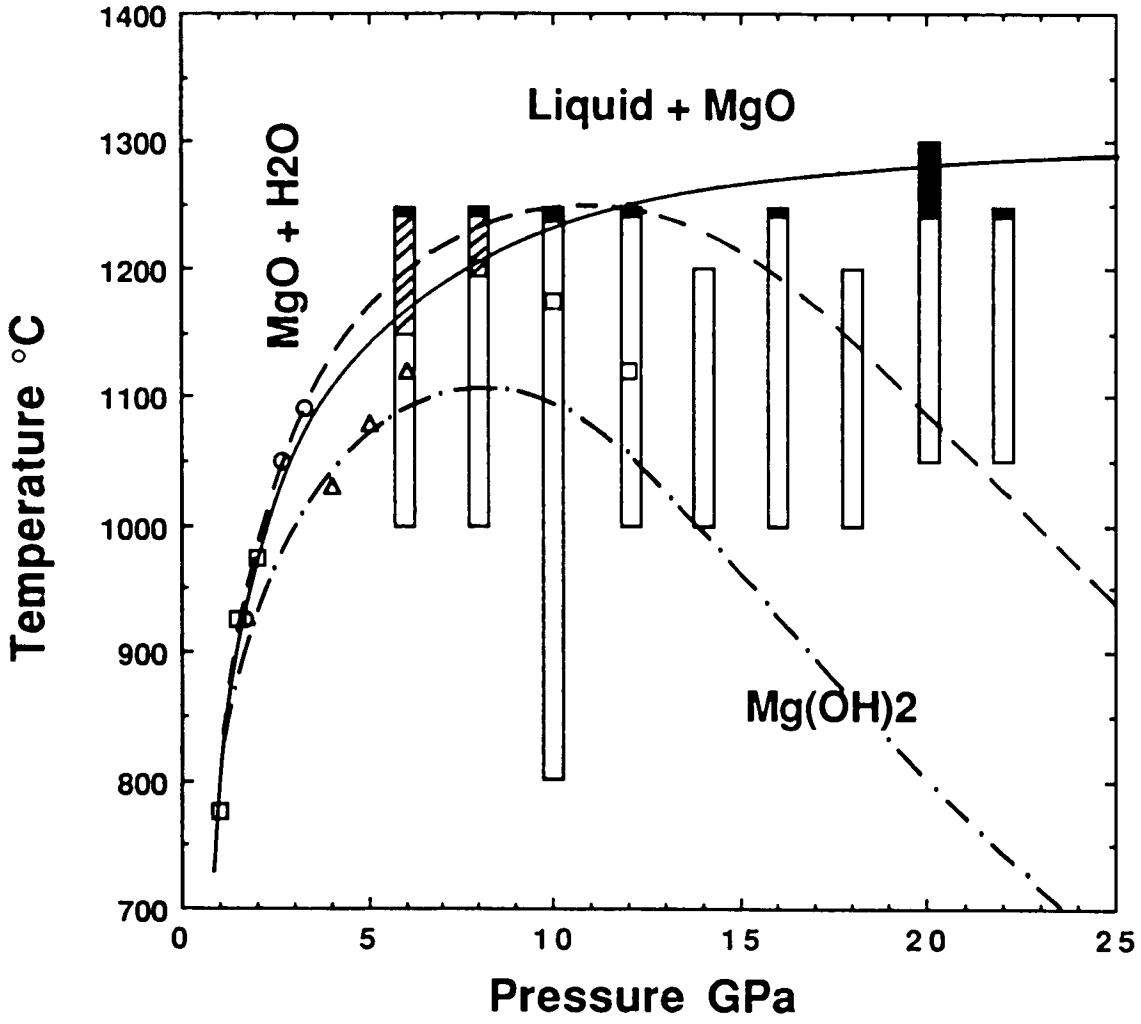

Figure 6.5 *Calculated dehydration curves of brucite using different values of K_T and K_T'. Symbols are the same as in Figure 6.1. 1: data from Fei (unpublished); 2: data from Saxena (1989); 3: data from Duffy and Ahrens (1 991); Number on the curve is the entropy of brucite suggested by this study.*

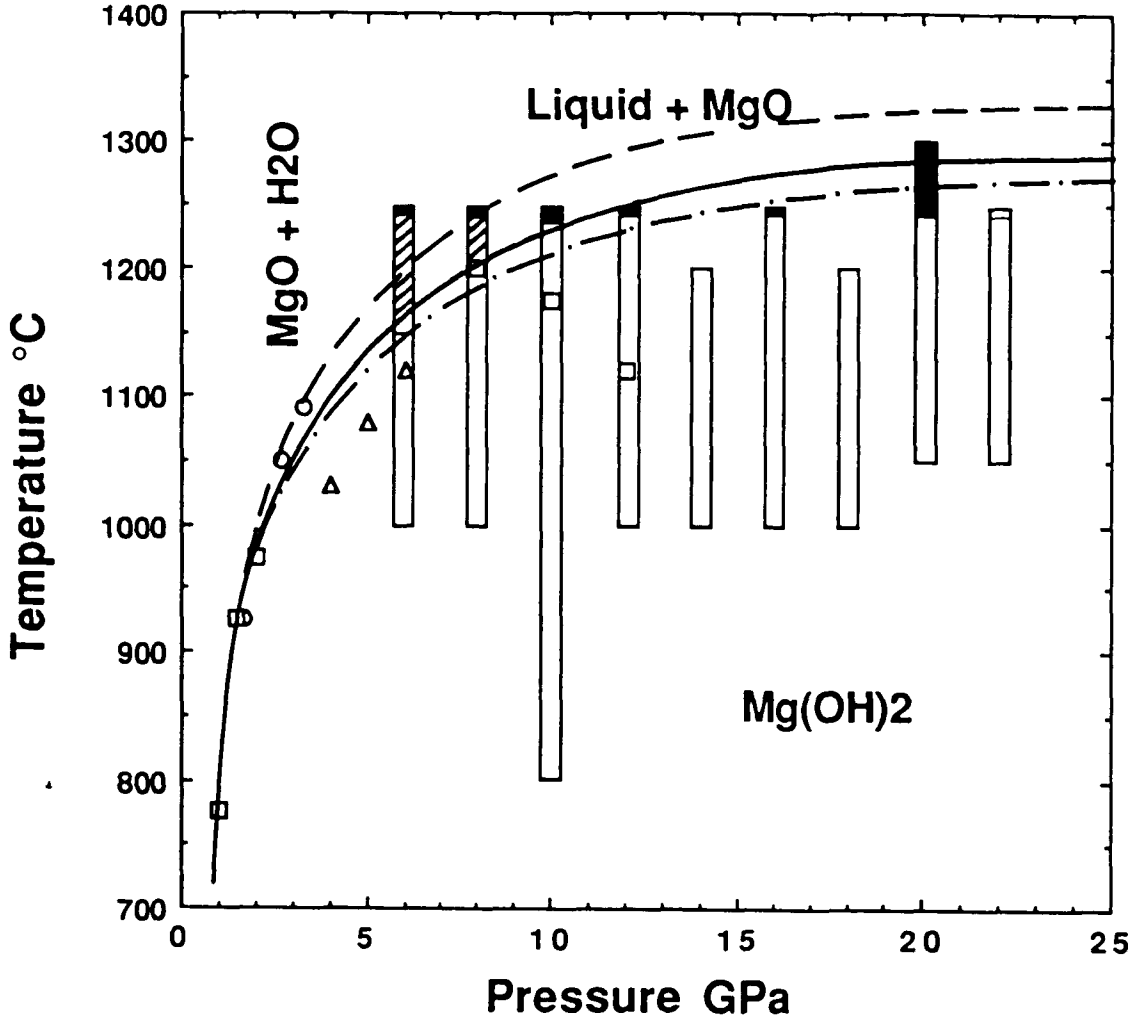

Figure 6.6 *Simulated dehydration curves at different standard entropy values of brucite. Symbols are the same as in Figure 6.1. Solid curve:* ΔS^{o}_{298} *= 63.6 J mol*$^{-1}$ *K*$^{-1}$*; Dashed curve:* ΔS^{o}_{298} *= 63.18 J mol*$^{-1}$ *K*$^{-1}$*(Robie et al., 1978); Dotted curve:* ΔS^{o}_{298} *= 64.4 J mol*$^{-1}$ *K*$^{-1}$ *(Holland and Powell, 1991).*

6.4. Stability of brucite in the mantle

From the experimental study between 6 and 22 GPa, the stability field of brucite

has been markedly extended above 10 GPa relative to the previous observations. However, both dehydration and melting still occur at temperatures that are lower than the expected mantle temperatures at pressures above 2 or 3 GPa depending on the geotherms (e.g., Brown and Mussett, 1984). Consequently, it can only be present in the colder subducted slabs, but not in the rest of the transition zone and the lower mantle.

Because of the limited stability field, brucite is unlikely to be involved in some of the mantle processes such as deep-focus earthquakes, which have recently been interpreted in terms of reactions involving water-bearing minerals (Meade and Jeanloz, 1989; Gasparik and Zhang, 1992), and viscosity reduction, which was considered to be associated with the presence of free water (McGovern and Schubert, 1989). However, it may play a role in generating the seismic low velocity zone, which has been interpreted in terms of incorporation of partial melt (e.g., Anderson and Bass,1984). This explanation, in turn, suggested the presence of volatiles such as water at relevant depths in order to depress the solidus of mantle materials. Provided that brucite is present below 100 km it will dehydrate, releasing water and causing melting.

Chapter 7

Conclusions and Comments

7.1 Melting of pyrope

Melting experiments were performed on the synthesized crystalline pyrope $Mg_3Al_2Si_3O_{12}$ at 2050 to 2500 °C and 10 to 16 GPa. Melting is congruent, and liquid was quenched to fine grains of pyrope. Our melting temperature at 10 GPa is in excellent agreement with the work of Irifune and Ohtani (1986). At pressures >10 GPa we observe melting temperatures that are much higher than those predicted by Irifune and Ohtani (1986), who fitted the existing data base to a Kraut-Kennedy equation. Within 3.5 and 10 GPa range, the slope of pyrope melting curve decreases from 82 °C/GPa to about 20 °C/GPa; whil between 10 and 16 GPa our melting data indicate a slope that is 67 °C/GPa.Such melting behavior is anomalous and has not been observed in other mantle minerals such as forsterite, enstatite, and coesite determined in Stony Brook and other laboratories. However, the increased melting slope above 10 GPa is consistent with the observations that liquidus phases change from olivine to aluminous garnet at high pressures in the multicomponent systems. No phase transformation was observed in the sample synthesized at 14.5 GPa and 2200 °C from oxide mixture of pyrope composition.

Using thermodynamic approach the melting data below 10 GPa can be well

described with the following data on pyrope liquid: V_{298} = 136.5 cm^3/mol; (α = 5.65 x 10^{-5}/K; K_T = 18.5 GPa; K_T' = 6.0. However, these data are unable to simulate a melting curve that showed an increased slope at certain pressure. By assuming complete disorders of Mg/Al between dodecahedral and octahedral sites and of Si/Al between tetrahedral and octahedral sites in crystalline pyrope, the calculated entropy of disordering is 18.7 J mol^{-1} K^{-1} but is far insufficient to yield a melting slope that is consistent with the experimental observations.

The melting data between 10 and 16 GPa can be fitted when liquid adopts different and larger values of K_T' above 10 GPa. This has been done by a method of trial and error. The resultant values are found to linearly increased with pressure. Using these values the calculated P-V relation indicates that pyrope liquid is considerably stiffened above 10 GPa, consistent with the observations and predictions that Al^{3+} in the liquid becomes six-coordinated above 6 to 10 G Pa.

7.2 Melting and subsolidus relations of silica polymorphs

Experiments were performed on amorphous silica at 1000 to 2850 °C and 9 to 14 GPa. The melting curve of coesite was extended from 8 GPa (Kanzaki,1990) to 13.7 GPa, and the melting temperatures indicated a slope almost independent of pressure. Our melting data did not confirm the prediction (Jackson, 1976) that the melting curve of coesite had a temperature maximum around 8 GPa and a large negative slope at higher pressures. Melting of stishovite was observed at 2850 °C and 14 GPa. For comparison, the melting temperatures inferred from the shock wave studies (Schmitt and Ahrens,1989)

are 3000±200 K. The triple point for coexisting coesite, stishovite and liquid was located at 2800 °C and 13.7 GPa, which was 600 °C higher than the previous estimation (Davis, 1972). The dP/dT slope of the coesite-stishovite transition observed at 2000 to 2800 °C was two and half times as large as indicated by the in situ X-ray study of Yagi and Akimoto (1976) below 1100 °C and by the quench experiments of Pacalo and Gasparik (1990) at 1050 and 1400 °C. At these relatively low temperatures, both Yagi and Akimoto (1976) and this study indicated the existence of metastable coesite in the stability field of stishovite, which made it difficult to determine the phase boundary.

Thermodynamic modeling on the coesite-stishovite boundary is rather difficult because it requires three-fold increase in the entropy change of the transition, which cannot be predicted from the existing heat capacity data base. Melting curve of quartz can be successfully modeled using the following data on SiO_2 liquid: V_{298} = 26.712 cm^3/mol; $\alpha = 1.0 \times 10^{-5}$ K^{-1}; K_T = 14.43 GPa; K_T' = 4.5. Melting curve of coesite can also be modeled using these data but requires larger heat capacity of coesite at high temperatures.

From the above data on SiO_2 liquid, the calculated melting points at room temperature for quartz and coesite were, respectively, 13 and 28 to 31.5 GPa. It implies that the amorphization of coesite observed at 30 to 35 GPa by Hemley et al. (1988) could be interpreted in terms of the crossing of the negative metastable extension of its melting curve, while the quartz-glass transformation should have occurred at much lower pressure than that demonstrated by Hemley et al. (1988).

7.3 Melting and dehydration of brucite

Quench experiments were performed on reagent $Mg(OH)_2$ at 6 to 22 GPa and 950 to 1250 °C. At pressures below 10 GPa, the dehydration temperatures increased with pressure, and are consistent with those of Johnson et al. (1991) and the extrapolation of the data of Irving et al. (1977). At 10, 12, 16, 20 and 22 GPa, brucite was observed to melt incongruently to periclase and liquid at 1250 °C, thus independent of pressure. Melting was also observed below 10 GPa, and was attributed to that of periclase + H_2O. Our study indicated that dehydration of brucite terminated at a pressure between 8 and10 GPa and a temperature between 1200 and 1250 °C with a melting curve rising from it. This relation has not been reported on brucite in the literatures but was observed in $Ca(OH)_2$ portlandite (Wyllie and Tuttle, 1960 and 1963). However, both observed (Johnson et al., 1991; Leinenweber et al., 1991) and predicted (Saxena, 1989; Duffy and Ahrens, 1991) temperature maximum in the dehydration curve has not been confirmed up to 22 GPa.

From this study, the stability field of brucite has been markedly extended above 10 GPa relative to the previous observations. However, both dehydration and melting still occur at temperatures that are lower than the expected mantle temperatures at relevant depths. Consequently, brucite can only be present in the colder subducted slabs, but not in the rest of the transition zone and lower mantle.

Thermodynamic modeling of the dehydration curve of brucite is very sensitive to the elastic data of brucite, particularly to the correct incorporation of

temperature dependence in bulk modulus. Using heat capacity and thermal expansion data of Saxena (1989) and compressibility data of Fei (unpublished), the simulated dehydration curve was in excellent agreement with the experimental observations below 10 GPa. The best value for the standard entropy of brucite at 298 K is 63.6 J mol^{-1} K^{-1}, which compares with a value of 63.18 J mol^{-1} K^{-1} from Robie et al. (1978) and of 64.4 J mol^{-1} K^{-1} from Holland and Powell (1991). The metastably extended dehydration curve does not show a temperature maximum at least to 30 GPa.

7.4 Comments

1. By stiffening pyrope liquid above 10 GPa the simulated melting curve was in excellent agreement with the experimental results in the entire P-T space. However, we consider it as a working model because it is difficult to evaluate whether the required large increase in K_T' is reasonable or not. The melting temperatures of pyrope are not expected to keep increasing at a slope of ~67 ^oC/GPa to very high pressures. In this regard, experiments performed above 20 GPa are useful.

2. Both melting of coesite and the coesite-stishovite transformation above 2000 ^oC can not be predicted using the existing thermochemical data on coesite and stishovite. Correct extrapolation of heat capacity data on both phases at high temperatures are required. This could be done by systematizing phase equilibrium data on the melting of coesite and on the transformations of quartz to coesite, coesite to stishovite and others involving stishovite in the system MgO-SiO_2. For coesite-stishovite transformation further experiments are needed

in three aspects: 1) evaluation of the previous determination below 1000 °C; 2) phase boundary in the temperature range of 1000 to 2000 °C; and 3) possibility of a nonquenchable phase transformation of coesite.

3. Dehydration curve of brucite and its metastable extension at high pressure are very sensitive to the physical properties of brucite (i.e., bulk modulus and its pressure derivative). Equation of state for water has not been experimentally determined at high pressures. Data on solubility of pericalse in water at high pressure and temperature are missing, and could be important in theoretical considerations.

Appendix

List of published and submitted abstracts and papers:

1. **Zhang J. (1988)**, Assessment of thermochemical data on magnesite, EOS Trans. AGU, 69, 473.

2. **Saxena, S. K., N. Charterjee, Y. Fei, and J. Zhang (1989)**, A critically assessed thermodynamic data base, EOS Trans. AGU, 70, 475.

3. **Saxena, S. K. and J. Zhang (1989)**, Assessed high-temperature thermochemical data on some solid, Phys. Chem. Solid, 50, 723-727.

4. **Saxena, S. K. and J. Zhang (1990)**, Thermochemical and pressure-volume temperature systematics of data on solids, examples: tungsten and MgO, Phys. Chem. Mineral., 17, 45-51.

5. **Shen, G., S. K. Saxena, and J. Zhang (1991)**, Assessment of the temperature dependence of thermal expansion and compressibility for silicates, EOS Trans. AGU, 72, 282.

6. **Zhang, J., C. T. Herzberg, and T. Gasparik (1991)**, Anormous melting behavior of crystalline pyrope $Mg_3Al_2Si_3O_{12}$: Implication for the melting of manesium perovskite, EOS Trans. AGU, 72, 317.

7. **Zhang, J., C. T. Herzberg, and T. Gasparik, and R. C. Liebermann (1991)**, Melting of coesite at 10-14 GPa, EOS Trans. AGU, 72, 436.

8. **Gasparik T, and J. Zhang (1992)**, Stability of hydrous phases at pressures corresponding to the Earth's transition zone,, Western Pacific Geophysics Meeting, EOS, 73, 53.

9. **Zhang, J., C. T. Herzberg, and T. Gasparik (1992)**, Meiting of crystalline pyrope $Mg_3Al_2Si_3O_{12}$ at 10 to 16 GPa, Geophys. Res. Lett., submitted.

10. **Zhang, J., R. C. Liebermann, T. Gasparik, C. T. Herzberg,and Y. Fei (1992)**, Melting and subsolidus relation of silica at 9 to 14 GPa, J. Geophys. Res., submitted.

11. **Zhang, J. and T. Gasparik (1992)**, Dehydration and melting of brucite $Mg(OH)_2$ up to 22 GPa, in preparation.

Bibliography

Akaogi, M., E. Ito, and A. Navrotsky, Olivine-modified spinel-spinel transitions in the system Mg_2SiO_4-Fe_2SiO_4: Calorimetric measurements, thermochemical calculation, and geophysical application, J. Geophys. Res., 94, 15671-15685, 1989.

Akaogi, M. and A. Navrotsky, The quartz-coesite-stishovite transformations: new calorimetric measurements and calculation of phase diagram, Phys. Earth Planet. Interior, 36, 124-134, 1984.

Akimoto, S., The system MgO-FeO-SiO_2 at high pressures and temperatures - phase equilibria and elastic properties, In The Upper Mantle, edited A. R. Ritsema, pp60-80, 1975.

Anderson, D. L., Isotopic evolution of the mantle: a model, Earth Planet. Sci. Lett., 35, 13-24, 1984.

Anderson, D. L. and K., Zou, Formulation of the thermodynamic functions for mantle minerals: MgO as an example, Phys. Chem. Minerals, 17, 138-150.,1989.

Angell, A. C., P. Cheesman, and S. Tamaddon, Pressure enhancement of ion mobilities in liquid silicates from computer simulation studies to 800 kilobars. Science, 218, 885-887, 1982.

Angell, A. C., P. Cheesman, and R. R. Kadiyala, Diffusivity and thermodynamic properties of diopside and jadeite by computer simulation studies, Chem. Geol., 62, 83-92, 1987.

Asamoto, R. R. and P. E. Novak, Tungsten-Rhenium thermocouples for use at high temperatures, Rev. Sci. Inst., 38, 1047-1052, 1967.

Barnes H. I. and W. G. Ernst, Ideality and ionization in hydrothermal fluids: the system MgO - H_2O - NaOH. Am. J. Sci. 261:129 - 150,1963.

Basset, W. A. and J. D. Barnett, Isothermal compression of stishovite and coesite up to 85 kbar at room temperature by X-ray diffraction, Phys. Earth Planet. Inter., 3, 54-60, 1970.

Berman, R. G. and T. H. Brown, Heat capacity of minerals in the system:K_2O-Na_2O-CaO-MgO-FeO-Fe_2O_3-Al_2O_3-TiO_2-SiO_2-CO_2-H_2O, representation, estimation and high temperature extrapolation, Contrib. Mineral. Petrol., 89, 168-183, 1985.

Bohlen, S. R. and A. L. Boettcher, The quartz+coesite transformation: A precise determination and the effects of other components, J. Geophys. Res., 87, 7073-7078, 1982.

Bottinga,Y. and D. Weill, Densities of liquid silicate systems calculated from partial molar volumes of oxide components, Am. J. Sci., 269-182, 1970.

Bottinga, Y., On the isothermal compressibility of silicate liquids at high pressure, Earth Planet. Sci. Lett., 74, 350-360, 1985.

Boyd, F. R. and J. L. England, Mantle minerals, Year Book Carnegie Inst. Washington, 61, 107-112, 1962.

Burnham C .W., J. R. Holloway, and N. F. Davis, Thermodynamic properties of water to 1000 °C and 10,000 bars. Geol. Soc. Am. Spec. Paper 132, 96 p., 1969.

Burton, B. P. and P. M. Davidson, In Advances in Physical Geochemistry, edited by S. K. Saxena, 1987.

Carmichael, R. S., Handbook of Physical Properties of Rocks, CRC Press, 1982.

Charlu, T. V., R. C. Newton, and O. J. Kleppa, Enthalpies of formation at 970 K of compounds in the system MgO-Al_2O_3-SiO_2 from high temperature solution calorimetry, Geochim. Cosmochim. Acta, 39, 1487-1497, 1975.

Chung, D. H., Elasticity of stishovite revisited, in High pressure Science Technology, edited by K D. Timmerhaus and M. S. Barber, pp97-108, 1979.

Davis, G. F., Equations of state and phase equilibria of stishovite and a coesitelike phase from shock-wave and other data, J. Geophys. Res., 77, 4920-4933, 1972.

Delany J. M. and H. C. Helgenson, Calculation of the thermodynamic consequences of dehydration in subducting oceanic crust to 100 Kb and 800 °C. Am. J. Sci. 278: 638 - 686,1978.

Duffy T. S. and T. J. Ahrens, The shock wave equation of state of brucite $Mg(OH)_2$. J. Geophys. Res. 96:14319 - 14330,1991.

Fei, Y. and S. K. Saxena, A thermochemical data base for phase equilibria in the system Fe-Mg-Si-O at high pressure and temperature, Phys. Chem. Minerals., 13, 311-324, 1986.

Fei, Y. and S. K. Saxena, An equation for the heat capacity of solids, Geochim. Cosmochim. Acta., 51, 251-254,1987.

Fei, Y., S. K. Saxena, and A. Navrotsky, Internally consistent data and equilibrium phase relations for compounds in the system MgO-SiO_2 at high pressure and high temperature, J. Geophys. Res., 95, 6915-6928, 1990.

Gasparik T., Transformation of enstatite-diopside-jadeite pyroxene to garnet. Contrib. Mineral. Petrol. 102: 389 - 405, 1989.

Gasparik T., Phase transitions in transition zone. J. Geophys. Res. 95: 1990.

Gasparik T, and J. Zhang, Stability of hydrous phases at pressures corresponding to the Earth's transition zone, (abstract), Western Pacific Conference, in press.

Haas, J. L. and J. R. Fisher, Simultaneous evaluation and correction of thermodynamic data, Am. J. Sci., 276, 525-545, 1976.

Halbach H. and N. D. Chartterjee, An empirical Redlich-Kwong type equation of state for water to 1000 °C and 200 Kbar. Contrib. Mineral. Petrol. 79: 337 - 345, 1982.

Halbse, T. and O. J. Kleppa, The thermochemistry of jadeite, Am. Mineral., 53, 1281-1291, 1968.

Haselton, H. T. and E. F. Westrum, Thermodynamics of grossular-pyrope garnets and their stabilities at high temperatures and high pressures, J. Geophys. Res., 85, 6973-6982, 1980.

Heinz, D. L. and R. Jeanloz, Measurement of the melting curve of $MgO_{.9}FeO_{.1}SiO_3$ perovskite at lower mantle conditions and its geophysical implications, J. Geophys. Res., 92, 11437-11444, 1987.

Helgeson H. C. and D. H. Kirkham, Theoretical prediction of the thermodynamic behavior of aqueous electrolytes at high pressures and temperatures: 1 Summary of the thermodynamic/electrostatic properties of solvent. Am. J. Sci. 274: 1089 - 1098, 1974.

Hemley, R. J., H. K. Mao, P.M. Bell and B. O. Mysen, Raman spectroscopy of SiO_2 glass at high pressure, Phys. Rev. Lett., 57, 747-750,1986.

Hemley, R. J., A. P. Jephcoat, H. K. Mao, L. C. Ming and M. H. Manghnani, Pressure-induced amorphization of crystalline silica, Nature, 334, 52-54, 1988.

Herzberg, C. T., The reaction forsterite+cordierite=aluminous orthopyroxene + spinel in the system $MgO-Al_2O_3-SiO_2$, Contrib. Mineral. Petrol.84, 84-90, 1983.

Herzberg, C. T., and M. J. O'Hara, Origin of mantle peridotite and komatiite by partial melting, Geophys. Res. Lett.,12, 541-544, 1985.

Herzberg, C. T., Magma density at high pressure, Part 1: The effect of composition on the elastic properties of silicate liquids, In Magmatic Processes: Physicochemical Principles, edited by B. O., Mysen, pp25-46,1987.

Herzberg, C. T., T. Gasparik, and H. Sawamoto, Origin of mantle peridotite: Constraints from melting experiments to 15 GPa, J. Geophys. Res., 95, 15779-15803, 1990.

Herzberg, C. T. and T. Gasparik, Garnet and pyroxenes in the mantle: A test of of the majorite fractionation hypothesis, J. Geophys. Res., 96, 16263-16274,1991.

Holland, T. J. B., Thermodynamic analysis of simple minerals, in Thermodynamics of Minerals and Melts, edited by R. C. Newton, A. Navrotsky, and B. J. Wood, ppl 9-34, 1981.

Holloway J. R., Fugacity and activity of molecular species in super-critical fluids. In Thermodynamics in Geology (ed. D. G. Fraser), pp. 16-181, Dordrecht - Holland, 1977.

Holm, J. L. and O. J. Kleppa, Thermodynamics of the disordering processin albite, Am. Mineral., 53, 123-133, 1968.

Irifune, T and E. Ohtani, Melting of pyrope $Mg_3Al_2Si_3O_{12}$ up to 10 GPa: Possibility of a pressure-induced structural change in pyrope melt, J. Geophys. Res., 91, 9357-9366, 1986.

Irving A. J., W. L. Huang, and P. J. Wyllie, Phase relations of portlandite, $Ca(OH)_2$ and brucite $Mg(OH)_2$ to 33 kilobars. Am J. Sci. 277: 313 -321, 1977.

Ito, E. and E. Takahashi, Melting of peridotite under the lower mantle condition, Nature, 328, 514-517, 1987.

Jackson, I., Melting of the silica isotypes SiO_2, BeF_2 and GeO_2 at elevated pressures, Phys. Earth Planet. Interior, 13, 218-231,1976.

James, F. and M. Roos, MINUIT, Computer Physics Communications., 10, 343-367, 1975.

Jeanloz, R. and E. Knittle, Reduction of mantle and core properties to a standard state by adiabatic decompression, in Chemistry and Physics of Terrestrial Planets, edited by S. K. Saxena, pp 275-309, 1986.

Johnson M. C., D. Walker, and S. K. Saxena, Brucite dehydration and the compressibility of water at very high pressure. EOS Trans. AGU, 72: 564, 1991.

Kanzaki, M, Melting of silica up to 7 GPa, J. Am. Ceram. Soc., 73, 3706-3707,1990.

Kanzaki M., Dehydration of brucite $Mg(OH)_2$ at high pressures: Detected by differential thermal analysis. Geophys. Res. Lett., 1991.

Kato, T. and M. Kumazawa, Melting experiments on natural lherzolite at 20 GPa: Formation of phase B with garnet, Geophys. Res. Lett., 13, 181-184, 1986.

Katsura, T. and E. Ito, The system Mg_2SiO_4-Fe_2SiO_4 at high pressures and high temepratures: Precise determination of stability of olivine, modified spinel, and spinel, J. Geophys. Res. 94, 15663-15670, 1989.

Kerrick D. M. and G. K. Jacobs, A modified Redlich - Kwong equation for H_2O, CO_2 and H_2O - CO_2 mixtures at elevated pressures and temperatures. Am. J. Sci., 281: 735 - 767,1981.

Kieffer, K., Thermodynamics and lattice vibrations of minerals: 1. Mineral heat capacities and their relationships to simple lattice vibrational models, Rev. Geophy. Space. Phys., 17, 1-19, 1979.

Knittle, E. and R. Jeanloz, Melting curve of $(Mg,Fe)SiO_3$ perovskite to 96 GPa, evidence for a structural transition in lower mantle melts, Geophys. Res. Lett., 16, 421-424, 1989.

Kuskov, O. L. and O. B. Fabrichnaya, The SiO_2 polymorphs: The equations of State and thermodynamic properties of phase transformation, Phys. Chem. Minerals, 14, 58-66, 1987.

Lane, D. L. and J. Ganguly, Al_2O_3 solubility in orthopyroxene in the system MgO-Al_2O_3-SiO_2: A reevaluation and mantle geotherm, J. Geophys. Res., 85, 6963-6972, 1980.

Lange, R. A. and I. S. E. Carmichael, Densities of Na_2O-K_2O-CaO-MgO-FeO-Fe_2O_3-Al_2O_3-TiO_2-SiO_2 liquids: New measurements and derived partial molar properties, Geochim. Cosmochim. 51, 2931-2946, 1987.

Leinenweber K., D. J. Weidner, M. Vaughan, O. Shimomuna, T. Kato, H. Morijima, J. Chen, and T. Kikegawa, In situ X-ray study of dehydration of brucite. EOS Trans. AGU, 72: 437, 1991.

Levien, L. and C. T. Prewitt, High - pressure crystal structure and compressibility of coesite, Am. Mineral., 66, 324-333, 1981.

Liebermann, R. C., C. T. Prewitt, and D. J. Weidner, Large-volume high pressure mineral physics in Japan, EOS, 66, 138-139, 1985.

Liebermann, R. C., A. E. Ringwood, and A. Major, Elasticity of poly-crystalline stishovite, Earth Planet. Sci. Lett, 32, 127-140, 1976.

McGovern P. J. and G. Schubert, Thermal evolution of the Earth: effects of volatile exchange between atmosphere and interior. Earth Planet. Sci. Lett-96: 27 - 37, 1989.

McMillan, P., Raman spectroscopy in mineralogy and geochemistry, Ann. Rev. Planet. Sci., 17, 255-283, 1989.

McMillan, P., M. Akaogi, E.Ohtani, O. Williams, R. Nieman, and R. Sato, Cation disorder in garnets along the $Mg_3Al_2Si_3O_{12}$ - $Mg_4Si_4O_{12}$ join: an Infrared, Raman and NMR study, Phys- Chem. Minerals., 16, 428-435, 1989.

Meade C. and R. Jeanloz, Acoustic emission from serpentine at high pressures and low temperatures: Implications for the origin of deep-focus earthquake. EOS Trans. AGU, 70 1321, 1989

Mishima, O., L. D. Calvert, and E. Whatley, "Melting ice" I at 77 K and 10 Kbar: a new method of making amorphous solids, Nature,310, 393-395, 1984.

Nelson, S. A. and I. S. E. Carmichael, Partial molar volumes of oxides components in silicate liquids, Contrib. Mineral. Petrol., 71, 117-124, 1979.

Ohtani, E. and M. Kumazawa, Melting of forsterite Mg_2SiO_4 up to 15 GPa, Phys. Earth. Inter., 27, 32-38, 1981.

Ohtani, E., F. Taulelle, and C. A. Angell, Al^{3+} coordination changes in liquid aluminosilicates under pressure, Nature, 314, 78-81, 1985.

Ohtani, E., T. Kato, and H. Sawamoto, Melting of a model chondritic mantle to 20 GPa, Nature, 322, 352-352, 1986.

Ohtani, E., Ultra - high pressure melting of a model chondritic mantle and

pyrolite compositions, in High Pressure Research in Mineral Physics, 87-93, edited by Manghnani M. H. and Y. Syono, Terra Publications, Tokyo, Japan, 1987.

Ohtani, E. and H. Sawamoto, Melting experiments on a model chondritic mantle compostion at 25 GPa, Geophys. Res. Lett., 14, 733-736, 1987.

Pacalo, R. E. G. and T. Gasparik, Reversals of the orthoenstatite-clinoenstatite transition at high pressures and high temperatures, J. Geophys. Res., 95, 15853-15858, 1990.

Presnall, D. C. and T. Gasparik, Melting of enstatite from 10 to 16.5 GPa, the beta phase-majorite eutectic at 16.5 GPa, and implications for the origin of the mantle, J. Geophys. Res., 15771-15777, 1990.

Richet, P. and Y. Bottinga, L. Danielou, J. P. Petitet, and C. Tequi, Thermodynamic properties of quartz, cristobalite and amorphous SiO_2: Drop calorimetry measurements between 1000 and 1800 K and a review from 0 to 2000 K. Geochim. Cosmochim. Acta. 46, 2269-2278., 1982.

Richet, P. and Y. Bottinga, Anorthite, andesine, wollastonite, diopside, cordierite, and pyrope: thermodynamics of melting, glass transitions, and properties of the amorphous phases, Earth Planet. Sci. lett., 67, 415-422, 1984.

Richet, P. and G. Fiquet, High-temperature heat capacity and premelting of minerals in the system MgO-CaO-Al_2O_3-SiO_2, J. Geophys. Res., 96, 445- 456, 1991.

Rigden, S. M., T. J. Ahrens, and E. M. Stopler, Shock compression of molten silicate: results for a model basaltic composition, J. Geophys.Res., 93, 367-382, 1988.

Rigden, S. M., T. J. Ahrens, and E. M. Stopler, High-pressure equation of state of molten anorthite and diopside, J. Geophys. Res., 94, 9508-9522, 1989.

Rivers, M. L. and I. S. E. Carmichael, Ultrasonic studies of silicate liquids, J. Geophys. Res., 92, 9247-9270, 1987.

Robertson, J. K. and P. J. Wyllie, Rock-water system, with special reference to the water-deficient region, Am. J. Sci., 271, 252-277, 1971.

Robie, R. A., B. S. Hemingway, and J. Fisher, Thermodynamic properties of minerals and related substances at 298.15 K and 1 bar (10^5 Pascals) and at high temperatures, U. S. Geol. Survey Bull., pp452, 1978.

Ross M. and F. H. Ree, Repulsive forces of simple molecules and mixtures at high density and temperature. J. Chem. Phys. 73: 6146 - 6152, 1980

Sasaki, S. and K. Nakazawa, Metal-silicate fractionation in the growing Earth: energy sourse for the terrestrial magma ocean, J. Geophys. Res., 91, 9231-9238., 1986.

Sato, Y., Pressure-volume relationship of stishovite under hydrostatic compression, Earth Planet. Sci. Lett., 34, 307-312, 1977.

Saxena, S. K. and Y. Fei, Fluids at crustal pressures and temperatures, Contrib. Mineral. Petrol., 95, 370-375, 1987a.

Saxena S. K. and Y. Fei, High pressure and high temperature fluid fugacity. Geochim. Cosmochim. Acta 51: 783 - 791, 1987b.

Saxena S. K. and Y. Fei, Fluid mixtures in the C - H - O system at high pressure and temperature. Geochim. Cosmochim. Acta 52: 505 - 512, 1988.

Saxena, S. K., Assessment of bulk modulus, thermal expansion and heat capacity of minerals, Geochim. Cosmochim. Acta, 53, 785-789, 1989.

Saxena, S. K. and J. Zhang, Assessed high-temperature thermochemical data on some solid, Phys. Chem. Solid, 50, 723-727, 1989.

Saxena, S. K. and J. Zhang, Thermochemical and pressure-volume temperature systematics of data on solids, examples: tungsten and MgO, Phys. Chem. Mineral., 17, 45-51, 1990.

Scarfe, C. M. and E. Takahashi, Melting of garnet peridotite to 13 GPa and the early history of the upper mantle, Nature, 322, 354-356, 1986.

Schmitt, D. R. and T. J. Ahrens, Shock temepratures in silica glass: Implications for modes of shock-induced deformation, phase transformation, and melting with pressure, J. Geophys. Res., 94, 5851-5871, 1989.

Schramke, J. A., D. M. Kerrick, and J. G., Blencoes, The experimental determination of the brucite=periclase+water equilibrium with a new volumetric technique, Am. Mineral., 67, 269-276, 1982.

Skinner, B. J., Thermal expansion, in Handbook of Physical Constants, edited by S. P. Clark, pp75-95, 1966.

Stebbins, J. F., 1. S. E. Carmichael., and L. K. Moret, Heat capacities and entropies of silicate liquids and glasses, Contrib. Mineral. Petrol., 86, 131-138, 1984.

Stebbins, J. F., and I. S. E. Carmichael., The heat of fusion of fayalite, Am. Mineral., 69, 292-297, 1984.

Stopler, E. M. and T. J. Ahrens, On the nature of pressure-induced coordination changes in silicate melts and glasses, Geophys. Res. Lett., 14, 1231-1233, 1987.

Suito, K., Phase relations of pure Mg_2SiO_4 up to 200 kilobars, in High Pressure Research: Application to Geophysics, ed. by Manghnani M. H. and S. Akomoto, Academic Press, New York, 365-371, 1977.

Takahashi, E. and C. M. Scarfe, Melting of peridotite to 14 GPa and genesis of komatiite, Nature, 315, 566-568, 1985.

Tan, H. and T. J. Ahrens, Shock induced polymorphic transition in quartz, carbon, and boron nitride, J. Appl. Phys., 67, 217-224, 1990.

Tequi, C., R. A. Robie, B. S. Heminway, D. R. Neuville, and P. Richet, Melting and thermodynamic properties of pyrope $Mg_3Al_2Si_3O_{12}$, Geochim. Cosmochim. Acta., 55, 1005-1010, 1991.

Walker, D., Lunar and terrestrial crust formation, J. Geophys. Res., 88, B17-B25, 1983.

Watanabe, H., Thermochemical properties of synthetic high-pressure compounds relevant to the Earth mantle, In High-Pressure Research in Geophysics, edited by S. Akimoto and M. H. and Manghnani, pp411-464, 1982.

Webb, S. L., The elasticity of the upper mantle orthosilicates olivine and garnet to 3 GPa, Phys. Chem. Mineral., 16, 684-692, 1989.

Weidner, D. J., J. D. Bass, A. E. Ringwood, and W. Singlar, The single crystal elastic moduli of stishovite, J. Geophys. Res., 87, 4740-4746, 1982.

Weidner, D. J. and H. R. Carleton, Elasticity of coesite, J. Geophys. Res., 82, 1334-1346, 1977.

Williams, Q. and R. Jeanloz, Spectroscopic evidence for pressure-induced coordination changes in silicate glasses and melts, Science, 239, 902-905, 1988.

Wyllie P. J. and O. F. Tuttle, The system CaO - H_2O - CO_2 and origin of carbonatites. J. Petrol. 1: 1 - 46, 1960.

Wyllie P. J. and O. F. Tuttle, The quenching technique in non-quenchable

systems: a discussion concerning the allaged decomposition of portlandite at high pressures. Am. J. Sci. 261: 983 - 988, 1963.

Yagi, T. and S. Akimoto, Direct determination of coesite-stishovite transition by in situ X-ray measurements, Tectonophysics, 35, 259-270, 1976.

Zhang, J., C. T. Herzberg, and T. Gasparik, Anormous melting behavior of crystalline pyrope $Mg_3Al_2Si_3O_{12}$: Implication for the melting of manesium perovskite, EOS, 71, 448, 1991.

Zhang, J., C. T. Herzberg, and T. Gasparik, and R. C. Liebermann, Melting of coesite at 10-14 GPa, EOS, 71, 436,1991.

Zhang, J., C. T. Herzberg, and T. Gasparik, and R. C. Liebermann, Melting and subsolidus relations of SiO_2 at 9-14 GPa, in preparation.